

University of New Hampshire

University of New Hampshire Scholars' Repository

Doctoral Dissertations

Student Scholarship

Spring 1997

Absorption and fluorescence spectra of sodium in an argon matrix

Alan Bruce Tutein

University of New Hampshire, Durham

Follow this and additional works at: <https://scholars.unh.edu/dissertation>

Recommended Citation

Tutein, Alan Bruce, "Absorption and fluorescence spectra of sodium in an argon matrix" (1997). *Doctoral Dissertations*. 1963.

<https://scholars.unh.edu/dissertation/1963>

This Dissertation is brought to you for free and open access by the Student Scholarship at University of New Hampshire Scholars' Repository. It has been accepted for inclusion in Doctoral Dissertations by an authorized administrator of University of New Hampshire Scholars' Repository. For more information, please contact Scholarly.Communication@unh.edu.

INFORMATION TO USERS

This manuscript has been reproduced from the microfilm master. UMI films the text directly from the original or copy submitted. Thus, some thesis and dissertation copies are in typewriter face, while others may be from any type of computer printer.

The quality of this reproduction is dependent upon the quality of the copy submitted. Broken or indistinct print, colored or poor quality illustrations and photographs, print bleedthrough, substandard margins, and improper alignment can adversely affect reproduction.

In the unlikely event that the author did not send UMI a complete manuscript and there are missing pages, these will be noted. Also, if unauthorized copyright material had to be removed, a note will indicate the deletion.

Oversize materials (e.g., maps, drawings, charts) are reproduced by sectioning the original, beginning at the upper left-hand corner and continuing from left to right in equal sections with small overlaps. Each original is also photographed in one exposure and is included in reduced form at the back of the book.

Photographs included in the original manuscript have been reproduced xerographically in this copy. Higher quality 6" x 9" black and white photographic prints are available for any photographs or illustrations appearing in this copy for an additional charge. Contact UMI directly to order.

UMI

**A Bell & Howell Information Company
300 North Zeeb Road, Ann Arbor MI 48106-1346 USA
313/761-4700 800/521-0600**

**ABSORPTION AND FLUORESCENCE SPECTRA OF
SODIUM IN AN ARGON MATRIX**

BY

Alan B. Tutein

B.S., University of New Hampshire (1990)

M.S., University of New Hampshire (1994)

DISSERTATION

Submitted to the University of New Hampshire
in partial fulfillment of
the requirements for the degree of

Doctor of Philosophy

in

Physics

May 1997

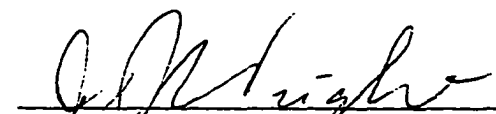
UMI Number: 9730846


**UMI Microform 9730846
Copyright 1997, by UMI Company. All rights reserved.**


**This microform edition is protected against unauthorized
copying under Title 17, United States Code.**


UMI
300 North Zeeb Road
Ann Arbor, MI 48103


This dissertation has been examined and approved.


Dissertation Director, J. J. Wright
Professor of Physics


L. C. Balling
Professor of Physics


J. F. Dawson
Professor of Physics


R. H. Lambert
Professor of Physics


H. R. Mayne
Professor of Chemistry

4/22/97
Date

Dedication

To my best friend and wife, Carrie.

Acknowledgments

I wish to thank my committee J. J. Wright, L. C. Balling, J. F. Dawson, R. H. Lambert, and H. R. Mayne.

I extend a special thanks to H. R. Mayne and R. P. White for allowing me to frequently bother them with questions and requests.

I am indebted to R. L. Kaufmann for the use of his computer resources. Thanks to his students (present and former), Dr. D. J. Larson, B. M. Ball, and I. Kontodinas, for putting up with me.

To my family and friends. Thank you for supporting me during these many years.

Table of Contents

Dedication	iii
Acknowledgments	iv
Abstract	x
1 Introduction	1
2 Method	5
2.1 Simulating the matrix trapping site	5
2.2 Calculating the Excited State Energies	12
2.2.1 An alkali in a rare gas matrix	12
2.3 Calculating the Absorption and Emission spectra	21
2.3.1 Absorption	21
2.3.2 Fluorescence	22
2.4 Potentials	29
2.4.1 Rare Gas-Rare Gas Interactions	29
3 Results and Conclusions	35
3.1 Characterization of the simulated matrix trapping site	35
3.2 Absorption results	36
3.3 Fluorescence results	46

4 Summary	56
A Useful Formulas	58
A.1 Spherical Harmonics	58
A.2 Wigner 3-j symbols	59
A.3 The integral of three Spherical Harmonics	59
B Proof of Hellman-Feynman Theorem	61
C Calculating the Perturbation Matrix, V_{ij}	62
C.1 Evaluation of matrix elements	64
C.2 Derivatives of the Matrix Elements for the P-state	66
C.2.1 Derivatives of V'_{00}	66
C.2.2 Derivatives of V'_{01}	66
C.2.3 Derivatives of V'_{02}	66
D Preprint–Structure of Na(3^2P)-Ar_n Clusters using Semiempirical Potentials	68
List of References	91

List of Tables

1.1	Experimental absorption peaks of Na in an Ar matrix	3
2.1	Ar _n cluster energies for n = 8...24	11
2.2	Sources for available Na-Ar dimer potentials	31
2.3	Ground state potential parameters used	32
2.4	Excited state potential parameters used	33
3.1	Free Na*Ar _n cluster transition wavelengths	50

List of Figures

1-1	Experimental absorption and blue site fluorescence of Na in Ar	2
2-1	NaAr _n coordinate system used.	6
2-2	Ar ₁₃ cluster	11
2-3	Na(3S)Ar ₆ isomers	13
2-4	Na*Ar _n coordinate system used.	14
2-5	Diagram of Σ and Π molecular orbitals	19
2-6	Histogram of the radial distribution of NaAr _n	24
2-7	Na(3P)Ar _n small cluster structures	28
2-8	Ar-Ar and Na-Ar ground state potentials compared	30
2-9	Morse potential showing the effect of Morse parameter ρ	33
2-10	Graph of all potentials used	34
3-1	Four sample nearest neighbor Ar locations for ground state Na	37
3-2	Orthogonal views of a sample ground state Na with nearest neighbor Ar atoms	38
3-3	Computed absorption spectrum using Saxon potentials	39
3-4	Computed absorption spectrum using Saxon $B^2\Sigma$ potential	41
3-5	Computed absorption spectrum using adjusted $B^2\Sigma$ potential	42
3-6	Computed absorption spectrum using Van Den Berg $B^2\Sigma$ potential	43

3-7	Computed absorption spectrum for Na surface site	45
3-8	Absorption and emission spectra using adjusted $B^2\Sigma$ potential	47
3-9	Emission spectrum using adjusted $B^2\Sigma$ potential	48
3-10	Uncorrected emission spectrum using adjusted $B^2\Sigma$ potential	49
3-11	Computed emission spectrum allowing all Ar atoms to move	53
3-12	Computed emission spectra allowing only Na atom to move	55

ABSTRACT

**ABSORPTION AND FLUORESCENCE SPECTRA OF SODIUM IN
AN ARGON MATRIX**

by

Alan B. Tutein
University of New Hampshire, May, 1997

A computer simulation of the formation of trapping sites for sodium atoms trapped in a solid argon matrix has been performed, using experimentally determined argon-argon and sodium-argon potentials available in the literature. The simulation method is a greatly simplified version of the more time-consuming molecular dynamics approach. Optical absorption and emission spectra corresponding to the matrix-perturbed 3s-3p sodium transition were calculated for each simulated trapping site, using first-order perturbation theory and the available sodium-argon dimer potentials. Two of the three requisite sodium-argon dimer potentials, the $X^2\Sigma$ and the $A^2\Pi$, have been determined experimentally, but for the $B^2\Sigma$ potential, only a theoretical calculation is available. The computer simulation produced only one type of trapping site, and a simple, one-parameter adjustment of the theoretical $B^2\Sigma$ potential brought the calculated absorption and emission spectra into good agreement with the absorption and emission observed for the dominant, thermally stable trapping site produced in experiments. This agreement was unique, in the sense that no adjustment of the $B^2\Sigma$ potential could reproduce the observed absorption and emission spectra for the relatively unstable or less probable trapping site formed in experiments.

Chapter 1

Introduction

A number of attempts have been made to understand the observed electronic spectra of an alkali atom trapped in a rare gas matrix in terms of model sites and known rare gas-rare gas and alkali-rare gas dimer potentials [1-7]. The presence of a single valence electron makes the alkali atom a good candidate for calculations of electronic structure in clusters and rare-gas solids. In addition, a large number of experiments examining the absorption and emission spectra of alkali atoms trapped in rare-gas solids have been performed [6, 8-23]. Most experiments involving a matrix isolated alkali atom have determined absorption and emission spectra corresponding to the transitions between the ground and first excited electronic states. These are also the states for which experimental dimer potentials are available. The purpose of this work was to generate possible matrix trapping sites by creating a computer simulation of the site formation. This simulation used existing experimental dimer potentials. For these simulated sites we have calculated the absorption and emission spectra and compared this with experimental data. We have chosen to simulate sites for sodium trapped in an argon matrix because this is the system for which two of the three requisite experimental Na-Ar [24-29] dimer potentials are available. Experimental dimer potentials are available for the Ar-Ar [30] ground state, the Na-Ar ground state, and one of

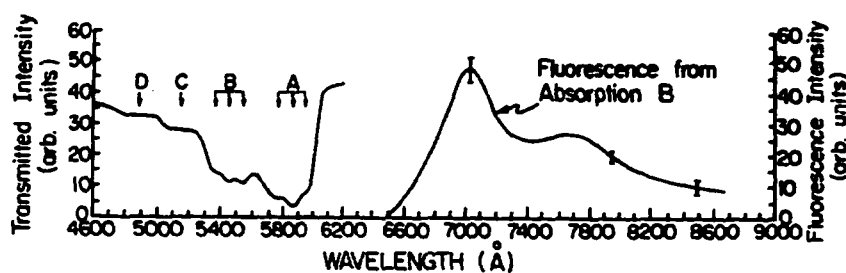


Figure 1-1: Experimental absorption and blue site fluorescence of Na in Ar. The left hand curve shows the transmitted intensity as a function of wavelength for Na atoms trapped in an Ar solid at 10 K [11]. Triplets are labeled A (Red) and B (Blue). Other absorption features (C and D) are also seen. The right hand curve shows the fluorescence intensity as a function of wavelength with the exciting laser tuned to the region of the B triplet.

the Na*-Ar excited states ($A^2\Pi$). For the other excited state potential ($B^2\Sigma$) we rely on a theoretical calculation as our starting point. These dimer potentials will be dealt with further in section 2.4.

The results from one of these experiments performed by Balling and Wright [11] are shown in figure 1-1. The left hand curve gives the transmitted intensity as a function of wavelength. The absorption features are labeled A through D; A and B are more often designated the “red triplet” and “blue triplet” respectively. The features labeled C and D represent other observed absorptions. More recent experiments by Tam and Fajardo [22] have shown C to be a triplet. Numerical values for the absorption peaks of sodium in an argon matrix at 10 K are given in table 1.1. This triplet structure is observed for both alkali and alkaline earth (groups I and II) atoms embedded in rare-gas solids. We note that the A and B triplets occur near and slightly blue-shifted respectively from the free sodium D lines (5890 Å and 5896 Å [31]). For this reason these absorption triplets are associated with transitions from the sodium $S_{1/2}$ to the first excited $P_{3/2,1/2}$ states. These free sodium states are perturbed by the presence of the argon matrix. The different triplets are believed to correspond to

absorptions from different sodium trapping sites, or local geometries. As can be seen in the right hand column of table 1.1, the B site is more thermally stable than the A site. The

Band	Absorption peak (\AA) [11]	Disappearance Temp.(K) [22]
A (Red)	5945 (20)	20
	5875 (20)	
	5775 (20)	
B (Blue)	5540 (10)	45
	5450 (10)	
	5360 (10)	
C(Violet)	5145 (15)	35
D	4880 (60)	45

Table 1.1: Experimental absorption peaks of Na atoms trapped in Ar matrices at 10K [11]. The numbers in parentheses are the experimental uncertainties. The right hand column gives the temperature above which these triplets are no longer observed [22].

observed absorptions labeled B disappear at 45 K while those labeled A disappear at a much lower temperature of 20 K (for reference the melting temperature of an argon matrix is 83.8 K [32]).

The right hand curve of figure 1-1 shows the fluorescence intensity as a function of wavelength after excitation with a laser tuned to the region of the thermally stable B triplet. The fluorescence is strongly red shifted compared with the free sodium lines. The fluorescence spectrum also shows a previously unexplained dual peak structure.

The method we used to generate the simulated matrix trapping sites will be dealt with in section 2.1. The calculation of the matrix perturbed sodium 3p states will be dealt with in section 2.2. The determination of the absorption and emission spectra from the calculated matrix trapping sites will be shown in section 2.3. The results of the perturbed 3s-3p absorp-

tion calculation, including the characterization of the matrix trapping site will be presented and discussed in chapter 3. The emission calculation results are also discussed and compared with experiment in chapter 3.

Chapter 2

Method

2.1 Simulating the matrix trapping site

In this section we present the method used to simulate the matrix trapping site with the sodium atom in its ground state. The method can be summarized as a greatly simplified semi-classical molecular dynamics simulation. In a semi-classical molecular dynamics approach, as in our work, the Born-Oppenheimer approximation [33] is used to separate electronic and nuclear motion. The nuclear motion is then solved for using classical dynamics. Typically, in a semi-classical molecular dynamics simulation, very small time steps are chosen such that the distance an individual atom travels in one time step is small. The complete details of the trajectory are then obtained by integrating the equations of motion. Since, in this work, we believe we do not need the full history of the atoms but only the minimum energy configuration, we do not require a full dynamics calculation. Because of the large reduction in computational overhead, we are able to deal with much larger clusters than could be treated using a full dynamics calculation.

We first address the calculation of the total energy of the sodium-argon cluster with the sodium in its ground state. For the alkali in its ground state, both the alkali electronic

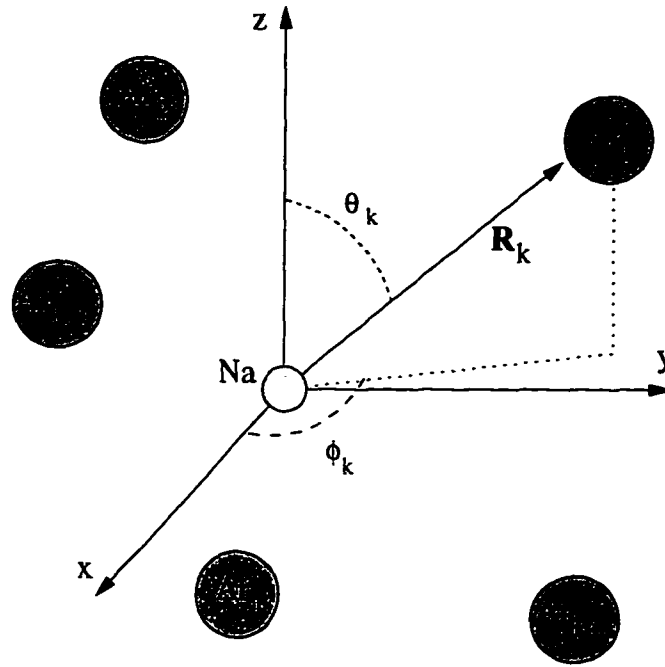


Figure 2-1: NaAr_n coordinate system used.

state and the rare-gas states have spherical symmetry and their interaction energy can be approximated as a pairwise sum over the ground state dimer potentials [34]. That is, with the alkali defined as the origin of the system, the total interaction energy is given as

$$V(\mathbf{R}_1, \mathbf{R}_2, \dots, \mathbf{R}_N) = \sum_{k=1}^N V_{X-RG}(|\mathbf{R}_k|) + \sum_{i=1}^N \sum_{j=i+1}^N V_{RG-RG}(|\mathbf{R}_i - \mathbf{R}_j|) \quad (2.1)$$

where V_{X-RG} is the $X^2\Sigma$ interaction of the ground state alkali atom with the rare-gas atoms, V_{RG-RG} is the interaction between rare-gas atoms, and \mathbf{R}_k is the vector to the k^{th} rare gas atom (figure 2-1). To determine the potential energy of a single atom we calculate that atom's portion of the total energy. For the sodium atom this is just the first sum in Equation (2.1).

For the k^{th} rare gas atom, the potential energy of that atom, V_k , is

$$V_k = V_{X-RG}(|\mathbf{R}_k|) + \sum_{i \neq k} V_{RG-RG}(|\mathbf{R}_i - \mathbf{R}_k|) \quad (2.2)$$

With this definition of the total interaction energy and the interaction of each atom in terms of the available sodium-rare gas and rare gas-rare gas dimer potentials, we can now describe our method of generating matrix trapping sites. For the results presented we started with a large, amorphous sphere of two hundred argon atoms with randomly chosen coordinates surrounding a central ground state sodium atom. This number of argon atoms represents between two and three atomic layers surrounding the sodium atom. This cluster size is a tradeoff between run time and the number of atomic layers. With this number of argon atoms, typical CPU times on an SGI Indigo2 were between 15 and 25 minutes and 1.5 to 2.5 hours on a Pentium 100MHz running Linux. The radius of the sphere used was about 15 Å. We found that any method which completely surrounded the sodium atom with argon atoms, that is, did not allow the sodium atom to be squeezed out, gave essentially the same results as our random sphere method. Any method where the sodium was not completely surrounded from the outset resulted in the sodium atom being squeezed out of the cluster for almost every run. This is because of the relative strengths of the sodium-argon and argon-argon interactions (see section 2.4). The sodium-argon interaction is smaller than the argon-argon interaction. Requiring the total cluster energy to be a minimum requires the sodium atom to be on the surface of the cluster. This will be discussed further in chapter 3 and results for the sodium atom on the surface of the cluster will be presented.

Our own simplification of a semi-classical molecular dynamics simulation was used. It can

also be considered a variation of the steepest descent method [35]. Our method was chosen because of its intuitive origin in classical mechanics. We start with the relationship between acceleration, \mathbf{a} , potential energy, V , and mass m , $\mathbf{a} = -\nabla V/m$. Given this relationship, for an atom with velocity $\dot{\mathbf{r}}_0 = \mathbf{0}$, and initial location \mathbf{r}_0 its position some time δt later is given as [36]

$$\mathbf{r}(\delta t) = \mathbf{r}_0 - \frac{1}{2} \left(\frac{\nabla V}{m} \right) \delta t^2 \quad (2.3)$$

This is essentially how a semi-classical molecular dynamics simulation would evolve at short times. For later times, the velocity would be non-zero and the equations of motion would have to be integrated to find the actual trajectory, adding computational complexity and time.

Because we are only interested in the final equilibrium positions and do not need information on the full path of the atom, we do not solve the full dynamics problem. Instead, we choose a maximum distance δr an atom is allowed to move. The atom that will move that distance, δr , in the minimum time is the one with the largest acceleration, $|\mathbf{a}|_{max} = \left| \frac{\nabla V}{m} \right|_{max}$. From Equation (2.3), this minimum time satisfies

$$\frac{1}{2} \delta t^2 = \frac{\delta r}{|\mathbf{a}|_{max}}$$

Substituting this into Equation (2.3) as our time step, steps are taken according to the following

$$\mathbf{r}_k(n+1) = \mathbf{r}_k(n) - \frac{\delta r}{|\mathbf{a}|_{max}} \cdot \frac{\nabla_k V_k}{m_k} \quad (2.4)$$

where δr is the maximum step size allowed for any single atom, V_k and m_k are the potential (Equation (2.2)) and mass respectively of the k^{th} atom, and n denotes the step number.

Only the atom with the largest acceleration will step δr , with all others stepping less. The determination of $|\mathbf{a}|_{\max}$ is performed at each step in the program. Thus each step represents a different elapsed time. We have denoted the coordinates with a lower case \mathbf{r} to indicate that this formula applies equally to sodium and argon atoms; that is, all atoms are allowed to move. This is another feature of this work. When generating the ground state cluster, no assumptions are made as to which atoms should move.

The maximum step size is started at a few Ångstrom and a trial step is taken. A trial step consists of moving all atoms, including the sodium atom, simultaneously. Each atom moves a distance given by Equation (2.4). If the total energy of the new cluster is lower than the previous energy, the step is kept and another step of that size is taken. If the energy increases, the step size is reduced by half and the trial step taken again. The procedure terminates either when 4000 steps have been taken or the step size is reduced below 0.001Å . The typical number of steps needed to find a minimum was 400 to 1600 steps. The minimum step size was chosen because it is half of the stated error in the best-known potential [26]. Any variation smaller than 0.001Å should affect the results less than errors in the potentials. Once a local minimum has been found each argon atom in the cluster is displaced a random distance between 0 and 1Å in a random direction. The sodium atom is excluded from this randomization because it was found that allowing the sodium atom to be randomly displaced might allow it to work its way to the surface of the cluster. After this randomization process, the minimization process is repeated and if a lower minimum is found it is kept; otherwise the randomization is repeated again. If the minimum energy structure does not change after three tries, the program is halted.

The program resulted in consistent formation of roughly spherical sites for sodium trapped

in our computer generated argon cluster. These results will be discussed further in chapter 3.

Before proceeding with any other calculations we needed to verify that our minimization procedure described above was giving reasonable results. To do this, several test cases, described in the following paragraphs, were run.

The easiest check to perform was to see if the program could correctly generate pure rare gas clusters. Several clusters containing only a few argon atoms were calculated. The structures associated with the local minima of these clusters followed closest packing, that is the atoms pack as spheres that are packed together as densely as possible. The overall interaction energies of several pure rare clusters generated by this program are compared with published results in table 2.1. The energy is given in normalized units, where all energies are divided by the magnitude of the argon-argon dimer potential well depth (99.554 cm^{-1} [30]). As can be seen, the results agree almost exactly. Generation of this table required several trials to find the global minimum due to the large number of local minima and the fact that our program is not designed to find the global minimum but only low lying local minima. The most well known structure consisting of pure argon is the Ar_{13} cluster. This icosahedral cluster demonstrates what is meant by closest packing. The high symmetry Ar_{13} cluster generated by our program is shown in figure 2-2. This near perfect agreement indicates that our program works well for pure argon clusters. The program generates clusters whose shape makes sense and whose energies and structures match work done by others.

Next we need to verify that the program works if all atoms are not identical. We expect closest packing of any argon atoms with the sodium atom residing on the outside. This is because the sodium-argon interaction energy is smaller than the argon-argon interaction energy (see section 2.4). Thus to minimize the total energy, the argon atoms will have

n	Reference Energy	Program Energy
8	-19.822	-19.821
9	-24.113	-24.113
10	-28.423	-28.422
11	-32.766	-32.766
12	-37.968	-37.968
13	-44.327	-44.327
14	-47.845	-47.845
15	-52.323	-52.323
16	-56.816	-56.816
17	-61.318	-61.318
18	-66.531	-66.531
19	-72.660	-72.660
20	-77.177	-77.177

Table 2.1: Ar_n cluster energies for $n = 8 \dots 20$ compared with results from ref. 37. Energy is given in normalized units.

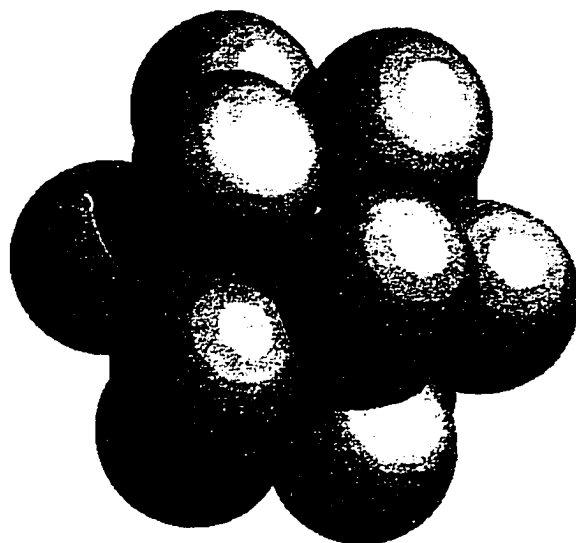


Figure 2-2: Ar_{13} cluster

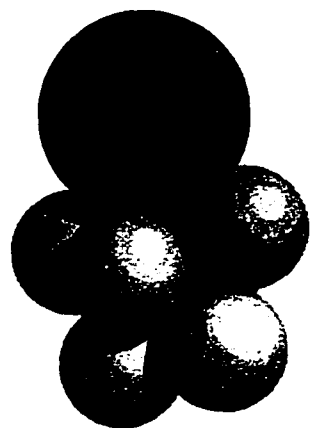
the maximum number of argon neighbors—the sodium will be outside a pure argon cluster. To check our calculation of a ground state sodium atom with several nearby argon atoms we compared the lowest four isomers of NaAr_6 to those found in the work of Tsouo *et al.* [3]. There is qualitative structural agreement between our work and that of Tsouo *et al.* Comparison of energies is not possible as their calculation of the interaction with the sodium relies on a different formulation of the interactions between sodium and argon and the argon-argon potential used was the Lennard-Jones approximation (we used the more accurate Aziz potential for this particular calculation—see section 2.4). We did however obtain energy trends that agreed with their results. See figure 2-3 for a summary of our results. These results were compared with figure 11 of Tsouo *et al.* These results led us to believe that our calculation of small clusters consisting of a single ground state sodium atom and multiple argon atoms was correct.

2.2 Calculating the Excited State Energies

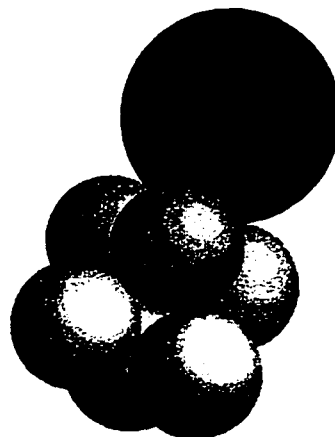
We wish to calculate the energy levels of an excited state alkali atom interacting with nearby rare gas atoms for our computer generated sites. The effect of a collection of rare gas atoms in perturbing the free alkali is considered for the sodium atom in its first excited state. The simplified dimer case is considered and it is shown how known dimer potentials can be used to approximate the solution for a large number of rare gas atoms.

2.2.1 An alkali in a rare gas matrix

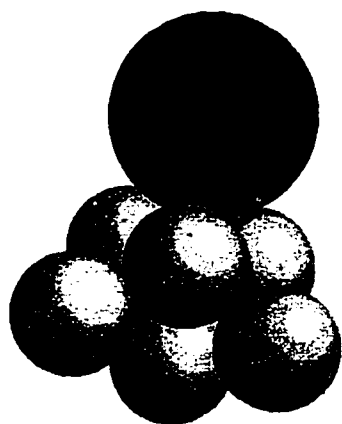
Consider a sodium atom, taken to be at the origin, with a valence electron e located at \mathbf{r} and N fixed argon atoms at positions $\mathbf{R}_1, \mathbf{R}_2, \dots, \mathbf{R}_N$ (figure 2-4).



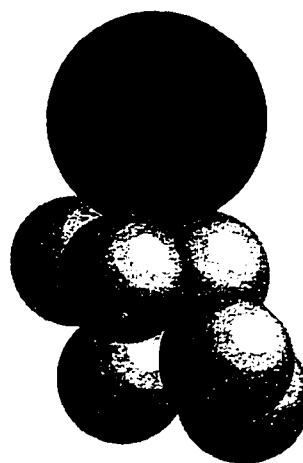
(a) a_1 (-1389 cm^{-1})



(b) b_1 (-1385 cm^{-1})



(c) c_1 (-1357 cm^{-1})



(d) d_1 (-1352 cm^{-1})

Figure 2-3: $\text{Na}(3\text{S})\text{Ar}_6$ isomers. Note that the labeling is that of reference 3.

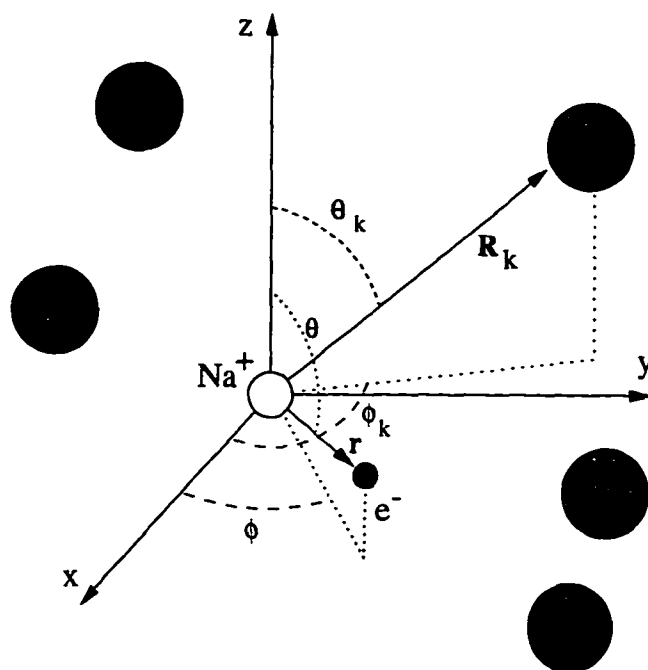


Figure 2-4: Na^+Ar_n coordinate system used.

We wish to calculate the electronic energy levels of the alkali atom valence electron, perturbed by the argon neighbors. We make the approximation that the electronic energy levels do not depend on the rare gas-rare gas interactions.

We limit the Hamiltonian of the perturbed alkali valence electron to

$$H = H_A + V_{A-RG_N}(\mathbf{r}; \mathbf{R}_1, \mathbf{R}_2, \dots, \mathbf{R}_N)$$

where H_A is the free alkali Hamiltonian and V_{A-RG} is the interaction of the alkali atom (core plus electron) with the rare gas atoms. The spin-orbit correction is often included but for sodium in argon is only a few wavenumbers [38]. It has also been assumed that the rare gas-rare gas interaction is independent of the valence electron location and that the electronic

energy levels also do not depend on the rare gas-rare gas interactions. The rare gas-rare gas interactions will be added later when calculating the total cluster energy.

We now examine the experimental results to estimate the order of magnitude of the effect of the matrix. The free atom transition energy weighted by the transition probability is $16,968 \text{ cm}^{-1}$ [31]. Of the triplet absorptions (sites A and B in figure 1-1), the transition energies observed in matrix isolated sodium vary between $16,821$ and $18,657 \text{ cm}^{-1}$ [11]. The maximum difference in energy introduced by the matrix is about ten percent of the free atom energy. For this reason, the new term in the Hamiltonian can be considered to be a perturbation of the free alkali Hamiltonian.

The ground state is non-degenerate and consists only of the alkali ground state wavefunction $|ns\rangle$ ($|n, l = 0, m = 0\rangle$). The expectation value of the energy in this state (ie. $\langle ns|H|ns\rangle$) is simply

$$E(\mathbf{R}_1, \mathbf{R}_2, \dots, \mathbf{R}_N) = E_{ns}^{(0)} + \sum_{k=1}^N \langle n, s | V_{A-RG}(\mathbf{r}; \mathbf{R}_k) | n, s \rangle$$

where $E_{ns}^{(0)}$ is the unperturbed ground state energy of the free alkali atom. This is Equation (2.1) without the rare gas-rare gas interaction. In that equation the unperturbed ground state energy, $E_{ns}^{(0)}$, is defined to be zero.

For states with $l \neq 0$, following standard degenerate perturbation methods (see for example Merzbacher [39]), the first order correction to the energy is the solution of

$$\det |V_{lm_i, lm_j} - E_{nlr}^{(1)} \delta_{m_i, m_j}| = 0$$

$E_{nlr}^{(1)}$ is the first order correction to the free alkali energy, $E_{nl}^{(0)}$, with r an index denoting the (possibly) split energies. V_{lm_i, lm_j} is defined as

$$V_{ij} \equiv \langle \Psi_{nlm_i}^{(0)} | V_{A-RG} | \Psi_{nlm_j}^{(0)} \rangle \quad (2.5)$$

Since this work deals only with transitions which have the same n and are not degenerate in l , a more concise notation is used

$$\det | V_{ij} - E^{(1)} \delta_{ij} | = 0 \quad (2.6)$$

The solutions to this equation give the first order corrections to the free alkali energies.

We now need to calculate the term V_{ij} in equations 2.5 and 2.6. It is well established that the potential energy of an excited alkali atom interacting with many nearby rare gas atoms is not simply the sum of the dimer interactions [40]. Baylis [34, 41] was the first to present a theoretical model for the interaction of an alkali atom in both the ground and excited state with several rare gas atoms. What follows is based on that work.

Consider the interaction of the alkali atom with the k^{th} rare gas atom, $V(\mathbf{r}, \mathbf{R}_k)$. The potential, $V(\mathbf{r}, \mathbf{R}_k)$, can be expanded in Legendre polynomials

$$V_{A-RG}(\mathbf{r}, \mathbf{R}_k) = \sum_L V_L(r, R_k) P_L(\hat{\mathbf{r}} \cdot \hat{\mathbf{R}}_k) \quad (2.7)$$

For now, the V_L can be considered coefficients of expansion. They will later be related to the experimental dimer potentials found in the literature.

Using this expansion we get

$$\begin{aligned}
 V_{ij} &= \sum_k \langle n, l = 1, m_i | V_{A-RG}(\mathbf{r}, \mathbf{R}_k) | n, l = 1, m_j \rangle \\
 &= \sum_L \sum_k \langle n, l = 1 | V_L(r, \mathbf{R}_k) | n, l = 1 \rangle \langle l = 1, m_i | P_L(\hat{\mathbf{r}} \cdot \hat{\mathbf{R}}_k) | l = 1, m_j \rangle \quad (2.8)
 \end{aligned}$$

As shown in Appendix C, the only allowed values of L are 0 and 2. It is shown in Appendix C that for the p state alkali, the angular dependent portion of Equation (2.8) ($L = 2$) can be expressed as

$$\langle m_i | P_2(\hat{\mathbf{r}} \cdot \hat{\mathbf{R}}_k) | m_j \rangle = \frac{4\pi}{5} \sum_{M=-2}^2 Y_{2,M}^*(\Omega_k) (-1)^{m_i} \sqrt{\frac{3}{2\pi}} \begin{pmatrix} 1 & 2 & 1 \\ m_j & M & -m_i \end{pmatrix}$$

Also shown in Appendix C is the calculation of the individual matrix elements V_{ij} . The final result for the p state alkali is

$$\begin{aligned}
 \mathbf{V} &= \sum_k V_0(R_k) \mathbf{I} + \frac{1}{10} \sum_k V_2(R_k) \times \quad (2.9) \\
 &\begin{bmatrix} -(3 \cos^2 \theta_k - 1) & -3\sqrt{2} \sin \theta_k \cos \theta_k e^{-i\phi_k} & -3 \sin^2 \theta_k e^{-2i\phi_k} \\ -3\sqrt{2} \sin \theta_k \cos \theta_k e^{i\phi_k} & 2(3 \cos^2 \theta_k - 1) & 3\sqrt{2} \sin \theta_k \cos \theta_k e^{-i\phi_k} \\ -3 \sin^2 \theta_k e^{2i\phi_k} & 3\sqrt{2} \sin \theta_k \cos \theta_k e^{i\phi_k} & -(3 \cos^2 \theta_k - 1) \end{bmatrix}
 \end{aligned}$$

where \mathbf{I} is the unit matrix and we have defined

$$V_0(R_k) = \langle nl | V_0(r, R_k) | nl \rangle$$

$$V_2(R_k) = \langle nl | V_2(r, R_k) | nl \rangle$$

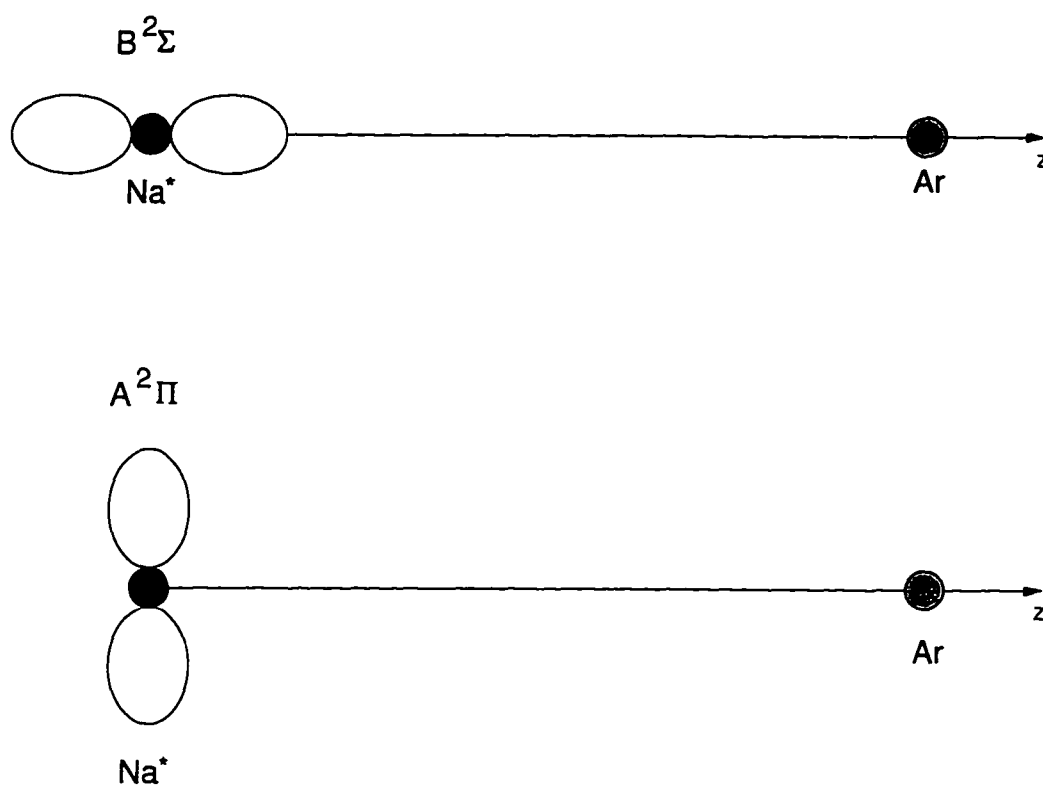
We note that in obtaining the matrix in Equation (2.9) the standard ordering for the magnetic quantum number has been assumed (1, 0, -1). Thus the upper left element corresponds to $m_i = m_j = 1$, the top row middle column to $m_i = 1, m_j = 0$, etc.

The relation between the coefficients of expansion, $V_L(r, R_k)$, and dimer potentials found in the experimental and theoretical literature must be established.

Consider a dimer consisting of one alkali atom and one rare gas atom. In Equation (2.9) any system of coordinate axes with the alkali defined as the origin can be chosen. A convenient choice for the quantization axis (z axis) is the interatomic axis. With this choice $\theta_k = 0$ and Equation (2.9) becomes

$$\mathbf{V} = \begin{bmatrix} V_0(R_k) - \frac{1}{5}V_2(R_k) & 0 & 0 \\ 0 & V_0(R_k) + \frac{2}{5}V_2(R_k) & 0 \\ 0 & 0 & V_0(R_k) - \frac{1}{5}V_2(R_k) \end{bmatrix} \quad (2.10)$$

We note that we end up with three energies, two of which are degenerate ($m_i = m_j = \pm 1$). Because of this degeneracy the electronic terms of the dimer are classified according to the absolute value of the projection of the orbital angular momentum along the quantization axis. This quantity is denoted $\Lambda (= |M_L|)$ and the terms are labeled according to the scheme $^{2S+1}\Lambda$. Note that the use of capital letters denotes the multiatom system. Because rare gas atoms are spherical, $l_{RG} = 0$. For this reason $M_L = m_l$ and $\Lambda = |m_l|$. Following the electronic term convention $\Lambda = 0$ is denoted Σ with the term being $B^2\Sigma$ while $\Lambda = 1$ is labeled $A^2\Pi$. A physical picture of the orientation of the atomic alkali orbital is given in figure 2-5.

Figure 2-5: Diagram of Σ and Π molecular orbitals

With this labeling in mind we see Equation (2.10) could also be written

$$\mathbf{V} = \begin{bmatrix} V_{A^2\Pi}(R_k) & 0 & 0 \\ 0 & V_{B^2\Sigma}(R_k) & 0 \\ 0 & 0 & V_{A^2\Pi}(R_k) \end{bmatrix} \quad (2.11)$$

Thus

$$V_{A^2\Pi} \equiv \langle \Psi_{n1\pm 1} | V_{A-RG} | \Psi_{n1\pm 1} \rangle = V_0 - \frac{1}{5}V_2$$

$$V_{B^2\Sigma} \equiv \langle \Psi_{n10} | V_{A-RG} | \Psi_{n10} \rangle = V_0 + \frac{2}{5}V_2$$

These two equations can be solved for V_0 and V_2 in terms of the dimer potentials.

$$V_0 = \frac{1}{3}(V_{B^2\Sigma} + 2V_{A^2\Pi})$$

$$V_2 = \frac{5}{3}(V_{B^2\Sigma} - V_{A^2\Pi})$$

With these two equations and Equation (2.9), we can solve the secular determinant (Equation (2.6)) for the first order correction to the free sodium energies given the experimental $A^2\Pi$ and $B^2\Sigma$ Na*-Ar dimer potentials.

We now have in place the tools to solve the secular determinant (Equation (2.6)) for the first order correction to the free alkali atom electronic energy. The three energies obtained give three electronic energy levels for the excited sodium atom interacting with the surrounding

argon atoms. For the excited state sodium atom the interaction energies are

$$E_i^*(\mathbf{R}_1, \mathbf{R}_2, \dots, \mathbf{R}_N) = E^{(0)} + E_i^{(1)}(\mathbf{R}_1, \mathbf{R}_2, \dots, \mathbf{R}_N) \quad (2.12)$$

where $E_i^{(1)}$ are the solutions to the secular determinant, with i an index denoting the three solutions. For the free sodium atom, the 3s-3p transition energy, $E^{(0)}$, is $16,968 \text{ cm}^{-1}$ [31].

There are several standard methods that can be used to solve for the eigenvectors and eigenvalues of this system. One is to write out the cubic equation and solve it directly. The resulting cubic is given as Equation (C.10). Another method is to use the Householder-Givens [35, 42] transform method in which a unitary transform that diagonalizes the matrix is calculated. This latter gives both the real roots and the complex coefficients of the corresponding eigenvectors. This is the method used because of the availability of the eigenvectors and its expandability if a larger basis set is required. It is also independent of the size of the matrix.

2.3 Calculating the Absorption and Emission spectra

2.3.1 Absorption

We now have in place the method for determining the matrix trapping site, its energy, and for calculating the electronic energy levels for the excited state alkali given the rare gas atom locations. It is now a simple matter to determine the absorption energies of these calculated clusters. We assume that the energies of the photons absorbed are given by the difference

between the excited state energies and the ground state energy.

$$\Delta E_i = E_i^*(\mathbf{R}_1, \mathbf{R}_2, \dots, \mathbf{R}_N) - E(\mathbf{R}_1, \mathbf{R}_2, \dots, \mathbf{R}_N) \quad (2.13)$$

where i is an index that denotes the three possible solutions in Equation (2.12). For convenience we order the energies from lowest to highest with the index, $i = 0 \dots 2$. Since there are three excited state levels there will be three (not necessarily unique) absorption energies.

2.3.2 Fluorescence

To determine the emission wavelength of the matrix isolated sodium we assume that the excited state system will relax to an energy minimum. The total interaction energy, $V^*(\mathbf{R}_1, \mathbf{R}_2, \dots, \mathbf{R}_N)$, is now given by the lowest excited state sodium energy obtained from Equation (2.12) plus the rare gas-rare gas interaction energy.

$$V^*(\mathbf{R}_1, \mathbf{R}_2, \dots, \mathbf{R}_N) = E_0^*(\mathbf{R}_1, \mathbf{R}_2, \dots, \mathbf{R}_N) + \sum_{i=1}^N \sum_{j=i+1}^N V_{RG-RG}(|\mathbf{R}_i - \mathbf{R}_j|) \quad (2.14)$$

We assume that the excited state lifetime is long compared to the relaxation time. This is a good assumption as typical excited state lifetimes are around 20ns [11] while molecular dynamics simulations indicate typical relaxation times are on the order of tens of picoseconds [7]. We have also assumed that following the lowest energy surface is sufficient to give the fluorescence. This is an intuitive assumption based on the expected excited state populations at thermodynamic equilibrium. Given the energy differences between the three absorption peaks, we can estimate the ratio of the populations of the middle state to the lowest state. Given typical experimental temperatures of 10 – 20K and energy differences of the order of

100 cm⁻¹ we obtain

$$\frac{E_{middle}}{E_{lowest}} \approx 10^{-4} - 10^{-7}$$

To further check this approach we examined the work of Krylov *et al.* [7]. They carried out a molecular dynamics calculation for barium in argon in which they followed each of the adiabatic energy surfaces. They allowed semi-classical “surface hopping” (hopping between energy surfaces) using the method of Tully [43], Kuntz [44], and more recently Jungwirth [45]. These results were also consistent with the assumption of thermodynamic equilibrium. As a check on our method and program we were able to reproduce their results and obtained extremely good agreement by only following the lowest energy state when calculating fluorescence.

There is one further complication that arises in our simulation. We have a limited cluster size. As discussed before, because of computational time considerations, we limit our simulation to 200 argon atoms. This gives us between two and three atomic layers surrounding the sodium. Starting with our computer generated matrix trapping sites and allowing the system to reach equilibrium with the sodium in the excited state, there is a drastic rearrangement of argon atoms in the cluster. In our model every atom in the cluster moved in response to the change in potential, corresponding to a liquification of our cluster. This is because there is no surrounding matrix to hold the argon atoms fixed. In the matrix environment such liquification is not realistic. The energy added during the optical transition should rapidly be distributed throughout the matrix. Only local argon atoms should rearrange, with the overall matrix remaining intact. To model this we froze every argon atom beyond the first set of nearest neighbors. The excited state sodium atom and the nearest argon atoms were

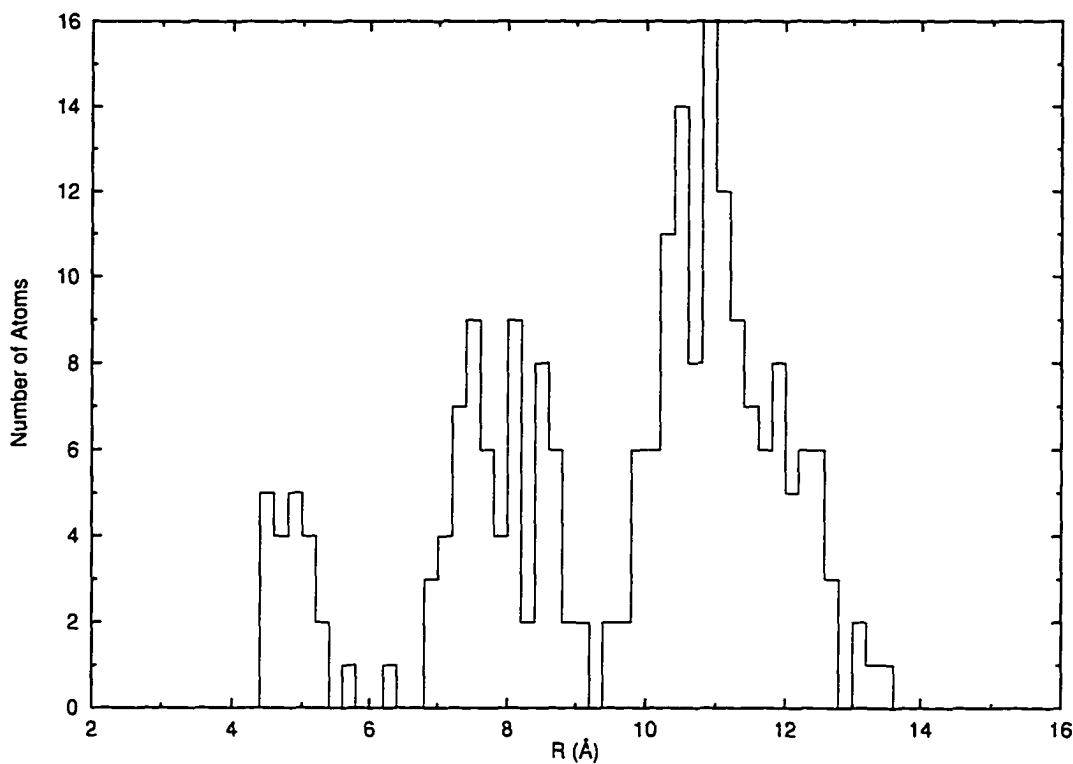


Figure 2-6: Histogram of the radial distribution of Ar atoms around the Na atom. The Ar atom distances from the Na atom are binned by 0.2 Å.

still allowed to move. Figure 2-6 shows a histogram of the argon atom locations relative to the ground state sodium for one of our computer generated matrix trapping sites. This figure shows that the first set of nearest neighbor atoms are spread out between roughly 4.3 Å and 5.5 Å but there is a clear lack of atoms at 6 Å. Thus, when calculating our trapping site with the sodium in its excited state we freeze every argon atom beyond 6 Å.

With the above limitations the relaxation procedure described in section 2.1 is repeated. However, in place of the $X^2\Sigma$ NaAr ground state potential used in Equations (2.4) and (2.1), the lowest Na*Ar energy surface given by Equation (2.12) is used. To obtain the gradient of the excited state surface needed in Equation (2.4) requires knowledge of the derivative of

the eigenvalues obtained by diagonalizing the matrix given by Equation (2.9). This problem is solved by use of the Hellman-Feynman theorem (see for example Merzbacher [39], pg 442). Given a complex Hermitian matrix \mathbf{V} (Equation (2.9) in our case), eigenvalues $E_i^{(1)}$ ($i = 0 \dots 2$), and their corresponding complex eigenvectors \mathbf{z}_i , we have the useful result

$$\frac{\partial E_i^{(1)}}{\partial (x_k)_j} = \mathbf{z}_i^\dagger \cdot \frac{\partial \mathbf{V}}{\partial (x_k)_j} \cdot \mathbf{z}_i \quad (2.15)$$

A short derivation of this equation is given in appendix B. This supports the decision to use the Householder-Givens transform which gives eigenvectors as well as eigenvalues. It is also possible to implicitly differentiate Equation (C.10) but this is error prone, more difficult to implement, and seems to be more subject to numerical roundoff errors. It is, however computationally much faster. An alternative method that others have used is to approximate the derivatives by moving each atom a small distance in each coordinate direction. This is several orders of magnitude slower than calculating the derivatives of the eigenvalues by either of the above methods.

No calculations of excited state $\text{Na}(3\text{P})\text{Ar}_n$ clusters are available to use as checks on our calculation of an excited state sodium interacting with many argon atoms. However, for small clusters, we can estimate the results. The special case of $\text{Na}(3\text{P})\text{Ar}_2$ has been done by Baylis [34]. In that work Baylis obtained an expression for the three energy levels as a function of the location of the two argon atoms. We found the following three electronic energy levels as a function of the Ar-Na-Ar angle, θ

$$V_0^*(R) = 2V_{A\Pi}(R) \quad (2.16)$$

$$V_{1,2}^*(R) = [V_{B\Sigma}(R) + V_{A\Pi}(R)] \pm [V_{B\Sigma}(R) - V_{A\Pi}(R)] \cos(\theta)$$

These expressions are identical to those of Baylis with the argon atoms assumed to be the same distance, R , from the sodium atom and to the same expression found in reference [46].

The expression for unequal NaAr distances is

$$\begin{aligned} V_0^*(R) &= V_{A\Pi}(R_1) + V_{A\Pi}(R_2) \\ V_{1,2}^*(R_1, R_2) &= \frac{1}{2} (a \pm \sqrt{b}) \end{aligned}$$

where

$$\begin{aligned} a &= \sum_{k=1}^2 [V_{B\Sigma}(R_k) + V_{A\Pi}(R_k)] \\ b &= \sum_{k=1}^2 [V_{B\Sigma}(R_k) - V_{A\Pi}(R_k)]^2 \\ &\quad + 2 [V_{B\Sigma}(R_1) - V_{A\Pi}(R_1)] [V_{B\Sigma}(R_2) - V_{A\Pi}(R_2)] \cos(\theta) \end{aligned}$$

This provided a numerical check on the program. Evaluating the above expressions for various values of R and θ and comparing these to the program results with the same values showed the program to be working.

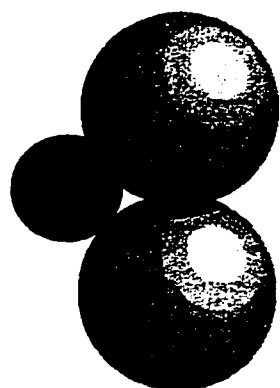
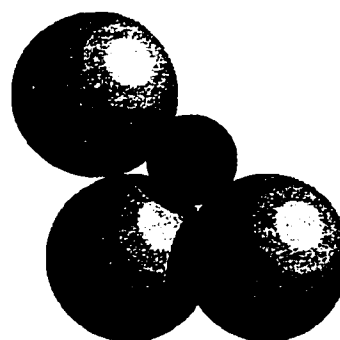
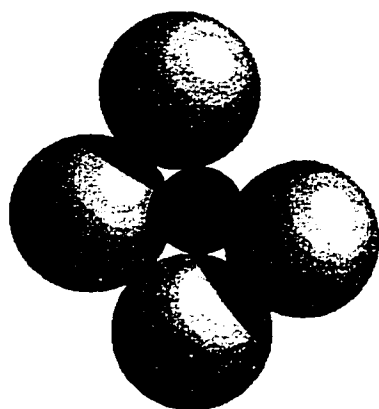
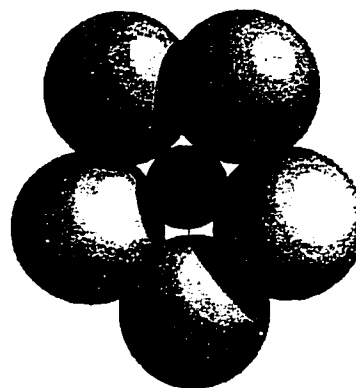
We note that $V_0^*(R)$ in Equation (2.17) is the lowest electronic energy solution for the relaxed atom case. The total energy of the Na^*Ar_2 system is

$$V_{min}^*(R, R_{ArAr}) = 2V_{A\Pi}(R) + V_{ArAr}(R_{ArAr}) \quad (2.17)$$

We would expect that for every argon atom added, the energetically preferred interaction is a Π type. Only a limited number of argon atoms can be added before we must consider the $B^2\Sigma$ interaction. Given the $A^2\Pi$ minimum location ($R_{Na^*Ar} = 2.907 \text{ \AA}$) and the ArAr minimum ($R_{ArAr} = 3.757 \text{ \AA}$) we can easily fit two argon atoms next to the excited state sodium. Both of these argon atoms will experience pure $A^2\Pi$ interactions. The distance between Ar_1 and Ar_2 should be the ArAr dimer distance and that between the sodium atom and the argon atoms should be the $A^2\Pi$ minimum distance. Thus the total energy should be twice the NaAr $A^2\Pi$ ($2 \cdot 563.4 \text{ cm}^{-1}$) energy plus the Ar-Ar interaction (99.6 cm^{-1}). This is exactly what is observed in the program test results and exactly what is expected from Equation (2.17). We expect (based on bond lengths) to be able to fit up to four argon atoms before we get non-additive effects. Once again this is observed in the test results. Thus for small excited state sodium-argon clusters with up to four argon atoms we obtain cluster energies which are the simply the sum of the Na*Ar $A^2\Pi$ and the ArAr interactions (purely additive) . Figure 2-7 shows these planar Na(3P)Ar_n clusters. The Π lobe is perpendicular to the plane of each cluster giving the lobe orientation pictured in figure 2-5 for each of the argon atoms. The Na(3P)Ar₅ cluster is still planar and all atoms experience pure $A^2\Pi$ interactions but the extra argon is “squeezed” in and no atoms are at their normal dimer distances: the Na*Ar distances are longer than for the Na*Ar dimer case and the ArAr distances are compressed compared with their dimer case.

Further checks of the whole system were done by hand calculating several excited state configurations. These calculations agreed exactly with the output of the program.

Further calculations of Na(3P)Ar_n for $n = 4, 5, 6, 7$ are presented in the preprint in appendix D. In all of the tests performed, the results were consistent with what was expected

(a) Na(3P)Ar₂(b) Na(3P)Ar₃(c) Na(3P)Ar₄(d) Na(3P)Ar₅Figure 2-7: Na(3P)Ar_n small cluster structures

and the conclusion was reached that the program performed both the ground and excited state calculations correctly.

Once the minimization procedure is completed we have a relaxed cluster consisting of an excited state sodium atom and many argon atoms. We once again assume a vertical transition. The fluorescence energy is given by the difference between the lowest excited state curve and the ground state as seen in Equation (2.13).

2.4 Potentials

2.4.1 Rare Gas-Rare Gas Interactions

Several potentials were used as input into the model. A Lennard-Jones approximation to the Ar-Ar potential [47] was used. One form of the Lennard-Jones (LJ) potential is

$$V_{LJ}(R) \equiv \epsilon \left[A \left(\frac{R_m}{R} \right)^n - B \left(\frac{R_m}{R} \right)^m \right]$$

with $A \equiv \frac{m}{n-m}$ and $B \equiv \frac{n}{n-m}$ (where $n > m$) and ϵ is the well depth at R_m , the well minimum. The form used for the Ar-Ar interaction is the LJ(12,6) which is

$$V_{LJ(12,6)}(R) = \epsilon \left[\left(\frac{R_m}{R} \right)^{12} - 2 \left(\frac{R_m}{R} \right)^6 \right]$$

A more accurate Ar-Ar potential form by Aziz *et al.* [30] was also used. The well depth of this Ar-Ar potential is $\epsilon = 99.738 \text{ cm}^{-1}$, and the minimum is $R_m = 3.7570 \text{ \AA}$. It was found that both Ar-Ar potentials gave essentially the same results. For the runs presented below the computationally simpler Lennard-Jones form was used, saving about a factor of two in

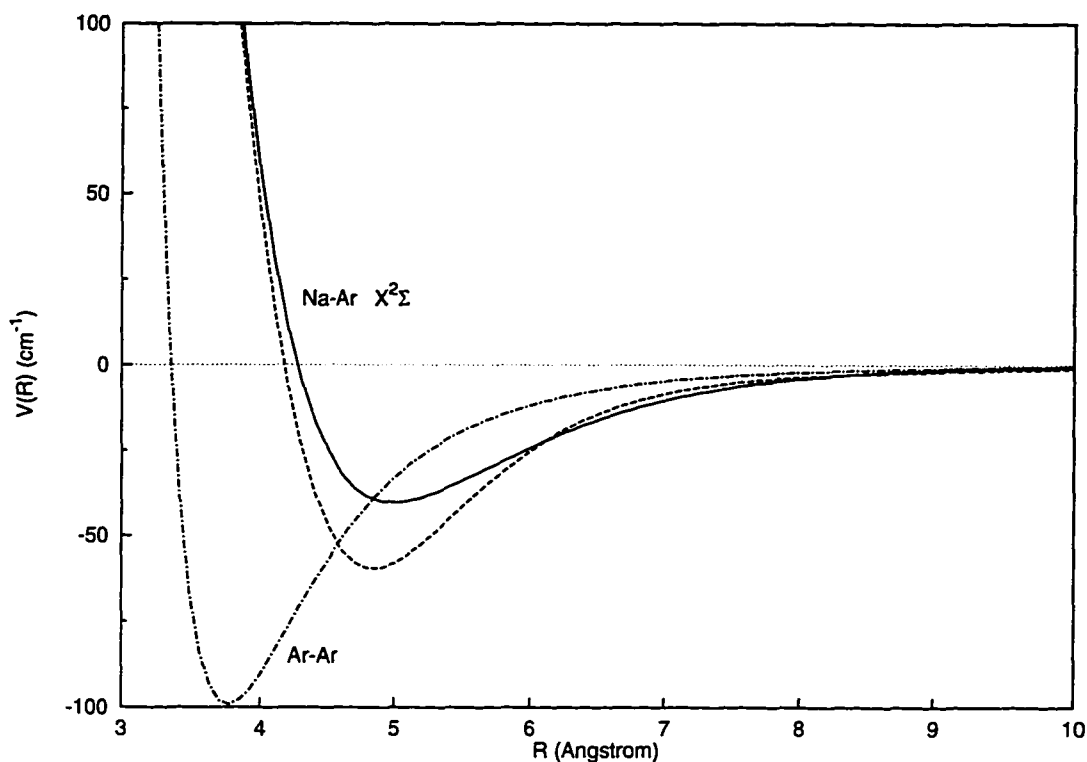


Figure 2-8: Ar-Ar and Na-Ar ground state potentials compared. The solid line represents the Na-Ar $X^2\Sigma$ dimer potential from ref. [26]. The dotted line represents the potential from ref. [25]. The dot-dash line is the Lennard Jones Ar-Ar dimer potential with parameters taken from ref. [30].

run time.

A short summary of the available sodium-argon potentials is given in table 2.2.

The Na-Ar $X^2\Sigma$ and $A^2\Pi$ dimer potentials used were taken from a spectroscopic determination by Tellinghuisen *et al.* [26]. A graph showing the argon-argon potential and the ground state sodium-argon dimer potentials used is given in figure 2-8.

To use the potentials of Tellinghuisen we needed an appropriate $B^2\Sigma$ dimer potential. Since there is no direct measurement of the shape of the $B^2\Sigma$ dimer potential and only a single measurement of its well location and depth from the experimental work of Van Den

Species	Source	$X^2\Sigma$	$A^2\Pi$	$B^2\Sigma$	Type
Na-Ar	24		✓		SLB
	25	✓	✓	✓	CI
	26	✓	✓		LS
	27	✓	✓	✓	CI
	28		✓	✓	PS
	29			✓	✓ [†]

Table 2.2: Sources for available Na-Ar dimer potentials

CI: *ab initio* configuration interaction

PS: Pseudopotential

SLB: Spectral Line Broadening

LS: high resolution laser spectroscopy

MB: Molecular Beam (†-only sensitive to well)

Berg [29], a Morse fit to the shape given by Saxon [25] was used as a starting point. The Morse potential is defined as [48]

$$V_{Morse}(R) \equiv \epsilon \left[e^{2\rho(1-\frac{R}{R_m})} - 2e^{\rho(1-\frac{R}{R_m})} \right] \quad (2.18)$$

where ϵ and R_m are the well depth and minimum respectively and ρ is called the Morse parameter and determines the shape of the potential. The Morse potential was chosen because it represents the most well-known three-parameter empirical dimer potential energy function [49]. An example of the effect of the Morse parameter is given in figure 2-9. Starting with the fit result of $\rho = 4.11$, the shape was adjusted until a single run of the program agreed with the experimental “Blue site” absorptions to within experimental error. The result was $\rho = 4.3$. This gives a slightly steeper wall than that of Saxon. The well depth, ϵ , and location, R_m , used were those of Saxon.

To see if the depth and minimum of the $B^2\Sigma$ potential obtained from Van Den Berg could

give results as good as the above, using the well depth and minimum of that work the shape was varied until once again the results closely match the experimental B site absorptions. It was found that for the trapping sites generated (which rely only on the $X^2\Sigma$ ground state Na-Ar dimer potential), no adjustment of the $B^2\Sigma$ potential could give absorptions in good agreement with the experimental A site absorptions. In addition, since our program finds the more thermally stable cluster formation (a local minimum), we would expect to find the thermally stable B site most or all of the time. It was found that with the well minimum at 6 Å (the upper limit of the error bars of Van Den Berg), the Morse parameter needed was $\rho = 5.5$, much steeper than that of Saxon. This result will be discussed in greater detail in section 3.2.

A convenient summary of the parameters used for the ground ($X^2\Sigma$) state Na-Ar dimer potential is given in table 2.3 and for the excited state dimer potentials ($A^2\Pi$ and $B^2\Sigma$) in table 2.4. These potentials are summarized and compared graphically in figure 2-10.

Designation [Source]	$X^2\Sigma$	
	ϵ (cm^{-1})	R_m (Å)
Best Potential [26]	40.4 ± 1.0	4.991 ± 0.002
Van Den Berg $B^2\Sigma$ [26]	40.4	4.991

Table 2.3: Ground state potential parameters used. Error is shown for information purposes only.

Designation [Source]	$A^2\Pi$			$B^2\Sigma$		
	ϵ (cm^{-1})	R_m (\AA)	ρ	ϵ (cm^{-1})	R_m (\AA)	ρ
Saxon [25]	492	2.91	NA	32.3	6.81	4.11†
Best Potential [25,26]††	563.4 ± 4.8	2.91 ± 0.05	5.29	32.3	6.81	4.3
Van Den Berg $B^2\Sigma$ [26,29]‡	563.4	2.91	5.29	30.7 ± 4.4	$5.50 \pm .53$	5.5

Table 2.4: Excited state potential parameters used. Error is shown for information purposes only.

†: Represents a force-fit to data given in [25]

††: $A^2\Pi$ from [26], $B^2\Sigma$ from [25] with ρ adjusted as described in text.

‡: $A^2\Pi$ from [26], $B^2\Sigma$ from [29] with ρ adjusted as described in text.

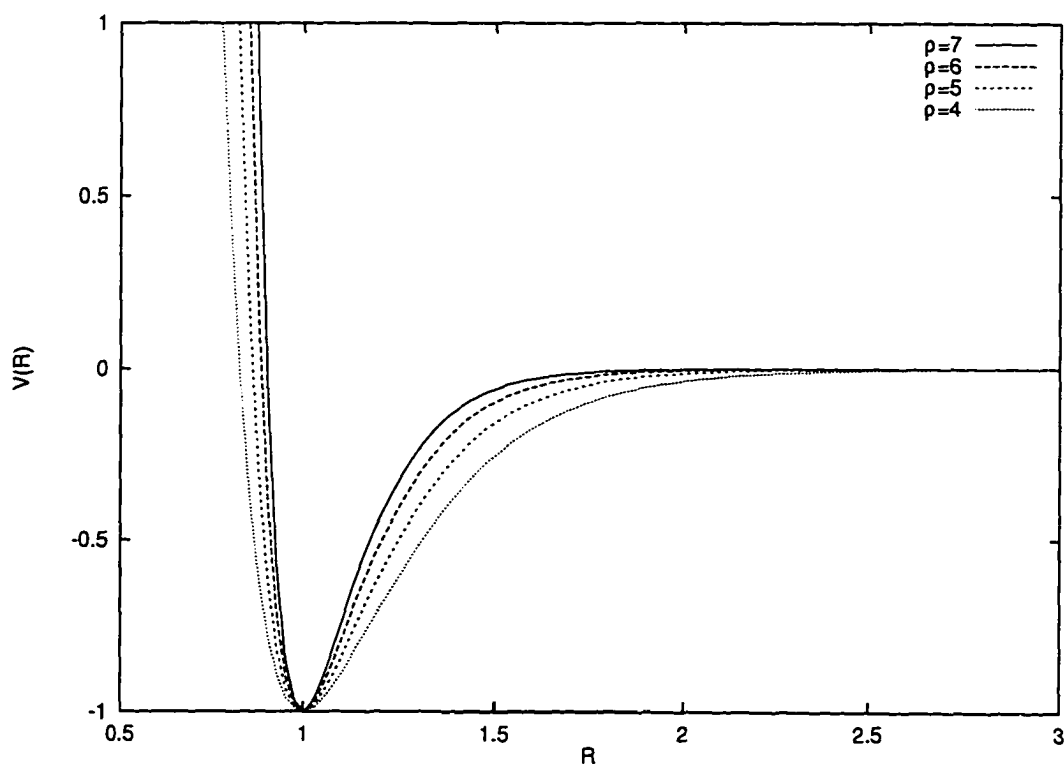


Figure 2-9: Graph of the standard Unit Morse Potential [48,49] showing effect of Morse parameter ρ

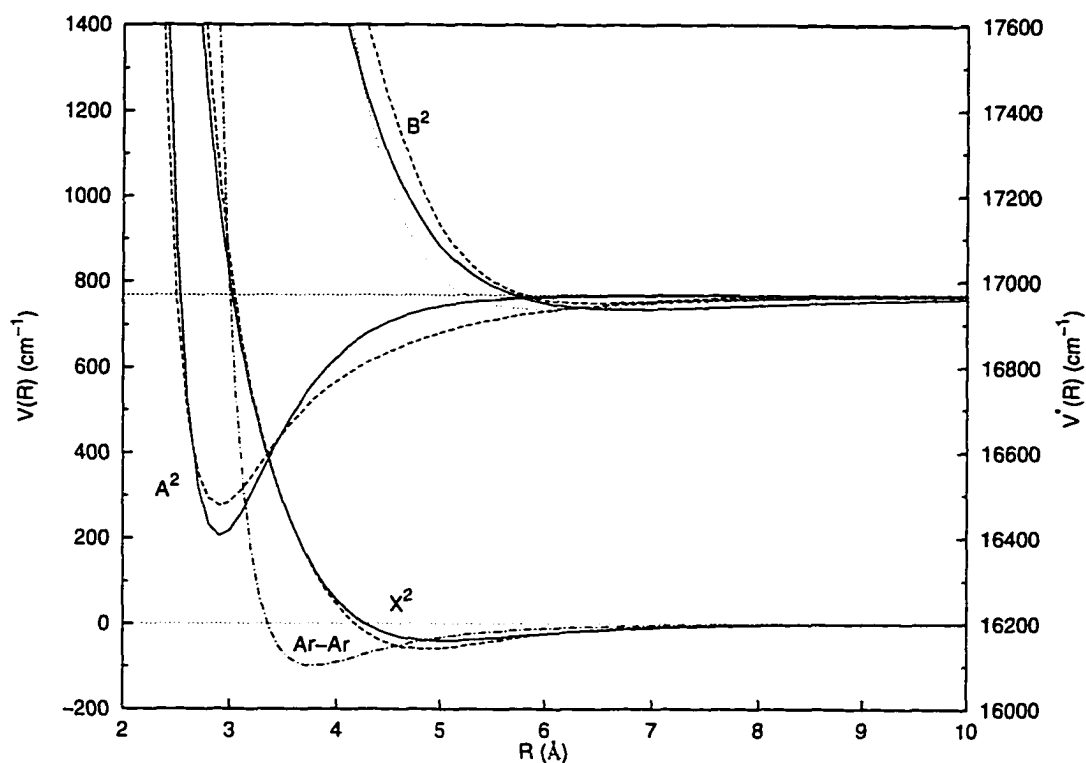


Figure 2-10: Graphical summary of all dimer potentials used. The solid line represents the Na-Ar $X^2\Sigma$ and Na*-Ar $A^2\Pi$ dimer potentials from ref. [26] with the Na*-Ar $B^2\Sigma$ dimer potential obtained as described in the text. The dotted line represents the set of potentials from ref. [25]. The dashed line for the $B^2\Sigma$ is an alternate version of the potential described in the text. The dot-dash line is the Lennard Jones Ar-Ar dimer potential with parameters taken from ref. [30].

Chapter 3

Results and Conclusions

3.1 Characterization of the simulated matrix trapping site

For each of the ground state sodium-argon potentials given previously in section 2.4, one hundred different trapping sites were generated. Later, a total of 1000 runs were performed using the Tellinghuisen $X^2\Sigma$ sodium-argon ground state dimer potential. In all runs the ground state trapping site was a roughly spherical site. We would expect this closest packing structure as both the Ar-Ar and Na-Ar ground state potentials are spherically symmetric. Deviations from a perfectly spherical site are due to the softness of the ground state Na-Ar potential well. To visually demonstrate the resulting site structure, space filled representations of the nearest neighbors from the first four runs using the Tellinghuisen $X^2\Sigma$ are shown in figure 3-1. We define the nearest neighbors as those which satisfy $R_k < 6 \text{ \AA}$. Figure 2-6 shows why this cutoff was chosen. It shows that the nearest neighbor atoms are spread out between roughly 4.3 \AA and 5.5 \AA but that there is a clear lack of atoms at 6 \AA .

The minimum of the ground state Na-Ar potential well is at 5.01 \AA . In the matrix the nearest neighbor argon atoms are located closer to the sodium atom than 5.01 \AA . This is because the Ar-Ar interaction is stronger and the large number of argon atoms tends to com-

press the sodium-argon distances. These nearest neighbor configurations shown in figure 3-1 demonstrate what is meant by roughly spherical. A further demonstration of this is shown in figure 3-2. In that figure a single computer generated ground state cluster is shown from all sides.

3.2 Absorption results

Given the computer simulated ground state trapping sites described in the previous section, the absorption of each individual simulated site was calculated. The absorption results are binned by wavelength and presented as histograms in figures 3-3, 3-4, 3-5, and 3-6. The absorption bin size is chosen to be 20 Å corresponding to the experimental error given by Balling *et al.* [11]. The dashed vertical lines on the left represent the experimental B site absorption peaks [11]. Also shown are the free sodium absorption lines (nearly overlapping vertical dotted lines) and the A site absorption peaks. The solid boxes are a histogram of the absorption wavelengths generated for this work.

Although not believed to be as accurate as experimentally derived potentials, the Saxon [25] sodium-argon dimer potentials are used in the literature. The most recent calculation [5] of a sodium atom in an argon matrix prior to this work uses the Saxon potential set. These potentials are used primarily because of the availability of the $B^2\Sigma$ potential and the belief that because all potentials are from one source they should be self-consistent—eliminating errors that potentials coming from several different, uncorrelated sources, might introduce. For this reason we also tried the full set of Saxon potentials. The calculated absorption results are shown in Figure 3-3. With the Saxon potentials, the largest simulated absorption

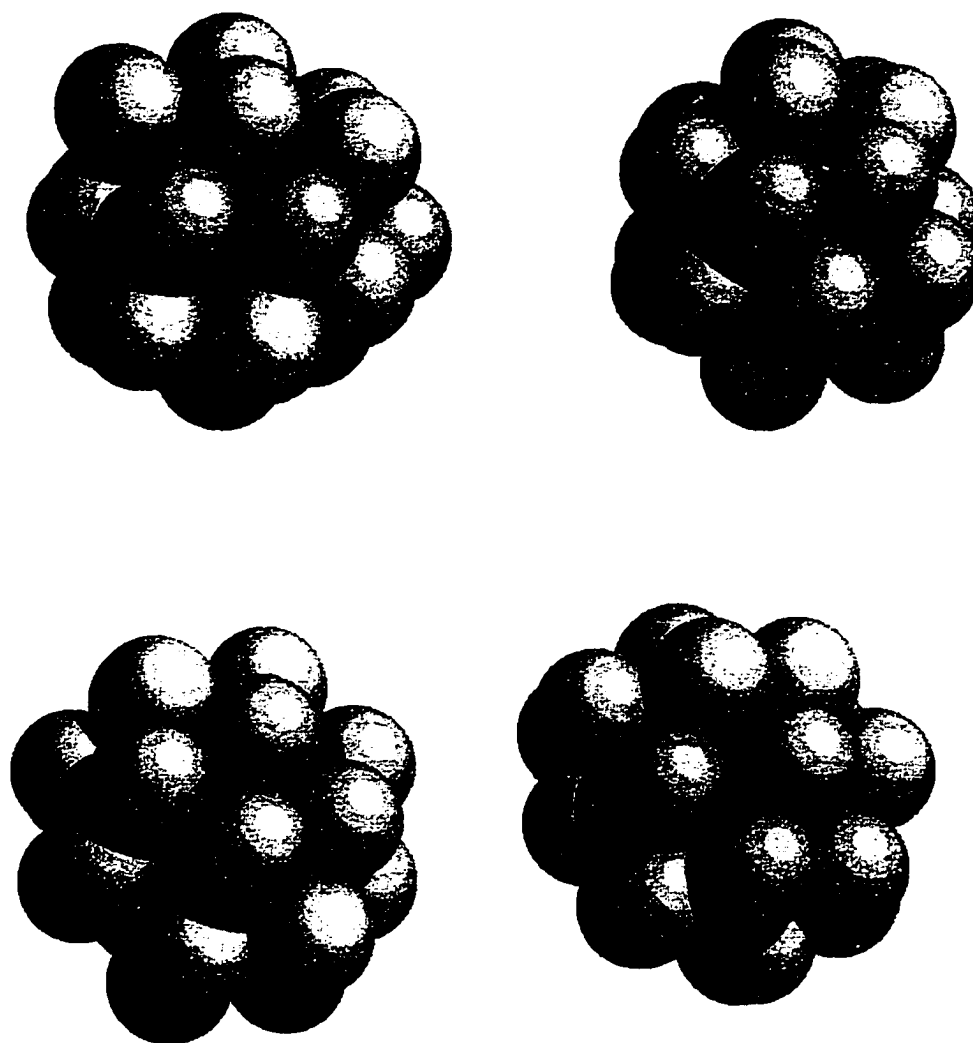


Figure 3-1: Four sample runs showing ground state Na with nearest neighbor Ar atoms ($R_k < 6 \text{ \AA}$).

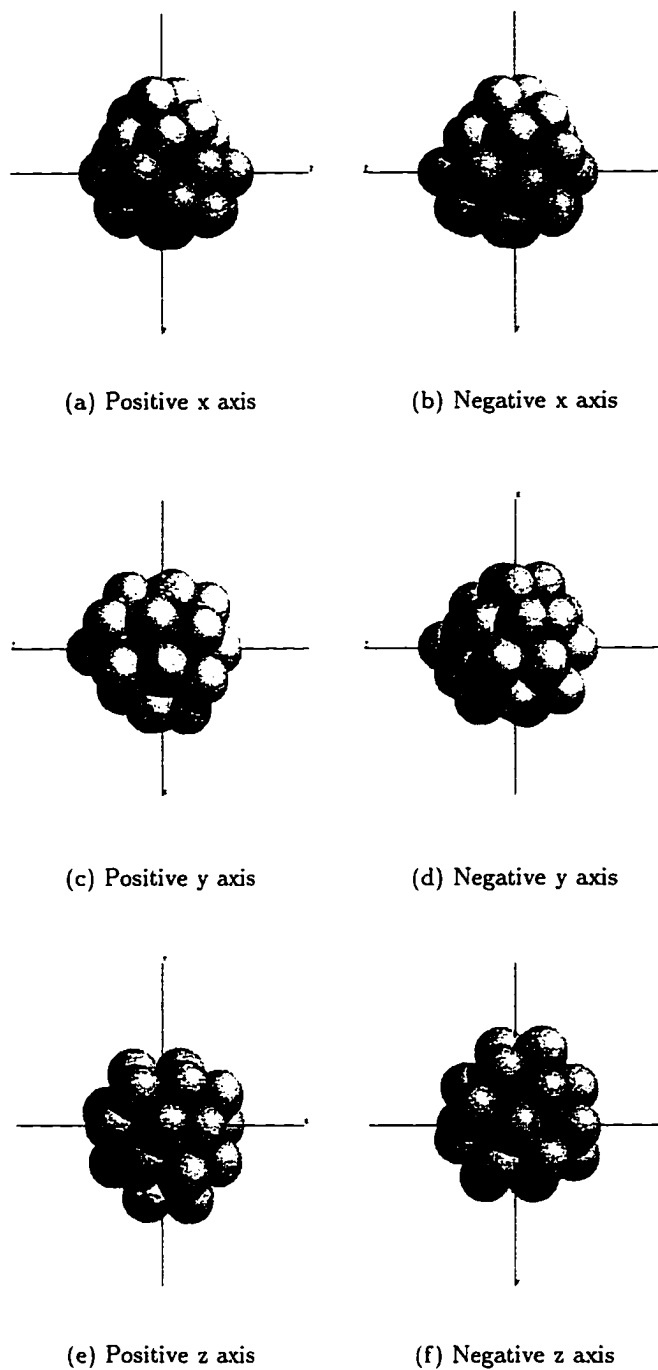


Figure 3-2: A single sample run showing ground state Na with nearest neighbor Ar atoms ($R_k < 6 \text{ \AA}$) seen from six views along the arbitrary space fixed coordinate system used in the program.

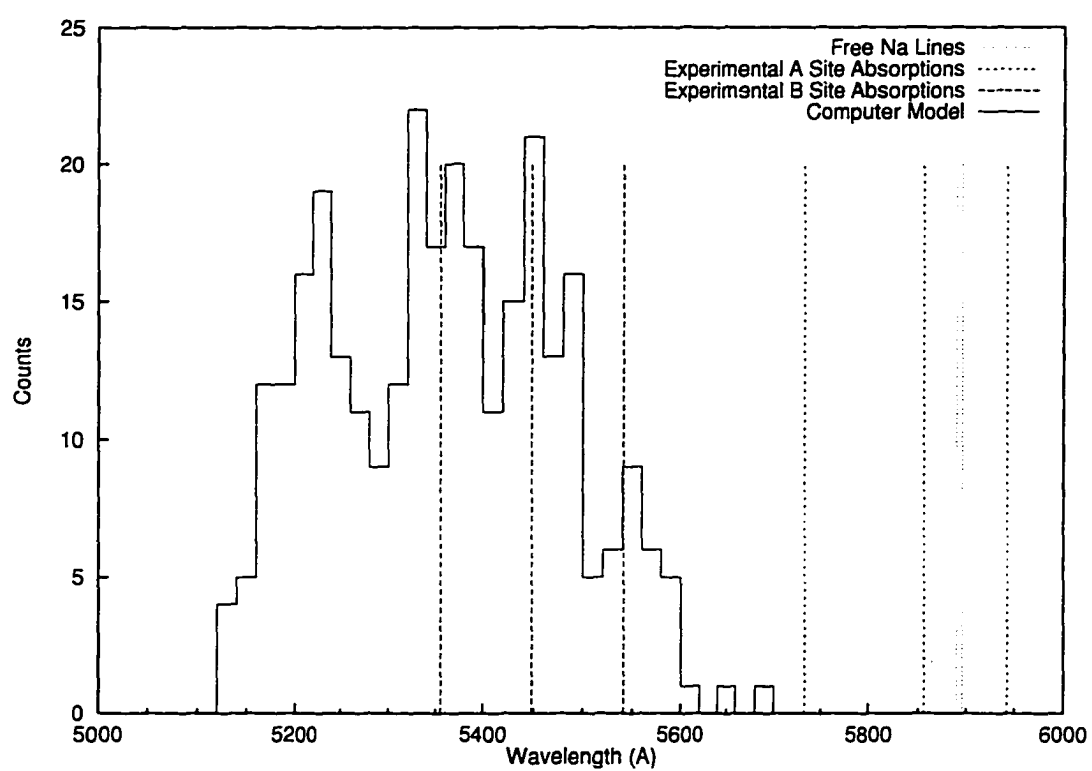


Figure 3-3: Computed absorption spectrum for one hundred runs using Saxon's [25] Na-Ar $X^2\Sigma$, $A^2\Pi$ and $B^2\Sigma$ dimer potentials compared with experiment.

wavelengths are blue shifted relative to the experimental B site absorptions. Triplet splitting is observed, but there is also a fourth, smaller peak at 5550 Å. These theoretical potentials are not as accurate as the corresponding experimentally measured potentials. It will be seen that using experimentally measured potentials gives better absorption results.

As previously stated in section 2.4, no experimental measurement of shape of the $B^2\Sigma$ Na*Ar dimer potential has been made. However, experimental Na-Ar $X^2\Sigma$ and Na*-Ar $A^2\Pi$ dimer potentials are available [26]. To use these experimental potentials, the Saxon $B^2\Sigma$ potential was adjusted to give good agreement between the calculated and the experimental matrix absorption results. Figure 3-4 shows the result of using the experimental $X^2\Sigma$ and $A^2\Pi$ dimer potentials together with a Morse fit to the Saxon $B^2\Sigma$ dimer potential. The calculated absorption spectrum shows a triplet structure that is red shifted when compared with the experimental B site absorption peaks. A small adjustment of the Morse parameter, ρ , from $\rho = 4.11$ to $\rho = 4.3$ gives calculated absorptions in better agreement with experiment. The absorption spectrum calculated with this “best $B^2\Sigma$ potential” is shown in Figure 3-5. We see a symmetric, triplet absorption spectrum with all three peaks matching the experimental peaks well.

Although, as previously stated, there exists no experimental measurement of shape of the $B^2\Sigma$ Na*Ar dimer potential, there is a measurement of its well parameters. Both the depth and the location of the well minimum have been measured by Van Den Berg *et al.* [29]. Initially the exact well location, $R_m = 5.5$ Å, quoted in that work was used. Since that work was not sensitive to the shape of the Na*-Ar $B^2\Sigma$ potential, a Morse potential fit to the shape derived by Saxon was used as a starting point. To obtain results consistent with the blue site a very steep potential had to be used ($\rho \approx 7$). We found that the best results (ie. those most

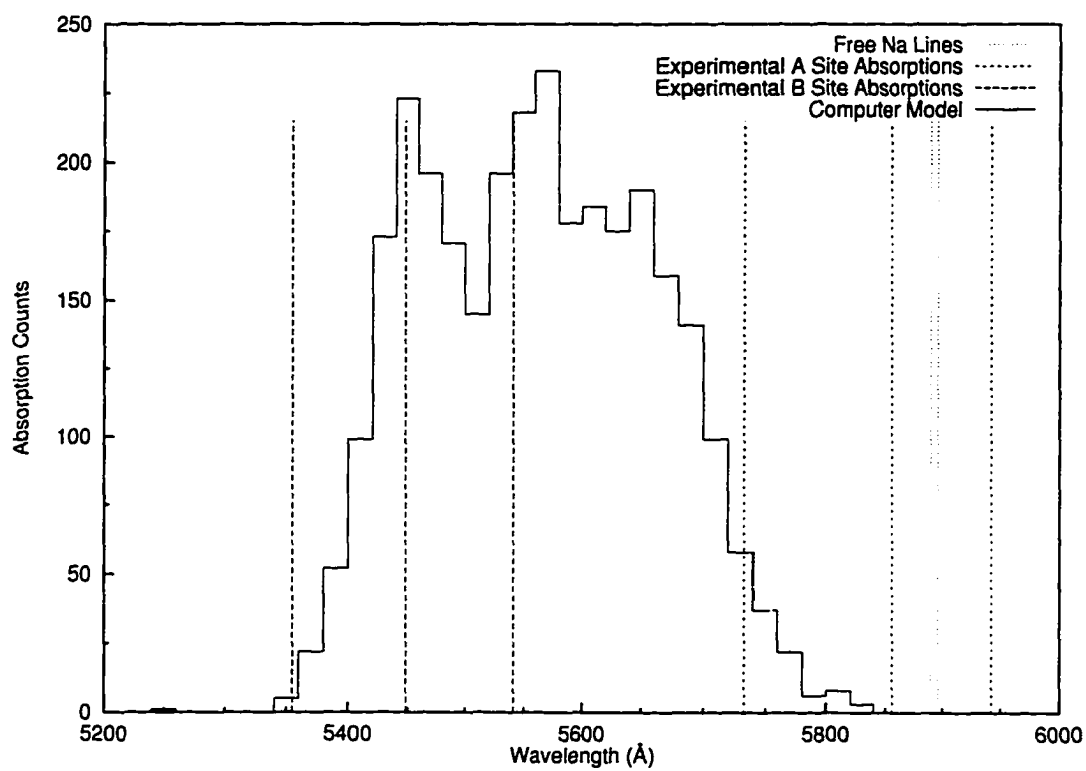


Figure 3-4: Computed absorption spectrum for one thousand runs using Tellitghuisen's [26] Na-Ar $X^2\Sigma$ and Na^{*}-Ar $A^2\Pi$ dimer potentials with Saxon's [25] Na^{*}-Ar $B^2\Sigma$ dimer potential compared with experiment.

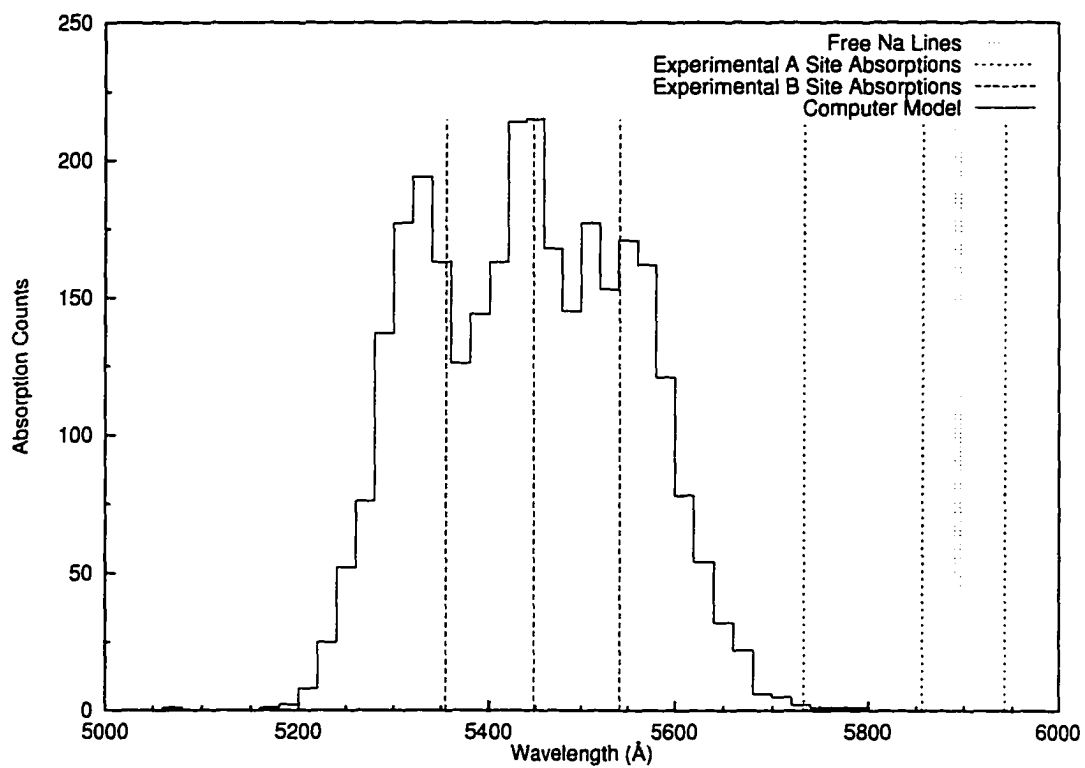


Figure 3-5: Computed absorption spectrum for one thousand runs using Tellinghuisen's [26] Na-Ar $X^2\Sigma$ and Na^{*}-Ar $A^2\Pi$ dimer potentials with the adjusted Na^{*}-Ar $B^2\Sigma$ dimer potential derived from Saxon [25] compared with experiment.

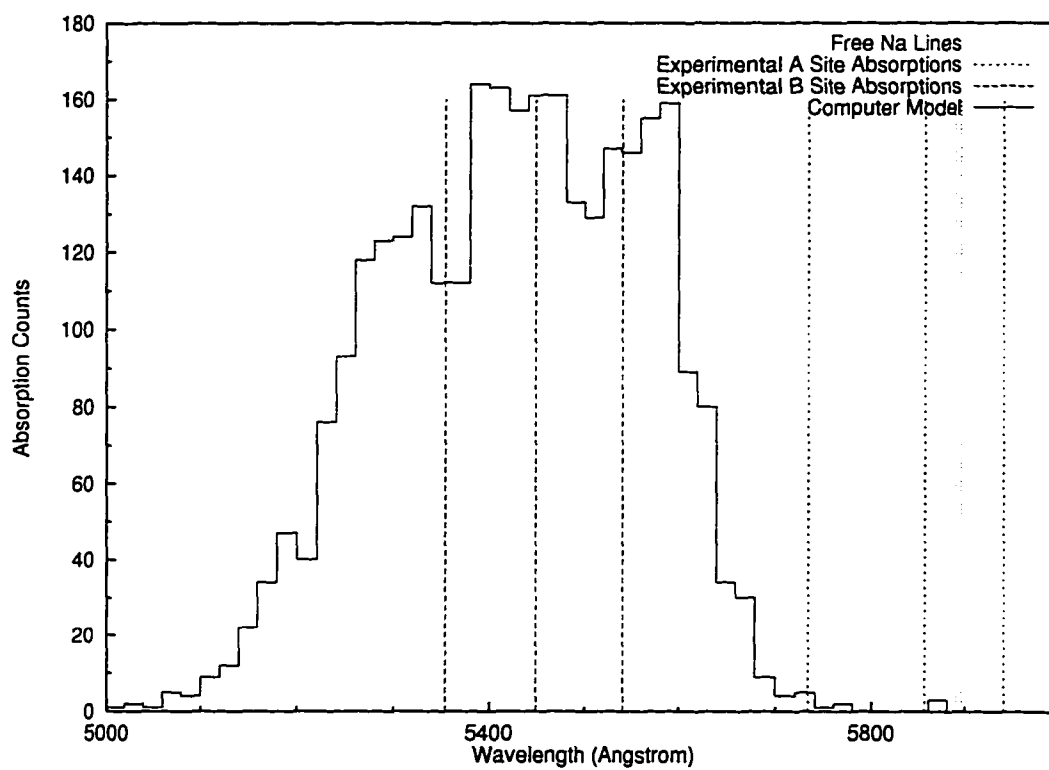


Figure 3-6: Computed absorption spectrum for one hundred runs using Tellinghuisen's [26] Na-Ar $X^2\Sigma$ and Na*-Ar $A^2\Pi$ dimer potentials with the Na*-Ar $B^2\Sigma$ dimer potential derived from Van Den Berg [29] compared with experiment

consistent with experiment) were obtained by using the upper limit on the experimental well minimum location ($R_m = 6 \text{ \AA}$). The final Morse parameter used was $\rho = 5.5$. These results are shown in figure 3-6. We see a triplet in the calculated absorptions but we also see that the peaks in the calculated results are quite wide. We also note that the spread in the absorption results is quite wide, spanning the wavelength range of 5000 \AA to 5800 \AA . We were able to draw several conclusions from this exercise. First, looking at the locations of the argon atoms relative to the sodium atom, we note that we are sampling the wall of the $B^2\Sigma$ potential (see figure 2-6). The larger Morse parameters correspond to steeper walls. It was observed that very large Morse parameters caused a more washed out set of absorptions. A very small Morse parameter caused the triplet to merge into one unresolved peak. These results are consistent with sampling the wall of the potential. A large Morse parameter means a very steep wall, therefore a small variation in atomic positions corresponds to a large variation in the size of the potential, or a very broad absorption spectrum. A very small Morse parameter corresponds to a shallow wall, a small $B^2\Sigma$ potential and therefore a small splitting, giving a single broad peak.

Since the A site is closer to the free sodium line(s) we also generated a surface trapping site as a possible candidate trapping site (figure 3-7). This was done by generating a large unrelaxed random cluster of argon atoms with a sodium at its surface and relaxing this structure. The results, shown in figure 3-7, show that the experimental absorption line that was slightly red-shifted compared with the free sodium absorption lines was not generated. It is unclear how a surface site can give absorptions that have a component greater than the free sodium absorption. This seems to require some sort of compression. The argument for that is most easily seen by examining a graph showing the dimer potentials used (figure 2-10). If

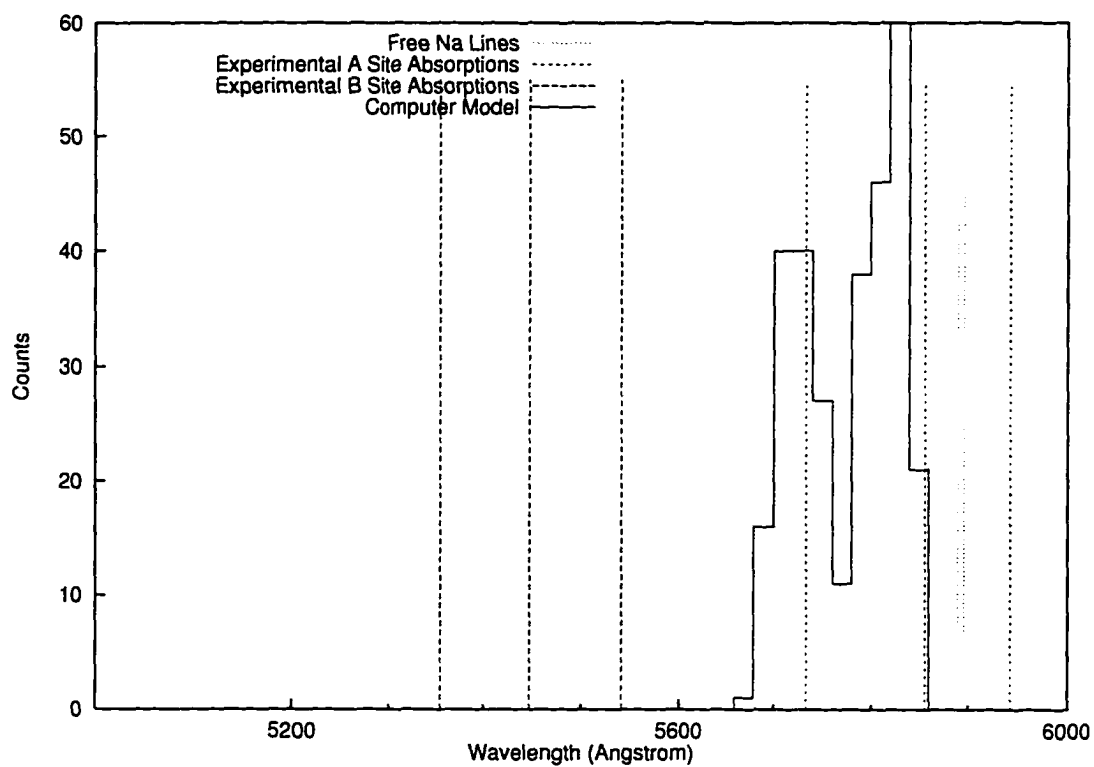


Figure 3-7: One hundred runs with sodium forced to reside on the surface of the simulated cluster. Tellinghuisen's [26] Na-Ar $X^2\Sigma$ and Na*-Ar $A^2\Pi$ dimer potentials with the Na*-Ar $B^2\Sigma$ dimer potential derived from Saxon [25] were used.

we believe that the experimental potentials are essentially correct (there seems no reason to argue against this), to get a transition energy that is smaller than the free atom line requires that argon atoms be squeezed in closer than the normal sodium-argon dimer distance. If this occurs, the ground state sodium-argon potential is higher in energy and one of the dimer energies is lower giving us the required smaller transition energy. The surface site also shows no triplet absorption structure. The degeneracy is not sufficiently split to produce more than two absorption lines. Our computer simulation supports the conclusion that the A site is not a surface site.

3.3 Fluorescence results

We discussed the method used to calculate the fluorescence in section 2.3.2. There we stated that we only allowed atoms closer than 6 Å to move when the sodium was in its excited state. Here we will also present results in which we allow all atoms to move (figure 3-11) and in which we only allow the sodium atom to move (figure 3-12).

For much of this discussion the reader is referred to the preprint presented in appendix D. This paper discusses the discovery of novel structures of Na^{*}-Ar_n clusters for small *n*. For *n* = 2, 3, 4, and 5 the clusters have a planar structure. The interaction between the excited sodium atom and the argon atoms is simply the sum of the individual Na^{*}-Ar A²Π dimer potentials. For *n* > 5 the interaction of additional argon atoms is dominated by the argon-argon dimer interactions. As additional argon atoms are added beyond *n* = 6, they form argon clusters with the Na^{*}-Ar₅ cluster on the surface. These cluster results are very important in explaining the matrix fluorescence results. The excited state cluster structures for small *n*

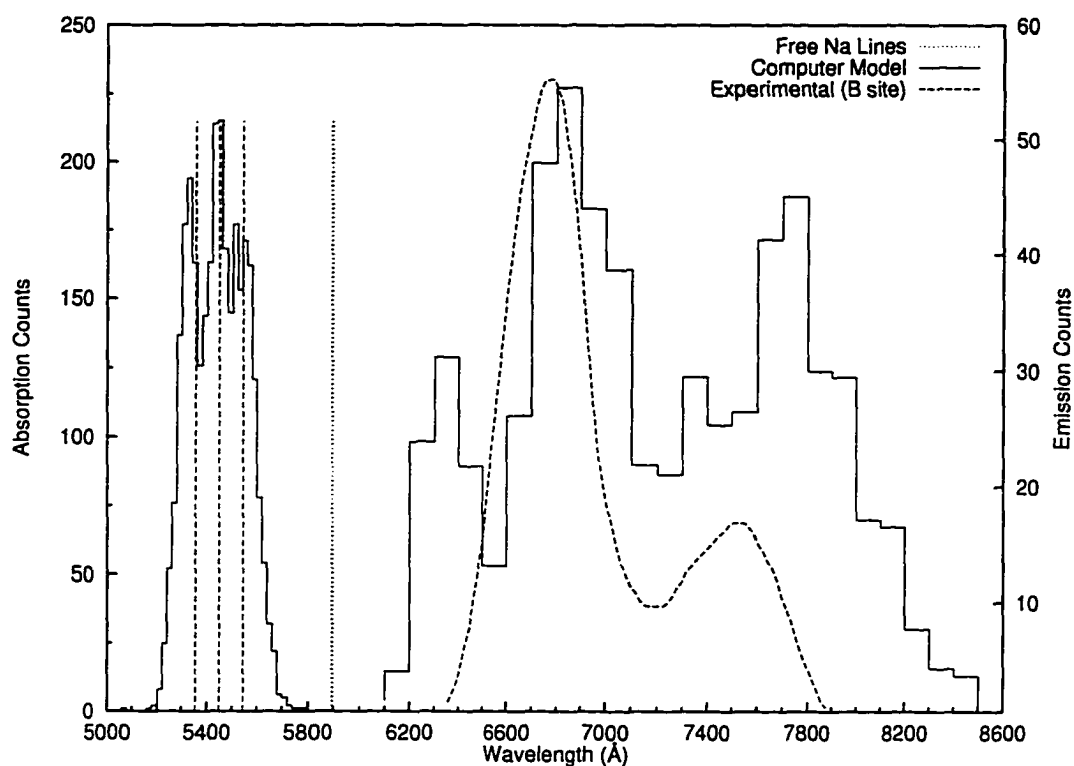


Figure 3-8: Computed absorption and fluorescence spectra for one thousand runs using Tellinghuisen's [26] Na-Ar $X^2\Sigma$ and Na*-Ar $A^2\Pi$ dimer potentials with the adjusted Na*-Ar $B^2\Sigma$ dimer potential derived from Saxon [25] compared with experiment.

are reproduced in figure 2-7.

We choose to concentrate on the fluorescence results from our "best $B^2\Sigma$ " potential, the potential with the adjusted Na*-Ar $B^2\Sigma$ dimer potential that gave good agreement with experimental absorptions. Our computer calculated fluorescence spectrum is presented in figures 3-8 and 3-9. We begin by examining both the calculated absorption and fluorescence results on one graph (figure 3-8). The first thing that we notice is that the calculated fluorescence results are red shifted relative to the absorption lines. We have succeeded in generating results which are consistent with experiment when we only consider the amount of the red

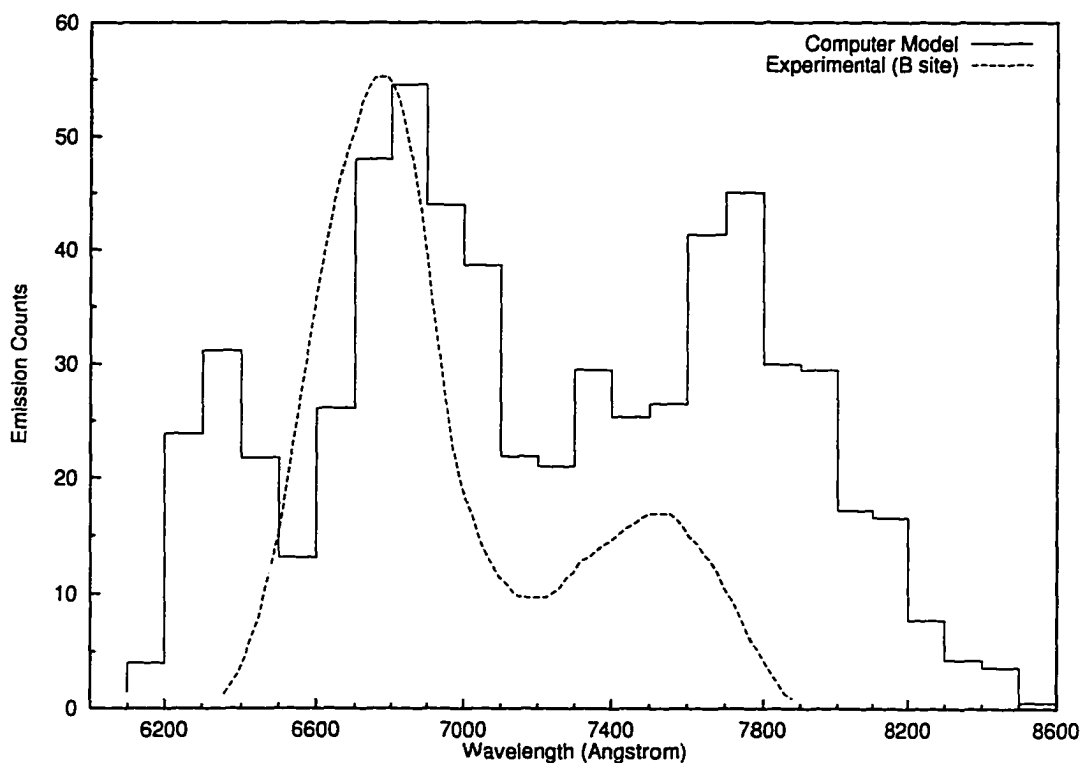


Figure 3-9: Computed fluorescence spectrum for one thousand runs using Tellinghuisen's [26] Na-Ar $X^2\Sigma$ and Na*-Ar $A^2\Pi$ dimer potentials with the adjusted Na*-Ar $B^2\Sigma$ dimer potential derived from Saxon [25] compared with experiment.

shift. Figure 3-9 examines only the calculated and experimental fluorescence results. These calculated emission spectra (figures 3-8 and 3-9) have been corrected for the transition rate for spontaneous emission in the dipole approximation (see Bransden [33], Section 4.3). For reference the uncorrected calculated emission spectrum is presented in figure 3-10. This figure should be compared directly with the corrected figure 3-9.

The first thing that strikes one upon examining the experimental B site emission results is the existence of two peaks. There are apparently two distinct structures that exist in the excited state matrix. Examining the corrected emission spectrum, figure 3-9, our simulation

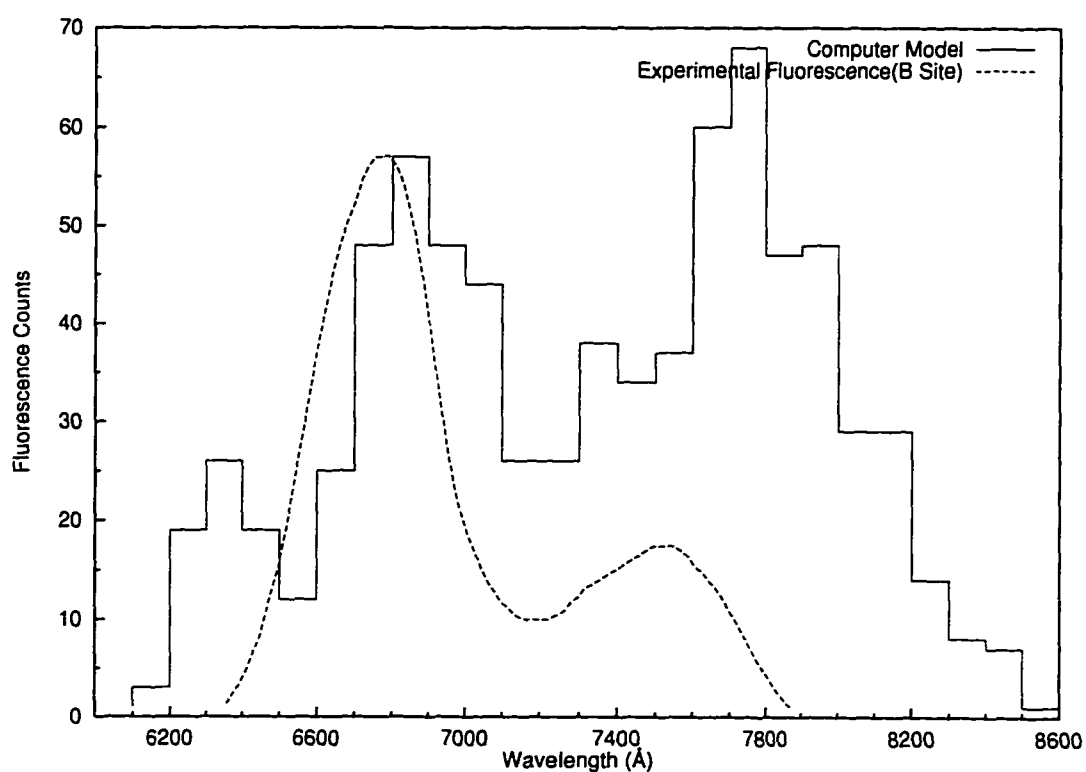


Figure 3-10: Uncorrected computed fluorescence spectrum for one thousand runs using Tellinghuisen's [26] Na-Ar $X^2\Sigma$ and Na^{*}-Ar $A^2\Pi$ dimer potentials with the adjusted Na^{*}-Ar $B^2\Sigma$ dimer potential derived from Saxon [25] compared with experiment. Not corrected for the transition rate for spontaneous emission.

n	Excited Energy (cm ⁻¹)	Ground Energy (cm ⁻¹)	λ (Å)
2	15841.2	1919.9	7183
3	15277.8	2892.7	8074
4	14716.4	3964.4	9301
5	14215.8	4023.3	9811

Table 3.1: Free Na*Ar_n cluster transition wavelengths

also gives two peaks in the correct region with a third smaller peak not seen in experiment. The most intense peak in the computational results has a peak wavelength very close to that of the experiment, the former appearing around 6800 Å and the latter around 6700 Å. There is also a peak in the calculated results at 6400 Å and another around 7800 Å. Considering the approximations going into our calculation, particularly the device of freezing all atoms beyond the nearest neighbors and the many competing interactions, the fluorescence agreement is quite good.

Close examination of the Na*Ar_n structures that gave rise to these peaks reveals that they correspond to the cluster structures formed and detailed in the preprint in appendix D. That is, when we examine the argon atoms closest to the sodium atom we find the same formations we find in bare clusters. The peak around 6800 Å corresponds to the Na*Ar₃ free cluster immersed in the matrix. The peak at 7800 Å corresponds to a Na*Ar₄ free cluster embedded in the matrix. The smaller peak located at 6400 Å, seen in our work but not in experiment, corresponds to a Na*Ar₂ free cluster embedded in the matrix.

Table 3.1 gives the energies and transition wavelengths associated with free Na*Ar_n clusters.

We note that the emission wavelengths generated in our calculated trapping sites are

blue shifted compared to those of the free $\text{Na}^*\text{-Ar}_n$ clusters. Much of this blue shift can be accounted for by the repulsive $B^2\Sigma$ potential. The remainder of it can be accounted for by the presence of the additional atoms in the matrix compared with the free cluster case. These additional argon atoms cause the ground state energy to be smaller, thus the sodium electronic transition energy is larger and the emission wavelengths are blue shifted. To give an example of this we randomly choose a cluster from our 1000 runs. The fluorescence wavelength of that simulated $\text{Na}^*\text{Ar}_{200}$ cluster is 7312 Å ($13,675 \text{ cm}^{-1}$). The interior contains a Na^*Ar_3 cluster. That is, there are three nearest neighbors in a planar configuration. If the repulsive $B^2\Sigma$ potential is set to zero and the emission recalculated for this particular cluster, we get a fluorescence wavelength of 7700 Å ($12,978 \text{ cm}^{-1}$). Thus the repulsive $B^2\Sigma$ potential is blue shifting our emission results by 400 Å (700 cm^{-1}). The remainder is accounted for by the presence of the additional atoms beyond the three nearest neighbors. The contribution of the nearest neighbors is largest but the other atoms cannot be neglected. The simulated $\text{Na}^*\text{Ar}_{200}$ cluster has a ground state energy of $1,855 \text{ cm}^{-1}$ while the Na^*Ar_3 cluster has an energy of $2,893 \text{ cm}^{-1}$. The pure $A^2\Pi$ interaction of the matrix is $-2,135 \text{ cm}^{-1}$ and that of the cluster is $-1,690 \text{ cm}^{-1}$. These differences between the $\text{Na}^*\text{Ar}_{200}$ and the Na^*Ar_3 clusters are because of the additional argon atoms. The simulated fluorescence spectrum in figure 3-9 shows three peaks. Clearly the calculated peak near 6400 Å, corresponding to $\text{Na}^*\text{-Ar}_2$, is not visible in the experimental results. Either nature does not form that nearest-neighbor configuration for the B site fluorescence or it is shifted toward the red and merges with the 6800 Å peak. The 7800 Å calculated emission peak is blue shifted relative to the experiment. This discrepancy could be due to errors in our $B^2\Sigma$ potential. This is the peak with nearest neighbors corresponding to the $\text{Na}^*\text{-Ar}_4$ cluster as discussed above.

To generate our calculated fluorescence results, we have frozen outer argon atoms in place to simulate the argon matrix holding these argon atoms in place. However, we still don't have a mechanism to account for the added potential of the matrix. Perhaps for the sites corresponding to this 7800 Å calculated emission, the atoms do not rearrange themselves as much as we observe even with our freezing all argon atoms beyond 6 Å. Another argument which seems to support this conclusion is the relative peak heights of the calculated emission results compared with those of the experiment. The more red shifted experimental emission peak is much smaller than the other. Clearly, this formation is much less frequent than our crude simulation indicates.

We need to examine our assumption that freezing all argon atoms except the nearest neighbors best simulates emission in the matrix environment. To this end, we examine what happens when all atoms are allowed to move and when only the sodium atom is allowed to move. Using the same set of potentials used in the calculation of the emission results shown in figure 3-9, all atoms were allowed to move. The results of one hundred emission calculations are presented in figure 3-11. There is a large discrepancy between the calculated and experimental B site emission results. The calculation wavelengths are as high as 9000 Å (figure 3-11). The highest wavelength in the experimental B site emission is only about 7900 Å. Close examination of the nearest neighbor configuration found a Na*Ar₅ cluster at the center of many (about 60%) of the simulation runs. The same arguments used above to explain the blue shift relative to the free cluster apply here. Clearly, allowing every atom to move causes compression of the local rare gas atoms and many runs ended up with the Na*Ar₅ cluster center. This gives results which, when compared with experiment, are unrealistic and no sites generated had fluorescence in the experimentally observed region. One further note

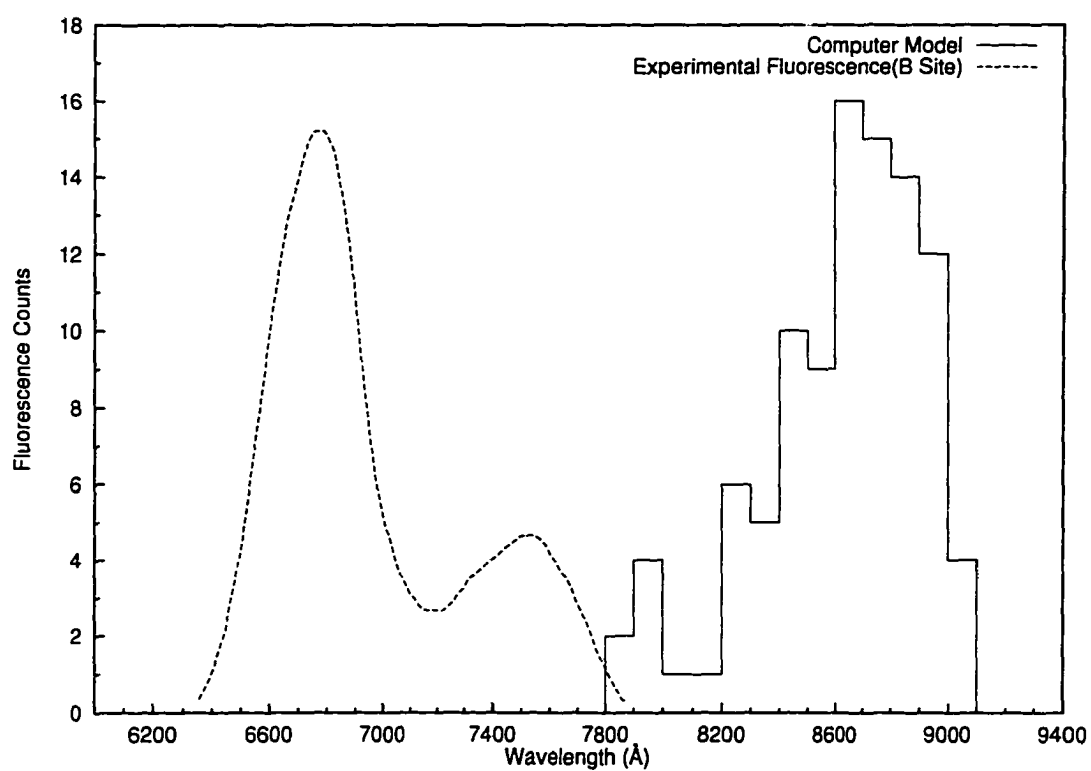


Figure 3-11: Computed emission spectrum for one hundred runs using the potentials of figure 3-9 with all atoms allowed to move when fluorescence is calculated.

is in order. We note that there are peaks in the calculated emission spectra at around 8000 Å, 8300 Å, 8500 Å, and 8700Å. These correspond to nearest neighbor configurations that look like $\text{Na}^*\text{-Ar}_n$ for n equals two, three, four, and five respectively.

A further set of trials allowing only the sodium to move were run (figure 3-12). This resulted in the nearly spherical cavity of the ground state (no argon atoms were allowed to move) with a sodium on one wall and fluorescence that was too blue relative to the experimentally measured B site emission. Clearly the local argon matrix must rearrange in order to get calculated red shifts consistent with experiment.

In conclusion, our arbitrary freezing of everything but the nearest neighbor argon atoms appears to give results consistent with experiment. If all argon atoms are allowed to rearrange, the emission is too red when compared with experiment. If only the sodium is allowed to move the results are too blue and many of the runs had emission wavelengths around the free sodium atom absorption lines.

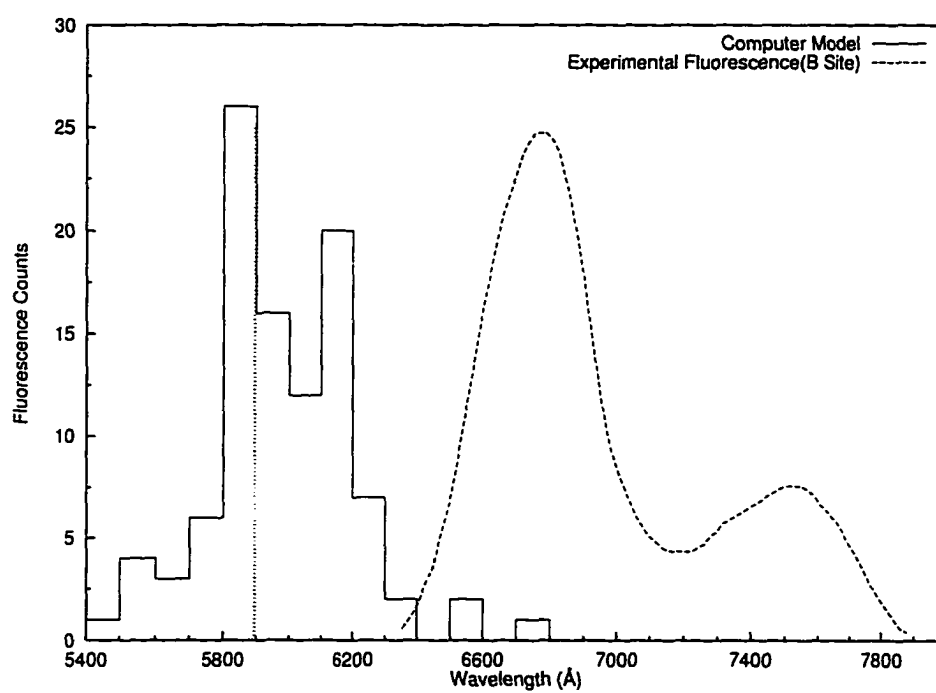


Figure 3-12: Computed emission spectra for one hundred runs using the potentials of figure 3-9 with only the Na atom allowed to move when fluorescence is calculated.

Chapter 4

Summary

A computer simulation of the formation of trapping sites for sodium atoms trapped in a solid argon matrix was performed. The resulting sites formed were all very similar, showing a roughly spherical shape. The method used to generate these sites appears to be capable of quantitatively reproducing the experimentally observed B site absorption triplet. A simple, one-parameter adjustment of the least well-known $B^2\Sigma$ sodium-argon dimer potential was necessary to bring the calculated absorption and emission spectra into good agreement with experiment. No adjustment of the $B^2\Sigma$ dimer potential could reproduce the observed absorption and emission spectra for other absorption features, making the assignment to the B site unique. This leads one to conclude that simulation, combined with experiment, might be used as a method to generate the experimentally inaccessible $B^2\Sigma$ dimer potential.

No candidates for the less thermally stable A site were obtained. The possibility of this site being a surface site was eliminated and arguments were given that lead one to believe it is an internal site with the argon atoms compressing the sodium-argon bond more than in the case of the B site. The absence of this A site in our method might be caused by the small number of argons in our simulation. This would lead to smaller compression forces and might explain the inability to compress the sodium-argon bonds sufficiently.

Because of the small number of argons used in this simulation, an artificial freezing of all but the sodium's nearest neighbor argons was necessary to simulate the bulk. This prevented liquification of our simulated cluster and gave calculated emission results consistent with experiment. A peak structure was observed in the calculated results. This structure is similar to that observed in experiment. The existence of these peaks was assigned to several unique nearest neighbor formations. These nearest neighbor formations matched those of free Na^*Ar_3 and Na^*Ar_4 clusters trapped in the argon matrix.

Given the simplicity of the simulation and the fact that one of the potentials is poorly known the results were surprisingly good. The match between the calculation and experiment was quite encouraging. The simulation method used appears to be capable of explaining some of the physics of matrix isolated sodium.

Appendix A

Useful Formulas

To convert from cm^{-1} to eV.

$$\hbar c = 197.32705359 \text{ eV} \cdot \text{nm}$$

$$\text{so } 8067.5 \text{ cm}^{-1} * \hbar c * 2\pi = 1.0 \text{ eV}$$

$$a_0 = 0.529177249 \text{ \AA}$$

$$k_{\text{Boltzman}} = 0.6950387 \text{ cm}^{-1}/\text{K}$$

If ΔE is given in wavenumbers (cm^{-1}) then the wavelength is given by

$$\lambda(\text{\AA}) = \frac{1.0 \times 10^8 \text{ \AA} \cdot \text{cm}^{-1}}{\Delta E(\text{cm}^{-1})}$$

A.1 Spherical Harmonics

$$Y_{0,0}(\Omega) = \sqrt{\frac{1}{4\pi}}$$

$$Y_{1,0}(\Omega) = \sqrt{\frac{3}{4\pi}} \cos \theta$$

$$Y_{1,\pm 1}(\Omega) = \mp \sqrt{\frac{3}{8\pi}} \sin \theta e^{\pm i\phi}$$

$$Y_{2,0}(\Omega) = \sqrt{\frac{5}{4\pi}} \left(\frac{3}{2} \cos^2(\theta) - \frac{1}{2} \right)$$

$$Y_{2,\pm 1}(\Omega) = \mp \sqrt{\frac{15}{8\pi}} \sin(\theta) \cos(\theta) e^{\pm i\phi}$$

$$Y_{2,\pm 2}(\Omega) = \frac{1}{4} \sqrt{\frac{15}{2\pi}} \sin^2(\theta) e^{\pm 2i\phi}$$

A.2 Wigner 3-j symbols

For what follows the reader is referred to Zare [50]. The 3j symbol is denoted as

$$\begin{pmatrix} l_1 & l_2 & l_3 \\ m_1 & m_2 & m_3 \end{pmatrix}$$

In general the 3-j symbol vanishes unless $m_1 + m_2 + m_3 = 0$. The angular momenta must also satisfy the triangle condition

$$|l_1 - l_2| \leq l_3 \leq l_1 + l_2 \quad (\text{A.1})$$

otherwise the 3j symbol is zero.

A.3 The integral of three Spherical Harmonics

The following integral is quite useful

$$\int d\Omega Y_{l_3 m_3}^*(\Omega) Y_{l_2 m_2}(\Omega) Y_{l_1 m_1}(\Omega) = (-1)^{m_3} \sqrt{\frac{(2l_1 + 1)(2l_2 + 1)(2l_3 + 1)}{4\pi}} \begin{pmatrix} l_1 & l_2 & l_3 \\ m_1 & m_2 & -m_3 \end{pmatrix} \begin{pmatrix} l_1 & l_2 & l_3 \\ 0 & 0 & 0 \end{pmatrix} \quad (\text{A.2})$$

Special Case:

$$\begin{pmatrix} j_1 & j_2 & j_3 \\ 0 & 0 & 0 \end{pmatrix} = \begin{cases} (-1)^g \sqrt{\frac{(2g-2j_1)!(2g-2j_2)!(2g-2j_3)!}{(2g+1)!}} \frac{g!}{(g-j_1)!(g-j_2)!(g-j_3)!} & j_1 + j_2 + j_3 \text{ even} \\ 0 & \text{otherwise} \end{cases} \quad (\text{A.3})$$

where we define $2g = j_1 + j_2 + j_3$.

Another special case:

$$\begin{pmatrix} j & 2 & j \\ -m & 0 & m \end{pmatrix} = (-1)^{j-m} \frac{3m^2 - j(j+1)}{\sqrt{(2j-1)j(j+1)(2j+1)(2j+3)}} \quad (\text{A.4})$$

$$\begin{pmatrix} j & j & 2 \\ m & -m-1 & 1 \end{pmatrix} = (-1)^{j-m} (2m+1) \sqrt{\frac{6(j+m+1)(j-m)}{(2j+3)(2j+2)(2j+1)(2j)(2j-1)}} \quad (\text{A.5})$$

$$\begin{pmatrix} j_1 & j_2 & j_1 + j_2 \\ m_1 & m_2 & m_1 + m_2 \end{pmatrix} = (-1)^{j_1 - j_2 + m_1 + m_2} \sqrt{\frac{(2j_1)!(2j_2)!(j_1 + j_2 + m_1 + m_2)!(j_1 + j_2 - m_1 - m_2)!}{(2j_1 + 2j_2 + 1)!(j_1 + m_1)!(j_1 - m_1)!(j_2 + m_2)!(j_2 - m_2)!}} \quad (\text{A.6})$$

Note also that the 3-j symbols are cyclic so any even permutation of the columns leaves the numeric value unchanged

$$\begin{pmatrix} j_1 & j_2 & j_3 \\ m_1 & m_2 & m_3 \end{pmatrix} = \begin{pmatrix} j_2 & j_3 & j_1 \\ m_2 & m_3 & m_1 \end{pmatrix} = \begin{pmatrix} j_3 & j_1 & j_2 \\ m_3 & m_1 & m_2 \end{pmatrix} \quad (\text{A.7})$$

Any odd permutation introduces a factor of $(-1)^{j_1+j_2+j_3}$

$$\begin{pmatrix} j_1 & j_2 & j_3 \\ m_1 & m_2 & m_3 \end{pmatrix} = (-1)^{j_1+j_2+j_3} \begin{pmatrix} j_3 & j_2 & j_1 \\ m_3 & m_2 & m_1 \end{pmatrix}$$

These conditions will help us rapidly calculate states.

Appendix B

Proof of Hellman-Feynman Theorem

Given a complex Hermitian matrix \mathbf{V} we can find the eigenvalues, λ_i ($i = 1 \dots N$), and their corresponding complex eigenvectors \mathbf{z}_i satisfying the standard eigenvalue-eigenvector problem

$$\mathbf{V} \cdot \mathbf{z}_i = \lambda_i \mathbf{z}_i.$$

To use the gradient method we need to know $\frac{\partial \lambda_i}{\partial (x_k)_j}$ where $(x_k)_j$ represents the j^{th} cartesian coordinate of the k^{th} RG atom.

Starting with

$$\lambda_i = \mathbf{z}_i^\dagger \cdot \mathbf{V} \cdot \mathbf{z}_i$$

where \mathbf{z}_i^\dagger is the Hermitian conjugate of \mathbf{z}_i

$$\begin{aligned} \frac{\partial \lambda_i}{\partial (x_k)_j} &= \frac{\partial \mathbf{z}_i^\dagger}{\partial (x_k)_j} \cdot \mathbf{V} \cdot \mathbf{z}_i + \mathbf{z}_i^\dagger \cdot \frac{\partial \mathbf{V}}{\partial (x_k)_j} \cdot \mathbf{z}_i + \mathbf{z}_i^\dagger \cdot \mathbf{V} \cdot \frac{\partial \mathbf{z}_i}{\partial (x_k)_j} \\ &= \frac{\partial \mathbf{z}_i^\dagger}{\partial (x_k)_j} \cdot \mathbf{z}_i \cdot \lambda_i + \mathbf{z}_i^\dagger \cdot \frac{\partial \mathbf{V}}{\partial (x_k)_j} \cdot \mathbf{z}_i + \mathbf{z}_i^\dagger \cdot \frac{\partial \mathbf{z}_i}{\partial (x_k)_j} \cdot \lambda_i \\ &= \mathbf{z}_i^\dagger \cdot \frac{\partial \mathbf{V}}{\partial (x_k)_j} \cdot \mathbf{z}_i + \left(\frac{\partial \mathbf{z}_i^\dagger}{\partial (x_k)_j} \mathbf{z}_i + \mathbf{z}_i^\dagger \cdot \frac{\partial \mathbf{z}_i}{\partial (x_k)_j} \right) \cdot \lambda_i \end{aligned} \quad (\text{B.1})$$

Where we have used the fact that \mathbf{V} is Hermitian.

Given the orthonormality of the eigenvectors $\mathbf{z}_i^\dagger \mathbf{z}_j = \delta_{i,j}$, we take the derivative of $\mathbf{z}_i^\dagger \cdot \mathbf{z}_i$

$$\begin{aligned} \frac{\partial (\mathbf{z}_i^\dagger \mathbf{z}_i)}{\partial (x_k)_j} &= \frac{\partial \mathbf{z}_i^\dagger}{\partial (x_k)_j} \cdot \mathbf{z}_i + \mathbf{z}_i^\dagger \cdot \frac{\partial \mathbf{z}_i}{\partial (x_k)_j} \\ &= \frac{\partial (1)}{\partial (x_k)_j} \\ &= 0. \end{aligned} \quad (\text{B.2})$$

Giving the useful result

$$\frac{\partial \lambda_i}{\partial (x_k)_j} = \mathbf{z}_i^\dagger \cdot \frac{\partial \mathbf{V}}{\partial (x_k)_j} \cdot \mathbf{z}_i \quad (\text{B.3})$$

Appendix C

Calculating the Perturbation Matrix, V_{ij}

We wish to calculate the angular portion of the matrix element V_{ij} given in Chapter 2 by Equation (2.8) reproduced here for reference.

$$\begin{aligned} V_{ij} &= \sum_k \langle n, l = 1, m_i | V(\mathbf{r}, \mathbf{R}_k) | n, l = 1, m_j \rangle \\ &= \sum_L \sum_k \langle n, l = 1 | V_L(r, R_k) | n, l = 1 \rangle \langle l = 1, m_i | P_L(\hat{r} \cdot \hat{R}_k) | l = 1, m_j \rangle \end{aligned}$$

To express the angular portion in terms of the location of the k^{th} RG atom, we use the addition theorem for spherical harmonics

$$P_L(\hat{r}, \hat{R}_k) = \frac{4\pi}{2L+1} \sum_M Y_{L,M}(\Omega) Y_{L,M}^*(\Omega_k)$$

the angular part of Equation (2.8) can be rewritten

$$\langle m_i | P_L(\hat{r} \cdot \hat{R}_k) | m_j \rangle = \frac{4\pi}{2L+1} \sum_M Y_{L,M}^*(\Omega_k) \int d\Omega Y_{1,m_i}^*(\Omega) Y_{L,M}(\Omega) Y_{1,m_j}(\Omega) \quad (C.1)$$

The above integral has a well known solution in terms of 3-j symbols. It is given in appendix A as Equation (A.2).

First we will consider the excited state (p state) as results here will be useful in the ground state. Using the triangle condition for 3-j symbols ($|l_1 - l_2| \leq l_3 \leq l_1 + l_2$) and identifying $l_1 = l_3 = 1$ we see that possible values of l_2 are $l_2 = 0, 1, 2$. Using Equation (A.3) we see that since $l_1 + l_2 + l_3$ must be even we can exclude $l_2 = 1$ leaving us with possible l_2 values of $l_2 = 0, 2$. So

$$V_{ij} = \sum_{k=1}^N \left\{ \langle np | V_0(r, R_k) | np \rangle \langle m_i | P_0(\hat{r} \cdot \hat{R}_k) | m_j \rangle + \langle np | V_2(r, R_k) | np \rangle \langle m_i | P_2(\hat{r} \cdot \hat{R}_k) | m_j \rangle \right\}$$

Consider the angular part of the first sum

$$\langle m_i | P_0(\hat{r} \cdot \hat{R}_k) | m_j \rangle = \langle m_i | 4\pi (Y_{0,0}(\Omega) Y_{0,0}^*(\Omega_k)) | m_j \rangle$$

$$\begin{aligned}
&= \int d\Omega Y_{1,m_i}(\Omega) Y_{1,m_j}(\Omega) \\
&= \delta_{m_i, m_j}
\end{aligned} \tag{C.2}$$

Now consider the angular part of the second sum

$$\begin{aligned}
\langle m_i | P_2(\hat{r} \cdot \hat{R}_k) | m_j \rangle &= \langle m_i | \frac{4\pi}{5} \sum_{M=-2}^2 Y_{2,M}(\Omega) Y_{2,M}^*(\Omega_k) | m_j \rangle \\
&= \frac{4\pi}{5} \sum_{M=-2}^2 Y_{2,M}^*(\Omega_k) \int d\Omega Y_{1,m_i}^*(\Omega) Y_{2,M}(\Omega) Y_{1,m_j}(\Omega)
\end{aligned} \tag{C.3}$$

For all V_{ij} we can evaluate $\begin{pmatrix} l_1 & l_2 & l_3 \\ 0 & 0 & 0 \end{pmatrix}$ using equation A.3. The result is

$$\begin{pmatrix} l_1 & l_2 & l_3 \\ 0 & 0 & 0 \end{pmatrix} = 2\sqrt{\frac{4}{5!}}$$

Thus,

$$\int d\Omega Y_{1,m_i}^*(\Omega) Y_{2,M}(\Omega) Y_{1,m_j}(\Omega) = (-1)^{m_i} \sqrt{\frac{3 \cdot 5 \cdot 3}{4\pi}} 2\sqrt{\frac{4}{5!}} \begin{pmatrix} 1 & 2 & 1 \\ m_j & M & -m_i \end{pmatrix} \tag{C.4}$$

Substituting C.4 into C.3 gives

$$\langle m_i | P_2(\hat{r} \cdot \hat{R}_k) | m_j \rangle = \frac{4\pi}{5} \sum_{M=-2}^2 Y_{2,M}^*(\Omega_k) (-1)^{m_i} \sqrt{\frac{3}{2\pi}} \begin{pmatrix} 1 & 2 & 1 \\ m_j & M & -m_i \end{pmatrix}$$

Or, using the fact that an odd column permutation introduces a factor of $(-1)^{j_1+j_2+j_3} = (-1)^4 = 1$

$$\langle m_i | P_2(\hat{r} \cdot \hat{R}_k) | m_j \rangle = \frac{4\pi}{5} \sum_{M=-2}^2 Y_{2,M}^*(\Omega_k) (-1)^{m_i} \sqrt{\frac{2}{2\pi}} \begin{pmatrix} 1 & 2 & 1 \\ -m_i & M & m_j \end{pmatrix}$$

Using the general condition on the magnetic quantum number for a 3j symbol we know $m_j + M - m_i = 0$.

For the ground state alkali atom (s state) our basis consists of the single basis function $\langle 00|$. Inserting $l_1 = l_3 = 0$ and using the triangle condition ($|l_1 - l_2| \leq l_3 \leq l_1 + l_2$) we see that there is only one possible value $l_2 = 0$.

$$V_{ij} = \sum_{k=1}^N \langle np | V_0(r, R_k) | np \rangle \langle m_i | P_0(\hat{r} \cdot \hat{R}_k) | m_j \rangle$$

We have already determined $\langle m_i | P_0(\hat{r} \cdot \hat{R}_k) | m_j \rangle = 1$ in Equation (C.2). The result is that

$V_{ij} = \sum_{k=1}^N \langle np | V_0(r, R_k) | np \rangle$. Thus the ground state has no angular dependence and is simply the sum of the dimer potentials.

C.1 Evaluation of matrix elements

For notational convenience in what follow, we will define

$$V_0(R_k) = \langle nl | V_0(r, R_k) | nl \rangle$$

and

$$V_2(R_k) = \langle nl | V_2(r, R_k) | nl \rangle$$

Since $V_{ij} = V_{ji}^*$ we need only calculate the members of the upper triangle of the matrix. As a sample let us do V_{00} . For V_{00} $m_i = m_j = 1$ thus $M = 0$.

$$V_{00} = \sum_k \left\{ V_0(R_k) + V_2(R_k) \frac{4\pi}{5} Y_{2,0}^*(\Omega_k) (-1)^1 \sqrt{\frac{3}{2\pi}} \begin{pmatrix} 1 & 2 & 1 \\ -1 & 0 & 1 \end{pmatrix} \right\}$$

Using Equation (A.4)

$$\begin{pmatrix} 1 & 2 & 1 \\ -1 & 0 & 1 \end{pmatrix} = (-1)^4 (-1)^0 \frac{1}{\sqrt{2 \cdot 3 \cdot 5}}$$

Finally

$$V_{00} = \sum_k \left\{ V_0(R_k) - V_2(R_k) \frac{1}{10} (3 \cos^2 \theta_k - 1) \right\}$$

For V_{11} , $m_i = m_j = 0$ so $M = 0$ we use Equation (A.3)

$$\begin{pmatrix} 1 & 2 & 1 \\ 0 & 0 & 0 \end{pmatrix} = (-1)^2 \sqrt{\frac{2 \cdot 1 \cdot 2}{5!}} \cdot 2 = 2 \cdot \frac{1}{\sqrt{2 \cdot 3 \cdot 5}}$$

$$V_{11} = \sum_k \left\{ V_0(R_k) + V_2(R_k) \frac{2}{10} (3 \cos^2 \theta_k - 1) \right\}$$

For V_{22} , $m_i = m_j = -1$ so $M = 0$ we see that $V_{22} = V_{00}$ since

$$\begin{pmatrix} 1 & 2 & 1 \\ 1 & 0 & -1 \end{pmatrix} = \begin{pmatrix} 1 & 2 & 1 \\ -1 & 0 & 1 \end{pmatrix}$$

For V_{01} , $m_i = 1$, $m_j = 0$ so $M = 1$ using Equation (A.5)

$$\begin{pmatrix} 1 & 2 & 1 \\ -1 & 1 & 0 \end{pmatrix} = -\sqrt{\frac{6 \cdot 2}{5!}} = -\sqrt{\frac{1}{10}}$$

$$\begin{aligned}
V_{01} &= \sum_k \left\{ V_0(R_k) - V_2(R_k) \frac{4\pi}{5} Y_{2,1}^*(\Omega_k) (-1)^1 \sqrt{\frac{3}{2\pi}} \sqrt{\frac{1}{10}} \right\} \\
&= \sum_k \left\{ V_0(R_k) - V_2(R_k) \frac{3\sqrt{2}}{10} \cos \theta \sin \theta e^{-i\phi} \right\}
\end{aligned} \tag{C.5}$$

For V_{02} , $m_i = 1$, $m_j = -1$ so $M = 2$ using Equation (A.7)

$$\begin{pmatrix} 1 & 2 & 1 \\ -1 & 2 & -1 \end{pmatrix} = \sqrt{\frac{1}{5}}$$

$$\begin{aligned}
V_{02} &= \sum_k \left\{ V_0(R_k) - V_2(R_k) \frac{4\pi}{5} Y_{2,2}^*(\Omega_k) (-1)^1 \sqrt{\frac{3}{2\pi}} \sqrt{\frac{1}{5}} \right\} \\
&= \sum_k \left\{ V_0(R_k) - V_2(R_k) \frac{3}{10} \sin^2 \theta e^{-2i\phi} \right\}
\end{aligned} \tag{C.6}$$

For V_{12} , $m_i = 0$, $m_j = -1$ so $M = 1$ we see that $V_{12} = -V_{01}$ since

$$\begin{pmatrix} 1 & 2 & 1 \\ 0 & 1 & -1 \end{pmatrix} = \begin{pmatrix} 1 & 2 & 1 \\ -1 & 1 & 0 \end{pmatrix}$$

where the minus sign comes from the $(-1)^{m_i}$.

Putting these together the final result is

$$\begin{aligned}
\mathbf{V} &= \sum_k \langle V_0(\mathbf{R}_k) \rangle \mathbf{I} + \frac{1}{10} \sum_k \langle V_2(\mathbf{R}_k) \rangle \times \\
&\begin{bmatrix} -(3 \cos^2 \theta_k - 1) & -3\sqrt{2} \sin \theta_k \cos \theta_k e^{-i\phi_k} & -3 \sin^2 \theta_k e^{-2i\phi_k} \\ -3\sqrt{2} \sin \theta_k \cos \theta_k e^{i\phi_k} & 2(3 \cos^2 \theta_k - 1) & 3\sqrt{2} \sin \theta_k \cos \theta_k e^{-i\phi_k} \\ -3 \sin^2 \theta_k e^{2i\phi_k} & 3\sqrt{2} \sin \theta_k \cos \theta_k e^{i\phi_k} & -(3 \cos^2 \theta_k - 1) \end{bmatrix}
\end{aligned} \tag{C.7}$$

where \mathbf{I} is the unit matrix.

For computational convenience, the cartesian form of this equation was used.

$$\begin{aligned}
\mathbf{V} &= \sum_k \langle V_0(\mathbf{R}_k) \rangle \mathbf{I} + \sum_k \frac{\langle V_2(\mathbf{R}_k) \rangle}{10} \times \\
&\begin{bmatrix} -\left(\frac{3z_k^2}{(x^2+y^2+z^2)} - 1\right) & -3\sqrt{2} \frac{z_k(x_k - iy_k)}{(x^2+y^2+z^2)} & -3 \frac{x_k^2 - y_k^2 - i \cdot 2x_k y_k}{(x^2+y^2+z^2)} \\ (V'_{01})^* & -2 \cdot (V'_{00}) & -(V'_{01}) \\ (V'_{02})^* & -(V'_{01})^* & (V'_{00}) \end{bmatrix}
\end{aligned} \tag{C.8}$$

where \mathbf{V}' has an obvious meaning. This result is identical to that given in the appendix of reference [38].

We can solve this using the Householder-Givens-Wilkinson method or by writing out the determinant directly and solving the resulting cubic. As a simplification we note that we can

solve the secular equation for V' and add the diagonal terms to get the perturbation term. That is to say we define $E' = E - V_0 - V_{RG}$. Compare

$$\det \begin{bmatrix} a - E' & c + i \cdot d & g + i \cdot f \\ c - i \cdot d & -2 \cdot a - E' & -(c + i \cdot d) \\ g - i \cdot f & -(c - i \cdot d) & a - E' \end{bmatrix} = 0 \quad (\text{C.9})$$

We obtain the cubic...

$$E^3 - \{g^2 + 2(c^2 + d^2) + 3a^2 + f^2\}E + \{2g(c^2 - d^2) + 2a[c^2 + d^2 - (f^2 + g^2)] + 2a^3 + 4cdf\} = 0 \quad (\text{C.10})$$

This can be solved by any standard cubic method to obtain the eigenvalues E (see for example [35]).

C.2 Derivatives of the Matrix Elements for the P-state

As seen in Equation (2.15) in order to use the gradient method we require the derivatives of the matrix given by Equation (2.9). These derivatives are presented below in cartesian coordinates.

C.2.1 Derivatives of V'_{00}

$$\begin{aligned} \frac{\partial V'_{00}}{\partial x} &= \frac{6xz^2}{(x^2 + y^2 + z^2)^2} \\ \frac{\partial V'_{00}}{\partial y} &= \frac{6yz^2}{(x^2 + y^2 + z^2)^2} \\ \frac{\partial V'_{00}}{\partial z} &= \frac{-6z(x^2 + y^2)}{(x^2 + y^2 + z^2)^2} \end{aligned} \quad (\text{C.11})$$

C.2.2 Derivatives of V'_{01}

$$\begin{aligned} \frac{\partial V'_{01}}{\partial x} &= 3\sqrt{2} \cdot \frac{z(x^2 - y^2 - z^2 - i \cdot 2xy)}{(x^2 + y^2 + z^2)^2} \\ \frac{\partial V'_{01}}{\partial y} &= 3\sqrt{2} \cdot \frac{z(2xy + i \cdot (x^2 - y^2 + z^2))}{(x^2 + y^2 + z^2)^2} \\ \frac{\partial V'_{01}}{\partial z} &= -3\sqrt{2} \cdot \frac{(x - i \cdot y)(x^2 + y^2 - z^2)}{(x^2 + y^2 + z^2)^2} \end{aligned} \quad (\text{C.12})$$

C.2.3 Derivatives of V'_{02}

$$\frac{\partial V'_{02}}{\partial x} = -6 \cdot \frac{(2y^2 + z^2) + i \cdot y(x^2 - y^2 - z^2)}{(x^2 + y^2 + z^2)^2}$$

$$\begin{aligned}\frac{\partial V'_{02}}{\partial y} &= 6 \cdot \frac{y(2x^2 + z^2) + i \cdot x(x^2 - y^2 + z^2)}{(x^2 + y^2 + z^2)^2} \\ \frac{\partial V'_{02}}{\partial z} &= 6z \cdot \frac{(x^2 - y^2) - i \cdot 2xy}{(x^2 + y^2 + z^2)^2}\end{aligned}\tag{C.13}$$

Appendix D

Preprint–Structure of $\text{Na}(3^2\text{P})\text{-Ar}_n$ Clusters using Semiempirical Potentials

Structure of Na(3^2P)-Ar_n Clusters using Semiempirical Potentials

Alan B. Tutein^a and Howard R. Mayne^b

Departments of Physics and Chemistry
University of New Hampshire
Durham, NH 03824

ABSTRACT

We have calculated the minimum energy geometries of clusters formed by electronically-excited sodium atoms in their (3^2P) state with argon atoms. The potential energy functions needed to describe interactions with an open-shell atom are not pairwise additive. Those used here were constructed using a first-order perturbation treatment. The semiempirical potentials used as input were derived from direct spectroscopic evidence, in the case of the $A^2\Pi$ potential, and indirectly from matrix isolation data for the $B^2\Sigma$. We find the clusters to be planar for $n=2-5$. Additional argon atoms form an argon subcluster, avoiding the perpendicular to the Na^*-Ar_5 plane. We have investigated the sensitivity of the cluster geometry to variations in the potential parameters. We have also calculated geometric isomers for the Na^*-Ar_5 case. The significance of these findings for fluorescence experiments in cryoscopic rare gas matrices is discussed.

- a. Department of Physics
- b. Department of Chemistry

I. Introduction

In recent years there has been considerable interest in the study of microclusters, as experimental techniques capable of forming and characterizing such species have developed. In addition, there has been considerable theoretical and computational activity. The literature is vast, and we refer the reader to recent reviews.¹⁻⁵

One motivation for such work is to deepen our understanding of the microscopic details of solvation. There have been a large number of studies which have investigated the structure of heterogeneous clusters in which a single molecule or atom is "dissolved" in a cluster of rare gas atoms.⁶⁻²⁴ An advantage of clusters is that such parameters as the size and energy content (or temperature) of the cluster can be to some extent controlled. One area of interest has been the investigation of solvation effects as a function of the number of atoms in the solvent cluster. For instance, the infrared spectroscopy of SF₆-Ar_n system⁷⁻⁹ has been the object of considerable research. There has also been considerable interest recently in the effect on electronic spectra of aromatics in rare gas clusters.^{11-16,22,23}

While these systems are relatively anisotropic, most modeling calculations have used pairwise-additive electronically adiabatic potentials between the rare gas atoms and the heteroatom or individual atoms of the molecule. Relatively few studies have been carried out on clusters in which the potential cannot be modeled in this fashion. Effects of the role of three body interactions have been investigated.⁹

For several open shell atoms, however, the potential cannot be modeled by a single potential energy curve. For instance, in the recent investigation of Ba atoms desorbing from an argon cluster, Jungwirth and Gerber¹⁸ use a Σ and a Π -type potential in their modeling of Ba* desorbing from an Ar cluster. In a recent study of B-Ar_n cluster geometries, Alexander and coworkers^{19,20} used a similar formulation for the B-Ar potential.

We have chosen to carry out investigations on the electronically-excited Na(3²P)-Ar_n system. The fact that p orbitals are involved in the bonding means that nonadditive effects are extremely important. In addition, the interaction is both strong and highly anisotropic. In the study of B-Ar_n clusters referred to above, the B-Ar interaction is comparable in energy to the Ar-Ar energy. For excited state sodium, by contrast, the Π potential is much stronger than that between the rare gas atoms, and this causes the metal atom to have a profound organizing effect on the solvent.

The Na-Ar_n cluster has been the object of considerable interest as a model system in cryogenic matrix studies.^{17,25-31} The sodium atom acts as a chromophore; the 3²S→3²P optical transition lines serve as a probe of the local environment of the Na(3²S) atom. In addition, fluorescence lines yield information on solvent rearrangement after the excitation. There is a profound qualitative contrast between the Na-Ar interaction in the electronic ground state, and in some of the excited states. In the groundstate, the interaction is relatively weak. In the excited (A²Π) state, however, the excimer potential is strongly bound. In addition, if the symmetry of the system is lowered (as is the case in a cluster) the Na*-Ar interaction is anisotropic. Thus, there is the possibility of strong solvent reorganization effects on optical excitation of Na atoms within an Ar_n matrix. In fact, recent work on large clusters has shown this to be the case.³² This work³² has also yielded model Na*-Ar potentials which are in reasonable agreement with both absorption and emission spectra for Na in argon matrices.

We use these potentials here to investigate the structure of small Na(3²P)-Ar_n clusters. We find the potential energy global minimum for these excited state clusters for n=2 through 17. We comment on the role played by the anisotropy of the potential. We discuss possible isomers for the Na*-Ar₅ case, and generalize to larger structures. Finally, we comment on how an understanding of the cluster structure for small clusters can yield insight into details of macroscopic solvent rearrangement and relate our findings to matrix fluorescence data.

II. Calculation of Cluster Potential Geometry

(a) Formalism

To describe the interaction between a P atom and an S atom, potential energy curves of both Σ and Π symmetry must be considered. In order to calculate the interaction between a P atom and several S atoms, these potentials must be combined in a non-pairwise additive manner. We use here the perturbation technique proposed by Baylis,³³ which was developed for clusters by Balling and Wright (BW),³⁴ and more recently by Boatz and Fajardo (BF).³¹ We will consider here the case of a Na(3²P) atom interacting with n argon atoms.

The one-electron Hamiltonian for the sodium atom interacting with n argon atoms treated as point perturbbers is:

$$\mathbf{H} = \mathbf{H}_0(\mathbf{x}) + \sum_i^n v(\mathbf{x}, \mathbf{R}_i)$$

where \mathbf{x} denotes the electronic coordinate of the Na atom, and \mathbf{R}_i is the displacement of the i th argon atom. \mathbf{H}_0 is the unperturbed one-electron Hamiltonian:

$$\mathbf{H}_0 |p(\mathbf{x})\rangle = E_0 |p(\mathbf{x})\rangle$$

where E_0 is the eigenenergy for the 3p valence orbital. The potential $v(\mathbf{x}, \mathbf{R}_i)$ is a perturbation potential due the interaction between the electron and a point (argon atom) perturber at \mathbf{R}_i .

Following BW and BF we carry out a first-order perturbation calculation in the minimal p basis set: $\{p_m\} = \{p_1, p_0, p_{-1}\}$. This leads to a 3x3 secular determinant, whose solutions, E , are the electronic $\text{Na}^*\text{-Ar}_n$ energies:

$$\det | V_{mm'}(\mathbf{R}) - (E-E_0) \delta_{mm'} | = 0$$

where

$$V_{mm'}(\mathbf{R}) = \sum_i \langle m | v(\mathbf{x}, \mathbf{R}_i) | m' \rangle$$

is a function of the geometry of the n -atom argon subcluster, whose coordinates we denote by $\mathbf{R} = (R_{1x}, \dots, R_{nz})$. From this, we see that $E = E(\mathbf{R})$. We must therefore solve the secular determinant for each cluster geometry. Putting in the explicit functions for the p basis yields for the solutions:

$$E(\mathbf{R}) = \sum_i^n (V_0(\mathbf{R}_i) \mathbf{I} + (1/10) V_2(\mathbf{R}_i) \mathbf{M})$$

where $R_i = |\mathbf{R}_i|$, \mathbf{I} is the unit matrix and \mathbf{M} is a matrix containing angle-dependent terms given by BF (their treatment corrects a typographical error in the BW paper). The Legendre potential terms are related to the Σ and Π atom-atom potentials through:

$$3 V_0(\mathbf{R}_i) = V_{B\Sigma}(\mathbf{R}_i) + 2 V_{A\Pi}(\mathbf{R}_i)$$

$$3 V_2(\mathbf{R}_i) = 5 [V_{B\Sigma}(\mathbf{R}_i) - V_{A\Pi}(\mathbf{R}_i)]$$

where we have used the fact that the S and the P atom-atom interactions involved are the $B^2\Sigma$ and the $A^2\Pi$ $\text{Na}^*\text{-Ar}$ potential energy functions respectively.

The total energy of the Na^{*}-Ar_n cluster is given by

$$V(\mathbf{R}) = E(\mathbf{R}) + \sum_{j>k} V_{\text{Ar-Ar}}(r_{jk})$$

where $r_{jk} = |\mathbf{r}_{jk}| = |\mathbf{R}_j - \mathbf{R}_k|$, and $V_{\text{Ar-Ar}}(r)$ is the (assumed pairwise additive) Ar-Ar potential.

In obtaining geometries of the Na^{*}-Ar_n clusters, the lowest electronic eigenvalue was always used.

(b) Diatomic Potentials

The potential energy functions for Ar-Ar has been the subject of considerable research. We use the recent accurate fit potential of Aziz.³⁵ We use r for Ar-Ar interaction distances. In particular, the equilibrium distance is $r_e = 3.757 \text{ \AA}$, and the equilibrium well depth of 99.738 cm^{-1} will be denoted ϵ .

By contrast, the Na^{*}-Ar potentials are less well established. There is a spectroscopic potential available for the A²Π potential. Tellinghuisen et al.³⁶ extracted a potential curve from laser spectroscopy of the X-A transition. However, there is little data on the B²Σ potential. Pioneering ab initio studies^{37,38} show it is clearly much less strongly bound than is the A state, and also that it is much more repulsive at short range. There is also a small body of data from scattering experiments.^{39,40}

Several groups^{26,31,32} have used simplified B state potentials to model optical absorption of Na atoms in cryoscopic argon matrices. One recent study³² has been relatively successful in predicting the absorption spectrum from a limited number of matrix sites. This study fixed the B potential within a fairly narrow range of parameters. We use the potential derived from that work here. We show later that the cluster structures investigated here are unlikely to be very sensitive to the details of the potential used. We therefore use here a set of Morse parameters which fit reasonably well all experimental data for both absorption and emission spectra of Na in matrices.

Both the Na^{*}-Ar potentials are fit to Morse functions of the form:

$$V(R) = D X(R) (X(R) - 2)$$

where $X(R) = \exp[\rho (1-R/R_e)]$. Parameters are given in Table I, and the potential curves shown in Fig. 1. Also shown in Figure 1 is the $V_{\text{Ar-Ar}}(r)$ potential.

(c) Geometry Optimization

The global optimization was carried out using chiefly the Space-Fixed Modified Genetic Algorithm approach.⁴¹ This search is relatively fast. It also finds many local minima. In those cases where all local minima were required, the optimization search was restarted with a high penalty on the global minimum (GM). In addition, simulated annealing⁴² and steepest descents⁴³ from various candidate geometries were also employed.

III. Structure of Na($3^2P_{1/2}$)-Ar_n Clusters

(a) Na($2P$)-Ar₂ Clusters

An ab initio study of this system has recently been published.⁴⁴ We compare our semiempirical findings with these more accurate results here.

We show in Fig 2 the potential energy as a function of bond angle, θ , for a fixed value of $R(\text{Na}(2P)\text{-Ar})$ in C_{2v} geometry. There are three solutions to the secular determinant. At all angles the B_1 state has the lowest energy. The crossing of the diabatic B_2 and A_1 states near $\theta = 45$ degrees is a consequence of the planarity of the structure.⁴⁵ The results are in reasonable qualitative agreement with those of Langhoff.⁴⁴

In Fig 3 we show the minimum energy geometry for an $\text{Na}^*\text{-Ar}_n$ cluster for the simplest case, $n=2$. The C_{2v} geometry is trivial to predict: both Ar atoms lie at the equilibrium bond length, $R_{Ae} = 2.91 \text{ \AA}$, for the $A^2\Pi$ diatomic potential, with energy, $D_A = 563.4 \text{ cm}^{-1}$. The Ar-Ar bond length is $r_e = 3.757 \text{ \AA}$, with energy $\varepsilon = 99.738 \text{ cm}^{-1}$. The binding energy is therefore $2D_A + \varepsilon = 1226.5 \text{ cm}^{-1}$.

(b) Na($2P$)-Ar_n Clusters ($n = 2\text{-}17$)

The minimum energy geometries and energies of $\text{Na}^*\text{-Ar}_n$ ($n=2\text{-}17$) clusters are shown in figs 3 and 4. In order to facilitate discussion of the structure of the clusters and dynamics following excitation, we introduce here a descriptive notation. The notation is adapted from that proposed by Amar and Berry,⁴⁶ who used such a code in their study of Ar_7 clusters. As a simple example, our notation for the $\text{Na}^*\text{-Ar}_3$ minimum energy cluster is: $[0\ 0\ 0\ 1\ 2\ ;\ 3]$. The first five integers are used exactly as Amar and Berry use them; they denote

the number of argon atoms possessing a given number of nearest neighbor (NN) argon atoms. The number of NNs is listed from right to left, beginning at the semicolon. Thus, there are two argon atoms (the outer ones) with just one Ar NN, and one Ar atom (the central one) with two Ar NNs. There are no Ar atoms with three, four, or five NNs. The integer following the semicolon denotes the number of Ar atoms which are NN to the Na* atom; here three. Another simple case is that for Na*-Ar₅, which is denoted [0 0 0 5 0; 5]. As a more complex example, the Na*-Ar₆ structure shown in Fig 3 is given the notation: [0 0 2 4 0; 5]. This indicates that five argon atoms form the ring, and that the sixth argon atom is not part of the ring; furthermore, the sixth argon atom has two NNs. One useful property of the notation is that it allows a quick estimate of the total pairwise additive binding energy of the cluster. Clearly, each Ar atom which is NN to the Na* experiences the D_A attraction. The total Ar-Ar attraction can be found by summing the number of NN atoms, then dividing by two to include overcounting, and multiplying by ε. Thus, the approximate binding energy for Na*-Ar₆ is (5•D_A + (4•2 + 2•3)ε/2) = 3512 cm⁻¹. This is in fair agreement with the calculated value of 3402 cm⁻¹.

The n=3,4,5 clusters dramatically underline the tendency for the excited-state metal atom to organize the Ar atoms into a planar structure; All four argon atoms experience the strong Π attraction. The contrast with the Na(2S)-Ar_n clusters¹⁷ is striking. In the isotropic potential case, the Na-Ar attraction is weaker than the Ar-Ar interaction (D_X =40.4 cm⁻¹; ε = 99.7 cm⁻¹.) Therefore the cluster resembles Ar_n clusters, but with the Na atom on the outside of the cluster.

The contributions to the energy are also easily identified. Essentially, for n Ar atoms, (with n= 2-4) there are n D_A bond energies, plus (n-1) Ar-Ar nearest-neighbor interactions, ε. For n=2 through 4, all atom-atom distances are at the minimum for the pairwise interaction. This is reflected in the approximate binding energies. For instance, for n=4, the pairwise additive BE is 2551 cm⁻¹; the actual BE is 2604 cm⁻¹. The additional stabilization energy comes from second nearest neighbor Ar-Ar attractions.

By n= 5, however, there is some strain; the Na*-Ar pairwise attraction, being considerable stronger than the Ar-Ar attraction, wins out, and the Na-Ar bondlengths are the equilibrium distances for the A potential, R_{Ae}. The Ar-Ar bondlengths are slightly greater than r_e. The geometry has C₅ symmetry [0 0 0 5 0; 5]. The pairwise additive binding energy is 3312 cm⁻¹; the actual energy is 3189 cm⁻¹, showing the strain.

By n=6, however, two competing tendencies are clear. The Ar-Ar attraction competes with the A potential's attraction between Na* and the Ar

atoms. If we consider the interaction of the sixth Ar atom with the $\text{Na}^*\text{-Ar}_5$ moiety, this interplay becomes clear. The rare gas-rare-gas attraction is optimized by a perpendicular approach of the atom to the plane. However, this sixth atom would feel the strongly repulsive B $\text{Na}^*\text{-Rg}$ potential. The sixth argon atom thus coordinates to two of the argon atoms in the ring. If the sixth argon atom were to lie in the plane of the ring, the $R(\text{Na}^*\text{-Ar})$ bondlength would be large, and the attraction correspondingly small. The attraction of the $\text{Na}^*\text{-Ar}$ potential is therefore optimized by moving the atom slightly out of the plane of the ring, reducing the $R(\text{Na}^*\text{-Ar})$, but simultaneously minimizing the repulsive B interaction.

For $n=7$, we might expect there to be two competing isomers for the minimum energy geometry. Starting with the geometry for $\text{Na}^*\text{-Ar}_6$, we can add the seventh argon atom either on the same side of the ring ("syn") as the sixth Ar atom [0 1 2 4 0 ; 5], or on the opposite face ("anti"), with code [0 2 2 3 0 ; 5]. It is easy to estimate the binding energy from the code. We find that it is the structure with the tetrahedral Ar substructure [0 2 2 3 0 ; 5] which has the lower potential energy. Thus, one Ar atom adds above the Ar_5 ring, one below to obtain a C_{2v} geometry. As can be seen from Fig. 3, this is, indeed, the global minimum.

For $n=8$ through 13, the energetics of adding the n th atom to the $(n-1)$ cluster is straightforward: the $\text{Ar}(n)\text{-Ar}(n-1)$ attraction is optimized, resulting in the local tetrahedral structure so typical of the exterior pure argon clusters. This is clearly shown in the addition of the eighth argon atom to the $\text{Na}^*\text{-Ar}_7$. It is well known that the typical addition pathway for rare gas clusters is via addition to triangular faces. This addition results in an incremental increase in attraction of 3ϵ for each added argon atom, if only NN are considered. The optimal triangular face to add to is that of a tetrahedron, since the added atom also experiences second nearest- neighbor attraction from the argon on the opposite side of the face. Thus the GM of $\text{Na}^*\text{-Ar}_7$ is the "seed" from which the larger clusters can be constructed.⁴⁷

(c) Effect of Variation in the B Potential

While the Ar-Ar potential is now fairly well known,³⁵ the $\text{Na}^*\text{-Ar}$ pairwise potential energy functions used here as input to the secular determinant are not as well established. As discussed above, there is some experimental information on the $\text{Na}^*\text{-Ar}$ ($A^2\Pi$) potential. Therefore the potential used here is likely to be, at worst, semi-quantitative. In any case, there are unlikely to be any qualitative differences caused in the structures of the clusters by any reasonable variation in either the Ar-Ar or the $A^2\Pi$ potentials. The $B^2\Sigma$ potential function, by contrast, is very poorly known. We will therefore focus on possible qualitative effects on cluster geometry of varying this potential.

The B potential is "felt" only by Ar atoms both out of the plane of the ring, and relatively close to the Na atom. Furthermore, in the larger clusters, such extra-annular argon atoms will tend to experience strong attraction from the argon subcluster. Thus the greatest effect of any change in the potential will be on those clusters in which there are few extra-annular argons. In particular, Na*-Ar₆ and Na*-Ar₇ will be affected. We therefore restrict discussion to these clusters.

In what follows we consider the structure of the Na*-Ar₆ cluster by minimizing the potential energy of an Ar atom free to move in the field of a "frozen" Na*-Ar₅ ring as the B potential is varied. Clearly, the minimum energy location will lie on a vector whose projection into the plane of the ring bisects two Na*-Ar ring bonds. Thus, the only variables we need to describe the minimum energy location of the sixth argon atom are the polar variables (R,θ), where we take θ to be the angle from the C₅ axis of the ring.

There are three parameters for the Morse potential which models the B²Σ interaction: the well depth, D_B; the location of the well minimum, R_{Be}; and the Morse parameter, ρ_B. For reasons discussed above, the parameter values chosen for the rest of this work are: (32.3 cm⁻¹, 6.81 Å, 4.3) for (D_B,R_{Be},ρ_B). For a Morse potential, varying D changes the well depth and the slope of the potential everywhere. The parameter, ρ, governs the curvature at R_e, and hence the steepness of the repulsive wall, as well as the range of the attractive part of the potential. Increasing ρ has the effect of "tightening" the potential well. This therefore increases the repulsion of the potential at the values of R seen in this study.

We consider here the effects of varying each of these parameters in turn. Results for a 20% variation in each parameter taken individually for Na*-Ar₆ and Na*-Ar₇ respectively are shown in Figs 5 and 6.

We consider first Na*-Ar₆ [00240;5]. As can be seen from Fig 5(a), both R and θ are relatively insensitive to the well depth, D_B, increasing by less than 2% for a 40% change in D_B. Furthermore, it can be seen that the value of the R is considerably less than R_{Be}. In addition, we find that the distances from the two closest Ar atoms in the ring correspond to r_e, maximizing the Rg-Rg attraction. The sixth Ar atom is attempting to maximize the Ar-Ar attraction while minimizing the repulsion due to the B potential. In fact, the R value is close to that of the zero of the Morse potential, R₀, which is given by the solution of X(R) = exp(ρ(1-R/R_{m}))=2. That is,}

$$R_0 = R_{Be}(1 - \ln 2 / \rho_B)$$

It can be seen that R_0 is independent of D_B , which is also the case with the $R(D_B)$ of Fig 5(a). In addition, the value of θ is given by elementary trigonometry, simply by maintaining r_{Ar-Ar} at its minimum energy value, r_e , and holding the Na*-Ar distance at R_0 .

Variation of R and θ as the Morse parameter, ρ_B , is varied is shown in Fig 5(b). The behavior of R with ρ is instructive: It increases rapidly for low ρ , but less rapidly at large ρ . This is in keeping with the trend we see in $R_0(r)$. The angle, θ , also behaves as expected by constraining the Ar-Ar distance to its equilibrium distance, and keeping R at R_0 .

From the expression for R_0 above we would expect the most drastic change in the value of R to come with a change in R_{Be} . That this is the case is shown in Fig 5(c), where we see an essentially linear increase in R and θ with R_m at first, until $R = 5.74$ Ångstrom. By this value, the sixth argon atom has moved into the plane of the ring (as is evidenced by the value of $\theta = 90$ degrees) and is no longer influenced by the B potential.

For the Na*-Ar₇ case, the stable structure with the unperturbed potential is [02230;5], with $R=5.5$ Ång and $\theta = 70$ degrees. This geometry is not qualitatively affected by changes in the B potential. The structure affords not only optimal attraction of the extraannular argon atoms with the atoms of the ring, but also with each other. The argon subcluster is here tetrahedral, yielding extra binding energy from the atoms above and below the plane; the (R,θ) values correspond to a r_e value for Ar(6)-Ar(7).

Not surprisingly, then, both R and θ are extremely insensitive to the value of both D_B (fig 6(a)) and ρ (fig 6(b)). The greatest sensitivity is to the R_{Be} value, as it was for Na*-Ar₆. The finding here (fig 6(c)) is qualitatively the same as in the Ar₅ case: the extraannular argon atoms are "pushed" out of the ring, to some extent. However, in order to maintain the Rg-Rg interaction, the cluster retains its C_{2v} geometry, merely allowing the argon tetrahedron to distort to accommodate the repulsion from the B potential.

In conclusion, we have shown that the structure of the Na*-Ar₆ clusters is only slightly sensitive to details of the B potential – in particular, to the location of the zero of the potential or, equivalently, to the Morse parameter, ρ_B . Measurements of rotational constants could, in principle, lead to information on this parameter. The Na*-Ar₇ clusters are even less sensitive to changes in the $B^2\Sigma$

potential. Both geometries are dominated by the attractive $A^2\Pi$ and Rg-Rg potentials.

(d) Na^*-Ar_5 Geometric Isomers

As well as the global minimum of the potential energy, there are also several local minima – which we shall refer to as geometric isomers – which illustrate the role of the metal atom in influencing the “solvent” argon atoms. We have found that all the possible variations in structure are present in the isomers of Na^*-Ar_5 . The number of possible isomers grows very rapidly for the $n=6$ and 7 cases. In order to keep the treatment manageable, we focus here on the $n=5$ cases.

In what follows, we restrict ourselves to those isomers of Na^*-Ar_5 which have at least three argon atoms at NN distances from the $Na(3P)$ atom. We predict several more isomers with fewer “ring” argon atoms. However, these are of interest only for the variations in the geometries of the argon subcluster, and add little to the discussion of the effects of the excited state metal atom on the solvent. In any case, such isomers are very energetically unstable compared to those with more ring atoms.

The geometries and energies for the seven energetically lowest-lying isomers of Na^*-Ar_5 we have located (or predicted) are shown in Fig 7. We have already considered the global minimum (GM), I [0 0 0 5 0 ; 5], in some detail above.

In isomers II and III, four Ar atoms remain in the energetically-favorable ring configuration, as in the GM for Na^*-Ar_4 . However, the fifth atom is now no longer NN to the Na^* atom; instead, it is NN to two of the Ar atoms of the ring. There are two near-degenerate isomers, depending on whether the fifth argon bridges the central pair of argon atoms (resulting in a C_s geometry) or an outer pair of atoms (C_1). The energy difference between these structures and the GM derives from the loss of D_A ; there are still five Ar-Ar NN pairs, as there were in isomer I.

In isomer IV, the fifth Ar atom sits perpendicular to the plane of the ring near the shallow minimum of the $B^2\Sigma$ potential; that is, at R_{Be} . This minimum is “worth” 32.3 cm^{-1} . In order to include such isomers in our notational scheme, we need to amend the scheme. We denote Ar atoms which are attracted to the Na^* atom by the weak $B^2\Sigma$ potential in the following way. The number of NN Ar atoms is just as it was in Na^*-Ar_4 , as is the number of strongly-bound Ar atoms.

We denote this isomer by [0 0 0 2 2 ; 4 + 1], where the "+ 1" indicates an Ar atom weakly bound to the Na* (via the B²Σ). The rest of the structure is just as in the global minimum for Na*-Ar₅. This is reflected in the notation. The estimated binding energy for IV is 2583 cm⁻¹.

Isomers V, VI, and VII all have three-membered rings. The greatest Ar-Ar pairwise attraction is obtained by the tetrahedral disposition of atoms in isomer V, [0 1 3 0 1; 3], which has 7ε from the rare gas - rare gas interaction. Related, but less tightly held structures are the near-degenerate pair which both have code [0 10 4 0; 3]. These both have two argon atoms, each bridging two ring argons. In contrast to isomer V, though, the bridges are between different ring atoms. In order to distinguish between these two, we note that the slightly more stable structure has the two "non-ring" argon atoms on the same side of the plane of the ring, generating C_s geometry (or "syn"). The less stable of the structures is of C₂ geometry (or "anti").

The isomers for larger clusters share the same features as those explored for Na*-Ar₅. However, as we mentioned above, the number of them increases rapidly.

IV Conclusions

We have calculated the global minimum of Na*(3²P)-Ar_n clusters using a perturbation theory approach with semiempirical diatomic potentials. For clusters up to n=5, the structure is dominated by the strong A²Π interaction, leading to planar ring structures. For larger clusters, the Rg-Rg interaction is the dominant contribution, and the nonannular part of the cluster is similar to rare gas clusters.

We predict that variation in the relatively unknown B²Σ will have little effect on the geometry of these clusters. This potential will, however, be crucial in correctly assigning spectroscopic lines for optical excitations in Na(3²S)-Ar_n → Na*(3²P) -Ar_n clusters. It is through such measurements that the best experimental understanding of this component of the potential energy will come.

REFERENCES

1. A. W. Castleman and R. G. Keesee, *Ann. Rev. Phys. Chem.*, **37**, 525 (1986)
2. T. S. Zwier, *Ann. Rev. Phys. Chem.*, **47**, 205 (1996)
3. E. R. Bernstein, ed., *Atomic and Molecular Clusters, Studies in Physical and Theoretical Chemistry*, v 68, Elsevier, Amsterdam, 1990.
4. Q. Y. Shang and E. R. Bernstein, *Chem. Rev.*, **94**, 2015 (1994)
5. P. H. Hobza, H. L. Selzle, and E. W. Schlag, *Chem. Rev.*, **94**, 1767 (1994)
6. D. Eichenauer and R. J. LeRoy, *J. Chem. Phys.*, **88**, 2898 (1988)
7. X. J. Gu, D. J. Levandier, B. Zhang, G. Scoles, and D. Zhuang, *J. Chem. Phys.*, **93**, 4898 (1990)
8. D. J. Chartrand, J. C. Shelley, and R. J. LeRoy, *J. Phys. Chem.*, **95**, 8310 (1991).
9. D. J. Chartrand, R. J. LeRoy, A. Kumar, and W. J. Meath, *J. Chem. Phys.*, **98**, 5668(1993) .
10. L. Perera and F. G. Amar, *J. Chem. Phys.*, **93**, 4884 (1990)
11. M. Schmidt, J. Le Calvé, and M. Mons, *J. Chem. Phys.*, **98**, 6102 (1993)
12. L. E. Fried and S. Mukamel, *J. Chem. Phys.*, **96**, 116 (1992)
13. J. Bösiger, R. Knochenmuss, and S. Leutwyler, *Phys. Rev. Lett.*, **62**, 3058 (1989)
14. M. Y. Hahn and R. L. Whetten, *Phys. Rev. Lett.*, **61**, 1190 (1988)
15. X. Li, M. Y. Hahn, M. S. El-Shall, and R. L. Whetten, *J. Phys. Chem.*, **95**, 8524 (1991)
16. M. J. Ondrechen, Z. Berkovitch-Yellin, and J. Jortner, *J. Am. Chem. Soc.*, **103**, 6586 (1981)
17. C. Tsou, D. A. Estrin, and S. J. Singer, *J. Chem. Phys.*, **96**, 7977 (1992)

18. M. A. Osborne, M. A. Gaveau, C. Gee, O. Sublemontier, J. M. Mestdagh, and J. -P. Visticot, *J. Chem. Phys.*, **106**, 1449 (1997)
19. P. Jungwirth and R. B. Gerber, *J. Chem. Phys.*, **104**, 5803 (1996)
20. S. K. Gregurick, M. H. Alexander, and B. Hartke, *J. Chem. Phys.*, **104**, 2684 (1996)
21. M. H. Alexander, A. R. Walton, M. Yang, X. Yang, E. Hwang, and P. J. Dagdigian, *J. Chem. Phys.*, **106**, 6320 (1997)
22. G. S. Fanourgakis, S. C. Farantos, P. Parneix, and Ph. Bréchnignac, *J. Chem. Phys.*, **106**, 4954 (1997)
23. J. E. Adams and R. M. Stratt, *J. Chem. Phys.*, **105**, 1743 (1996)
24. A. Dullweber, M.P. Hodges, and D. J. Wales, *J. Chem. Phys.*, **106**, 1530 (1997)
25. L. C. Balling, M. D. Havey and J. F. Dawson, *J. Chem. Phys.*, **69**,1670 (1978)
26. L. C. Balling and J. J. Wright, *J. Chem. Phys.*, **81**, 675 (1984)
27. M. Hofmann, S. Leutwyler, and W. Schulze, *Chem. Phys.*, **40**, 145 (1979)
28. M. McCarty Jr. and G. W. Robinson, *Mol. Phys.*, **2**, 415 (1959)
29. B. Meyer, *J. Chem. Phys.*, **43**, 2986 (1965)
30. S. Tam and M. E. Fajardo, *J. Chem. Phys.*, **99**, 854 (1993)
31. J. A. Boatz and M. E. Fajardo, *J. Chem. Phys.*, **101**, 3472 (1994)
32. A. B. Tutein, Ph. D. Dissertation, University of New Hampshire, 1997.
33. W. E. Baylis, *J. Phys. B* **10**, L447 (1977).
34. L. C. Balling and J. J. Wright, *J. Chem. Phys.*, **79**, 2941 (1983)
35. R. A. Aziz, *J. Chem. Phys.*, **99**, 4518 (1993)
36. J. Tellinghuisen, A. Ragone, M. L. Kim, D. J. Auerbach, R. E. Smalley, L. Wharton, and D. H. Levy, *J. Chem. Phys.*, **71**, 1283 (1979)

37. W. E. Baylis, *J. Chem. Phys.*, **51**, 2665 (1969)
38. R. P. Saxon, R. E. Olson, and B. Liu, *J. Chem. Phys.*, **67**, 2692 (1977)
39. R. Düren, E. Hasselbrink and G. Moritz, *Z. Phys. A* **307**, 1 (1982)
40. F. Van Den Berg, R. Morgenstern, and C. Th. J. Alkemade,
Chem. Phys., **93**, 171 (1985)
41. J. A. Niese and H. R. Mayne, *J. Chem. Phys.*, **105**, 4700 (1996).
42. S. Kirkpatrick, C. D. Gelatt, and M. P. Vecchi, *Science* **220**, 671 (1983).
43. W. H. Press, S. A. Teukolsky, W. T. Vetterling, and B. P. Flannery,
Numerical Recipes, 2nd Ed. (Cambridge, NY, 1992)
44. P. W. Langhoff, *J. Phys. Chem.*, **100**, 2974 (1996).
45. K. M. Sando, G. J. Erickson, and R. C. Binning, *J. Phys. B* **12**, 2697 (1979).
46. F. G. Amar and R. S. Berry, *J. Chem. Phys.*, **85**, 5943 (1986)
47. M. R. Hoare and P. Pal, *J. Cryst. Growth*, **17**, 77(1972).

TABLE I

Parameters for the Morse potentials used for Na^{*}-Ar interaction. See text.

	D [cm ⁻¹]	Re [Ångstrom]	ρ
A ² Π	563.4	2.91	5.29
B ² Σ	32.3	6.81	4.4

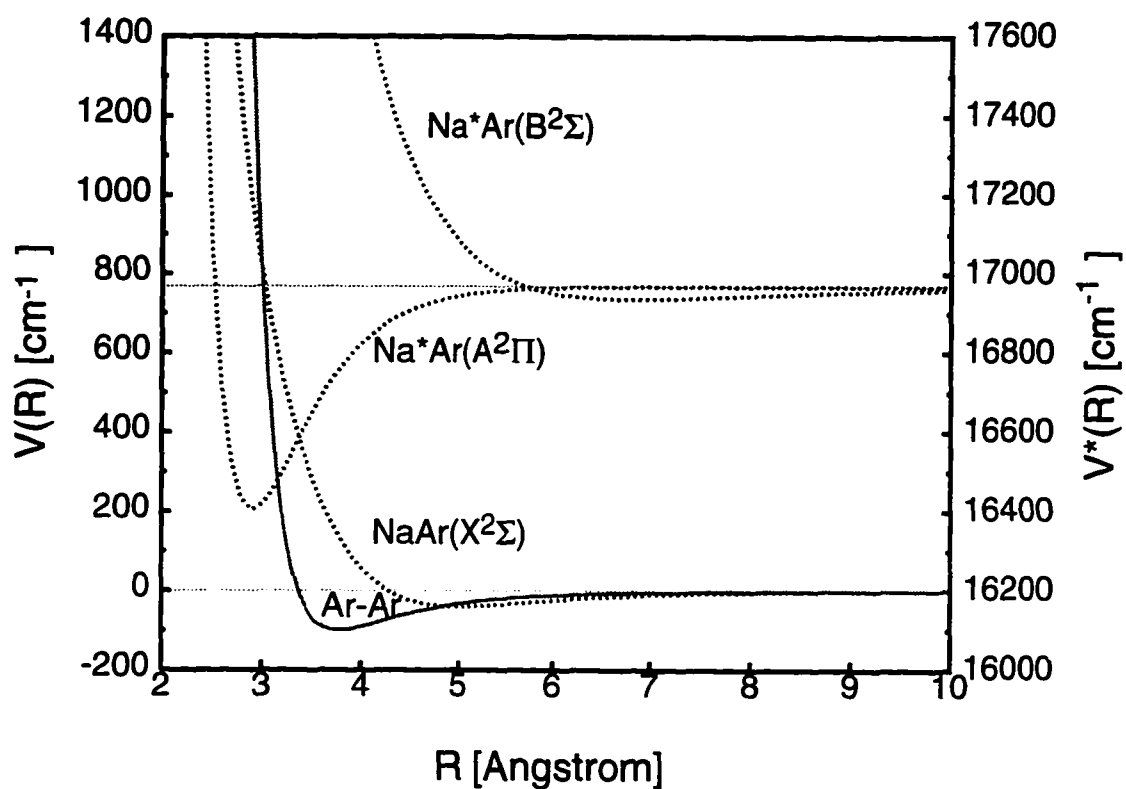


FIGURE 1

Pair potentials used here. The Ar-Ar pair potential is that of Aziz.³⁵ The $A^2\Pi$ potential for $\text{Na}(3^2P) - \text{Ar}$ is the Morse fit of Tellinghuisen et al.³⁶ The $B^2\Sigma$ potential for $\text{Na}(3^2P) - \text{Ar}$ is the best fit from a simulation of optical absorption spectra of sodium atoms in an argon matrix.³²

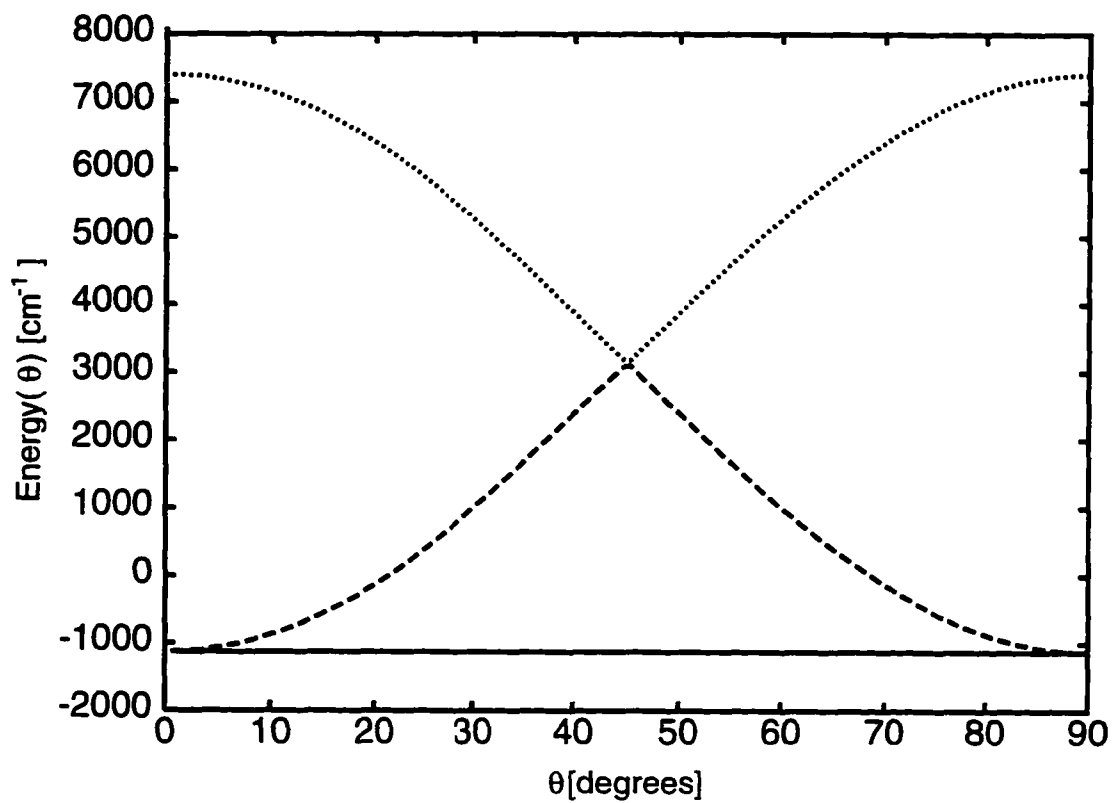


FIGURE 2

The three solutions of the secular determinant for $\text{Na}(3^2\text{P}) - \text{Ar}_2$ in C_{2v} geometry with $R(\text{Na-Ar}) = 4.0 \text{ \AA}$.

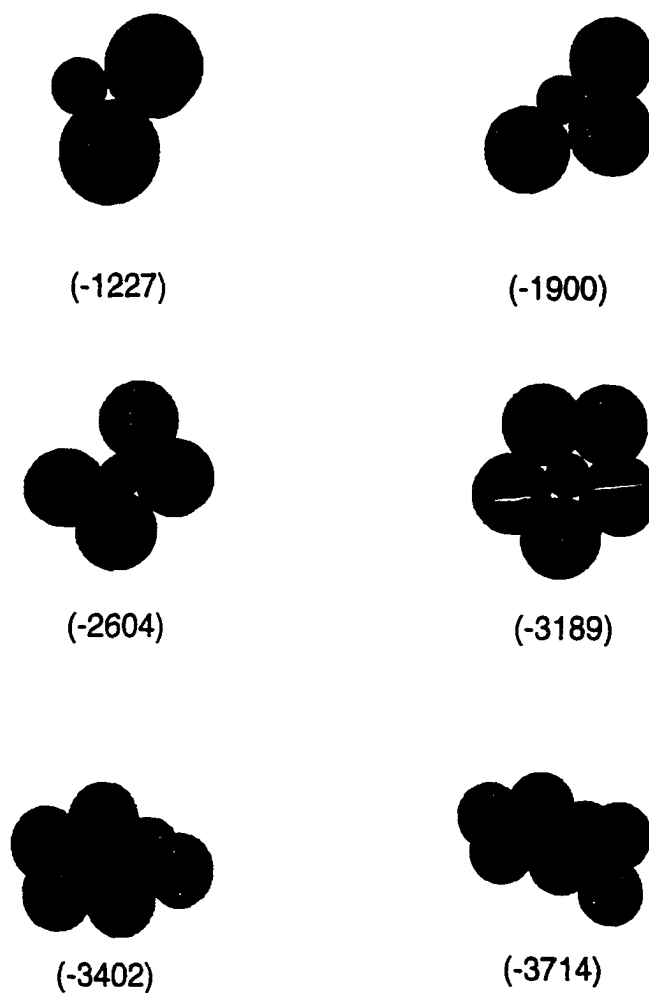


FIGURE 3

Minimum potential energy geometries for clusters $\text{Na}(3^2\text{P})-\text{Ar}_n$ for $n = 2$ through 7 . In parentheses the binding energy in cm^{-1} is given.

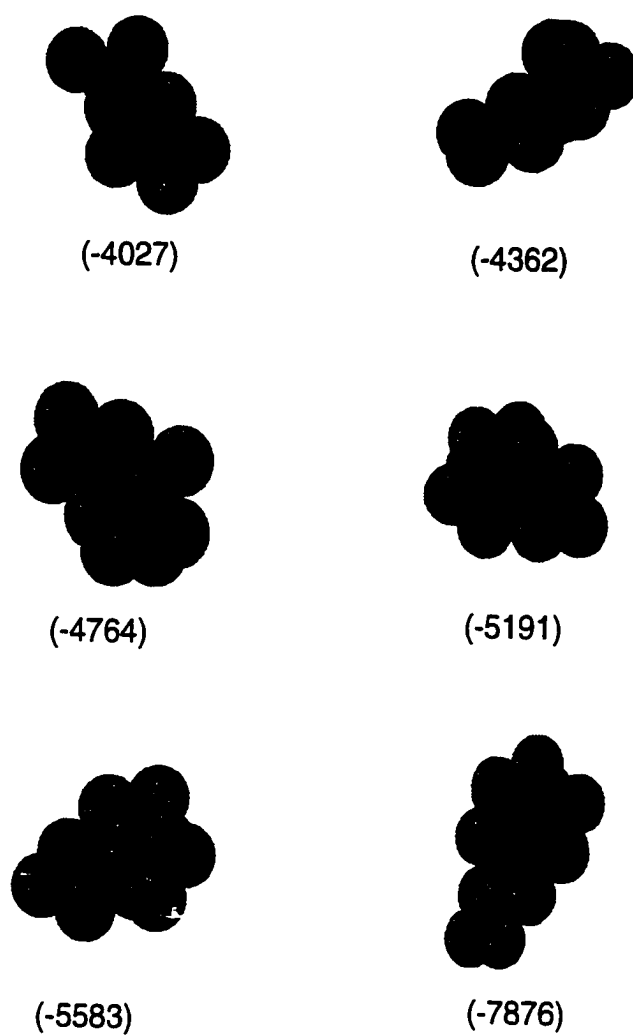


FIGURE 4

As in Figure 3, except $n = 8-12$ and 17.

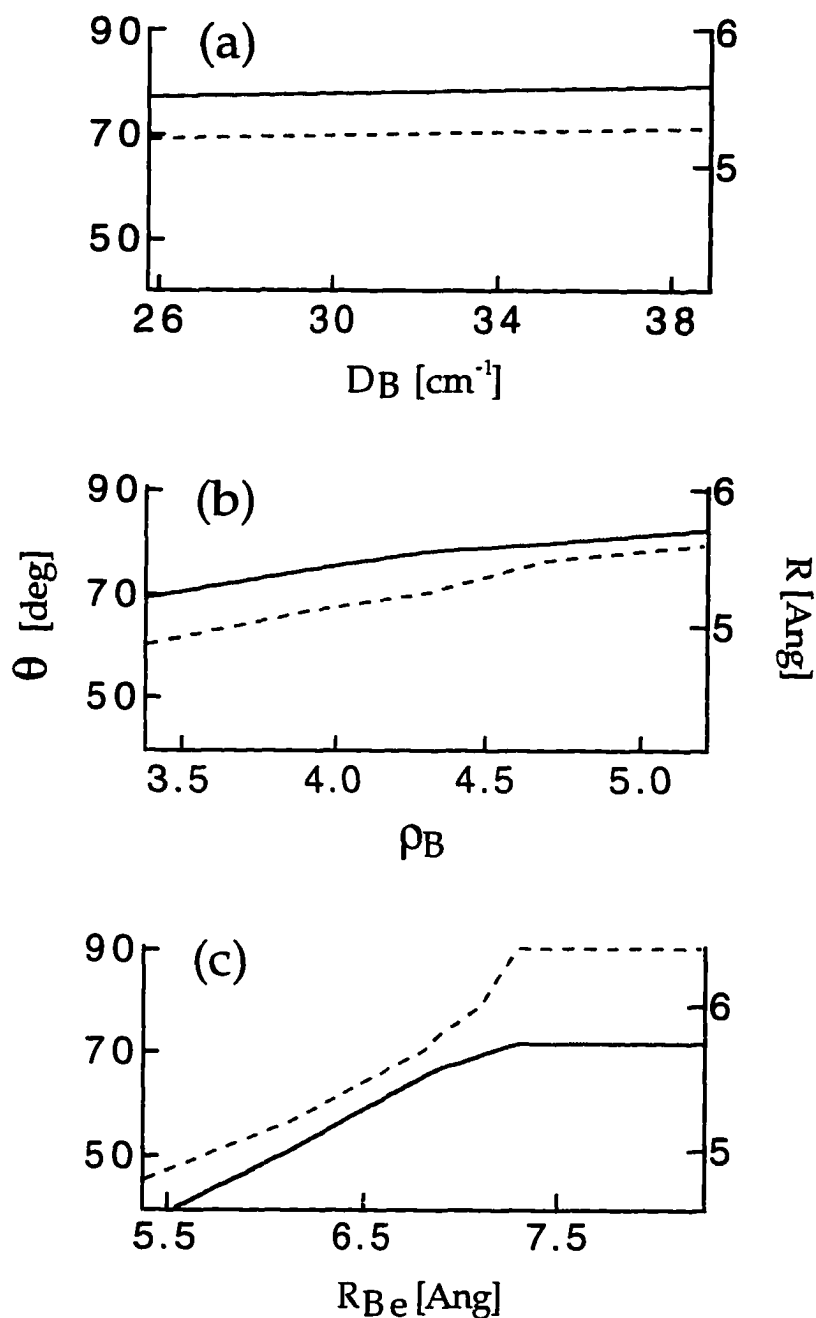


FIGURE 5

Effect on the geometry of $\text{Na}^*\text{-Ar}_6$ in C_s geometry of variations in the parameters of the B potential. Plotted are polar coordinates, (R, θ) of the minimum position of the sixth argon atom. The angle θ (dashed line) is measured from the C_5 symmetry axis of the $\text{Na}^*\text{-Ar}_5$ ring. At $\theta = 90$ degrees, the vector to the sixth argon atom would bisect the angle $\text{Ar}(4) - \text{Na} - \text{Ar}(5)$.

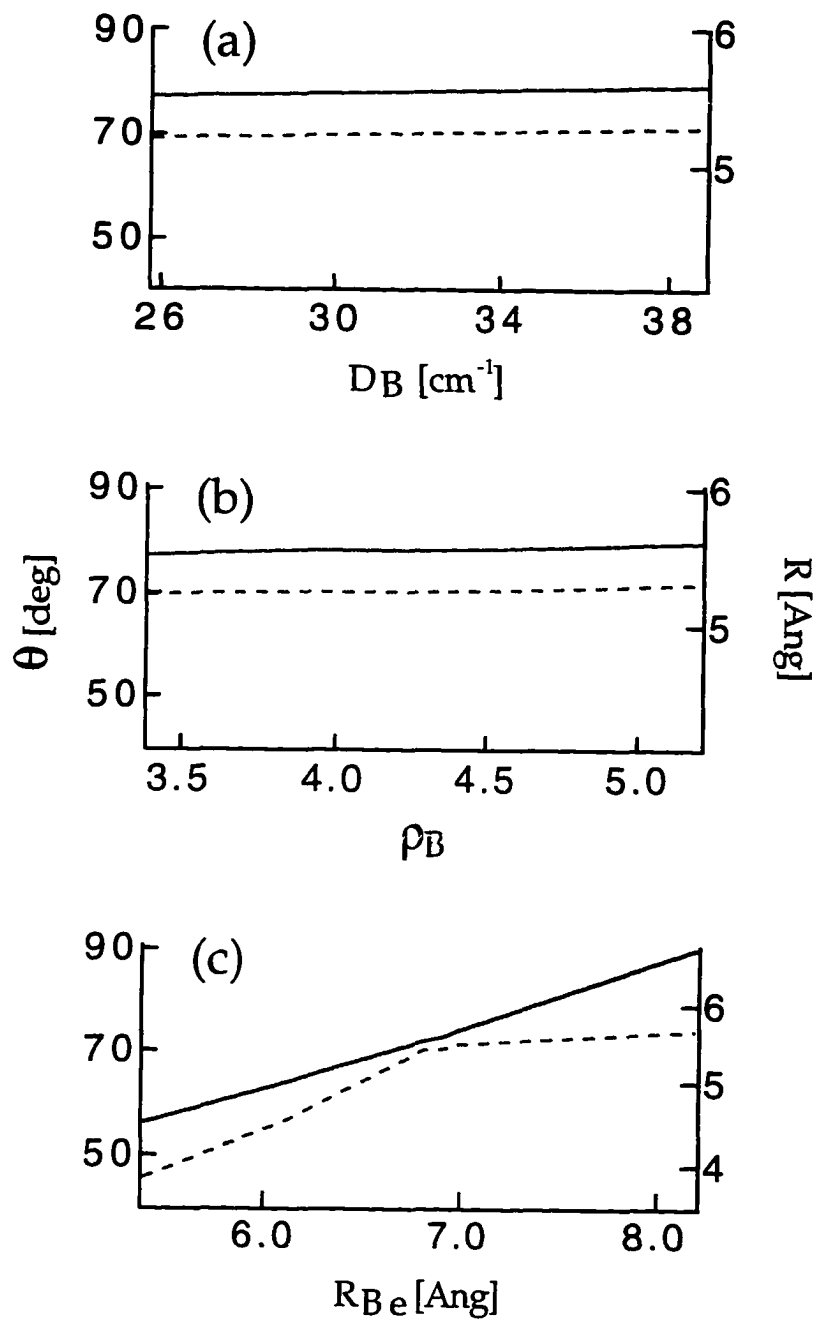


FIGURE 6

As in Figure 5 except for $\text{Na}^*\text{-Ar}_7$ in C_{2v} geometry. The angle, θ , refers to the coordinates of Ar(6). Ar(7) is at $(180-\theta)$.

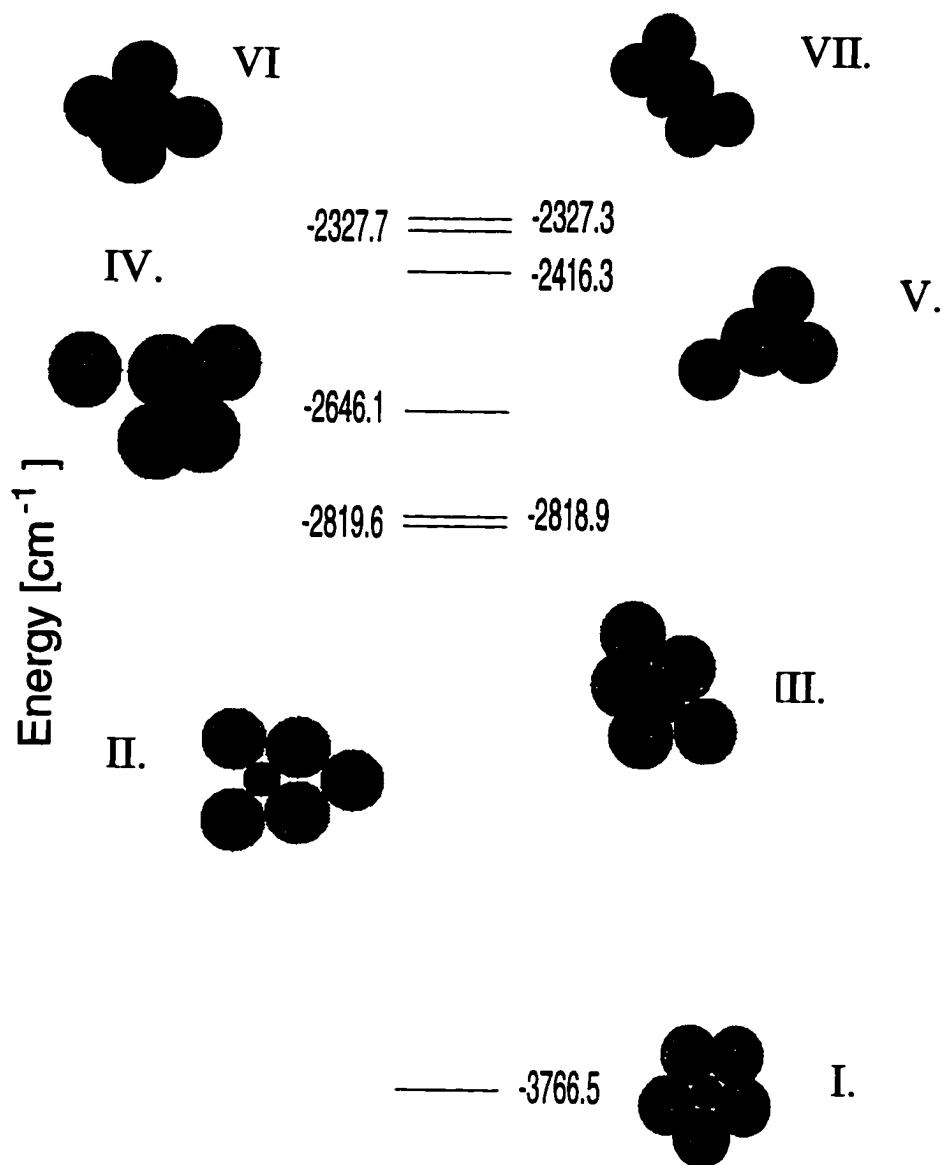


FIGURE 7

Geometries and energies for the seven energetically lowest-lying isomers of Na⁺-Ar₅.

List of References

- [1] L. C. Balling and J. J. Wright. Use of dimer potentials to calculate the energy levels of alkali atoms in rare-gas matrices. *J. Chem. Phys.*, 79:2941–2944, 1983.
- [2] L. C. Balling and J. J. Wright. Computer simulation of site formation for Na atoms trapped in Ar and Xe solids. *J. Chem. Phys.*, 81:675–679, 1984.
- [3] C. Tsoo, D. A. Estrin, and S. J. Singer. Electronic spectra of NaAr_4 and NaAr_6 : Isomerization and melting. *J. Chem. Phys.*, 96:7977–7991, 1992.
- [4] M. E. Fajardo. Classical Monte Carlo simulations of relaxed trapping site structures in Li atom doped solid Ne. *J. Chem. Phys.*, 98:119–125, 1993.
- [5] J. A. Boatz and M. E. Fajardo. Monte carlo simulations of the structures and optical absorption spectra of Na atoms in Ar clusters, surface, and solids. *J. Chem. Phys.*, 101:3472–3487, 1994.
- [6] J. P. Visticot, P. de Pujo, J. M Mestdagh, A. Lallement, J. Berlande, O. Sublemontier, P. Meyndier, and J. Cuvellier. Experiment versus molecular dynamics simulation: Spectroscopy of $\text{Ba}(\text{Ar})_n$ clusters. *J. Chem. Phys.*, 100:158–164, 1994.
- [7] A.I. Krylov, R.B. Gerber, M.A. Baveau, J.M.Mestdagh, B. Schilling, and J.P. Visticot. Spectroscopy, polarization and nonadiabatic dynamics of electronically excited $\text{Ba}(\text{Ar})_n$ clusters: Theory and experiment. *J. Chem. Phys.*, 104:3651–3663, 1996.
- [8] M. McCarty Jr. and G. W. Robinson. Environmental perturbations of foreign atoms and molecules in solid argon, krypton and xenon. *Mol. Phys.*, 2:415–430, 1959.
- [9] W. Weyhmann and F. M. Pipkin. Optical absorption spectra of alkali atoms in rare-gas matrices. *Phys. Rev.*, 137:A490–A497, 1965.
- [10] B Meyer. Absorption spectrum of Na and K in rare-gas matrices. *J. Chem. Phys.*, 43:2986–2992, 1965.
- [11] L. C. Balling, M. D. Havey, and J.F. Dawson. Absorption and emission spectra of Na atoms trapped in rare-gas matrices. *J. Chem. Phys.*, 69:1670–1675, 1978.
- [12] L. C. Balling, M. D. Havey, and J. J. Wright. Absorption and emission spectra of K atoms trapped in rare-gas matrices. *J. Chem. Phys.*, 70:2404–2408, 1979.
- [13] M. Hofmann, S. Leutwyler, and W. Schulze. Matrix isolation/aggregation of sodium atoms and molecules formed in a supersonic nozzle beam. *Chem. Phys.*, 40:145–152, 1979.
- [14] T. Welker and T. P. Martin. Optical absorption of matrix isolated Li, Na, and Ag clusters and microcrystals. *J. Chem. Phys.*, 70(12):5683–5691, 1979.

- [15] J. J. Wright and L. C. Balling. Absorption and emission spectra of Na atoms trapped in a Ne matrix. *J. Chem. Phys.*, 73:994–996, 1980.
- [16] J. J. Wright and L. C. Balling. Absorption and emission spectra of Li atoms trapped in rare gas matrices. *J. Chem. Phys.*, 73:3103–3106, 1980.
- [17] J. Hormes and B. Karrasch. Absorption spectra of Na and Na₂ in inert gas matrices. *Chem. Phys.*, 70:29–37, 1982.
- [18] H. Kuppelmaier, H.-J. Stöckmann, A. Steinmetz, E. Görlach, and H. Ackermann. Jahn-Teller effect of K atoms isolated in Ar matrices. *Phys. Letters*, 98A:187–191, 1983.
- [19] J. Rose, D. Smith, D.E. Williamson, P. N. Schatz, and M. C. M. O'Brien. Magnetic circular dichroism and the jahn-teller effect in the $^2S \rightarrow ^2P$ transition of sodium and lithium atoms isolated in xenon matrices. *J. Phys. Chem.*, 90:2608–2615, 1986.
- [20] A. Schrimpf, G. Sulzer, H.-J. Stöckmann, and H. Ackermann. Correlation of electron spin resonance and optical absorption of K atoms in solid Ar. *Z. Phys. B*, 67:531–539, 1987.
- [21] M. E. Fajardo. Matrix isolation spectroscopy of metal atoms generated by laser ablation: II. the Li/Ne, Li/D₂, and Li/H₂ systems. *J. Chem. Phys.*, 98:110–118, 1993.
- [22] S. Tam and M. E. Fajardo. Matrix isolation spectroscopy of metal atoms generated by laser ablation. III the Na/Ar, Na/Kr, and Na/Xe systems. *J. Chem. Phys.*, 99:854–860, 1993.
- [23] R.A. Corbin and M.E. Fajardo. Optical absorptions of Li atoms in mixed Ar/Xe matrices. *J. Chem. Phys.*, 101:2678–2683, 1994.
- [24] G. York, R. Scheps, and A. Gallagher. Continuum radiation and potentials of Na-noble gas molecules. *J. Chem. Phys.*, 63:1052–1064, 1975.
- [25] R.P. Saxon, R.E. Olson, and B. Liu. *Ab initio* calculations for the $X^2\Sigma$, $A^2\Pi$, and $B^2\Sigma$ state of NaAr: Emission spectra and cross sections for fine-structure transitions in Na-Ar collisions. *J. Chem. Phys.*, 67:2692–2702, 1977.
- [26] J. Tellinghuisen, A. Ragone, M. L. Kim, D.J. Auerbach, R.E. Smalley, L. Wharton, and D.H. Levy. The dispersed fluorescence spectrum of NaAr: Ground and excited state potential curves. *J. Chem. Phys.*, 71:1283–1291, 1979.
- [27] B. C. Laskowski, S.R. Langhoff, and J.R. Stallcop. Theoretical calculation of low-lying state of NaAr and NaXe. *J. Chem. Phys.*, 75:815–827, 1981.
- [28] R. Düren, E. Hasselbrink, and G. Moritz. On the interaction of excited alkali atoms with rare gas targets in scattering processes. *Z. Phys. A*, 307:1–11, 1982.
- [29] F. Van Den Berg, R. Morgenstern, and C. Th. J. Alkemade. Investigation of the $B^2\Sigma$ and test of the $A^2\Pi$ interaction potential for Na(3^2P)-Ar from high-resolution differential scattering measurements. *Chem. Phys.*, 93:171–178, 1985.

- [30] R. A. Aziz. A highly accurate interatomic potential for argon. *J. Chem. Phys.*, 99:4518–4525, 1993.
- [31] C. E. Moore. *Atomic Energy Levels*, volume 1. Natl. Bur. Stand., 1971.
- [32] C. Kittel. *Introduction to Solid State Physics*. Wiley, New York, 1986.
- [33] B.H. Bransden and C.J. Joachain. *Physics of Atoms and Molecules*. Longman, New York, 1983.
- [34] W. E. Baylis. Three-body alkali-noble-gas interactions and secondary satellites. *J. Phys. B*, 10:L477–L481, 1977.
- [35] W. H. Press, S. A. Teulosky, W. T. Vetterling, and B. P. Flannery. *Numerical Recipes in C: The Art of Scientific Computing*. Cambridge University Press, Cambridge, 1992.
- [36] D. Halliday and R. Resnick. *Fundamental of Physics*. John Wiley & Sons, Inc., New York, 1988.
- [37] C. D. Maranas and C. A. Floudas. A global optimization approach for Lennard-Jones microclusters. *J. Chem. Phys.*, 97:7667–7678, 1992.
- [38] W.G. Lawrence and V.A. Apkarian. Many-body potentials of an open shell atom: Spectroscopy of spin-orbit transitions in iodine in crystalline Xe and Kr. *J. Chem. Phys.*, 101:1820–1831, 1994.
- [39] E. Merzbacher. *Quantum Mechanics*. John Wiley & Sons, New York, 1970.
- [40] H. Margenau and N. R. Kestner. *Theory of Intermolecular Forces*. Pergamon, New York, 1969. chap 5.
- [41] W. E. Baylis. Semiempirical, pseudopotential calculation of alkali-noble-gas interatomic potentials. *J. Chem. Phys.*, 51:2665–2669, 1969.
- [42] D. J. Mueller. Householder's method for complex matrices and eigensystems of hermitian matrices. *Numerische Mathematik*, 8:72–92, 1966.
- [43] J.C. Tully and R.K. Preston. Trajectory surface hopping approach to nonadiabatic molecular collisions: The reaction of H^+ with D_2 . *J. Chem. Phys.*, 55:562–571, 1971.
- [44] P.J. Kuntz. Classical path surface-hopping dynamics. I. General theory and illustrative trajectories. *J. Chem. Phys.*, 95:141–155, 1991.
- [45] P. Jungwirth and R.B. Gerber. Quantum dynamics simulations of nonadiabatic processes in many-atom systems: Photoexcited $Ba(Ar)_{10}$ and $Ba(Ar)_{20}$ clusters. *J. Chem. Phys.*, 104:5803–5814, 1996.
- [46] K.M. Sando, G.J. Erickson, and R.C. Binning Jr. Extended pairwise additivity: interactions of degenerate atoms with rare-gas atoms. *J. Phys. B*, 12:2697–2795, 1979.
- [47] G.-Q.Xu, R.J. Holland, S.L. Bernasek, and J. C. Tully. Dynamics of cluster scattering from surfaces. *J. Chem. Phys.*, 90:3831, 1989.

- [48] G. Herzberg. *Molecular Spectra and Molecular Structure, I. Spectra of Diatomic Molecules*. D. Van Nostrand Company, Inc, Princeton, NJ, second edition, 1950.
- [49] I. N. Levine. *Molecular Spectroscopy*. John Wiley & Sons, Inc., 1975.
- [50] Richard N Zare. *Angular momentum : understanding spatial aspects in chemistry and physics*. Wiley, New York, 1988.